AFIT/GAE/ENY/93D-20

A STUDY OF GRAPHITE PEEK COMPOSITE WITH CENTRAL ELLIPTICAL HOLES UNDER TENSION

THESIS

Bill J. Lau, Captain, USAF

AFIT/GAE/ENY/93D-20

Approved for public release; distribution unlimited

The views expressed in this thesis are those of the author and do not reflect the official policy or position of the Department of Defense or the U. S. Government.

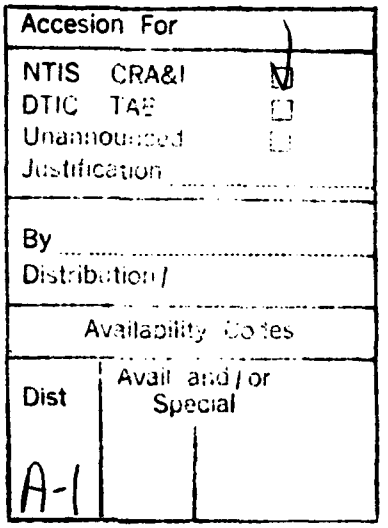

AFIT/GAE/ENY/93D-20

A STUDY OF GRAPHITE PEEK COMPOSITE WITH CENTRAL ELLIPTICAL HOLES UNDER TENSION

THESIS

Presented to the Faculty of the Graduate School of Engineering

of the Air Force Institute of Technology

Air University

In Partial Fulfillment of the

Requirements for the Degree of

Master of Science in Aeronautical Engineering

Bill J. Lau, B.S.A.E.

Captain, USAF

December 1993

Acknowledgments

An effort of this magnitude cannot be undertaken lightly or without assistance, and there are a number of people who merit special mention in this regard.

First, I would like to thank Dr. Anthony Palazotto, my thesis advisor, for the basic idea that started this whole thing rolling, and all the help he provided along the way. He helped keep me focused and ensured I didn't get too far behind. Special thanks also go to Dr. R.S. Sandhu of Wright Lab for sponsoring this research and guiding me along the way. His knowledge in this field is extensive, and he put hings in perspective. His office gratiously provided a place to work at and free use of their computer resources, as well as their supply cabinet. Dr. Greg Schoeppner and Mr. Forrest Sandow both provided answers and assistance, too, and always with a smile.

The Composites Facility in Building 65 and Beta Industries did a great job manufacturing my test specimens, and without their help no study would have been possible. Thanks to everyone there who was part of the Gr/PEEK team.

A lot of time and effort went into attaching strain gages to 60-plus specimens, and I appreciate the expertise provided by the folks of the Instrumentation Lab in Building 65. I thank everyone who got involved in this task, and put in some overtime to get it done quickly.

Alas, these gages didn't last long, and thanks go to Mr. Don Cook and Mr. Larry Bates for conducting the numerous tests required in this effort. They were very helpful and pleasant to be around. I looked forward to every testing day, and was sorry it was all over so soon.

Finally, a special thank you to my family: my wife, Sue, and my daughter, Sarah, for the sacrifices made during the last 18 months, and reminding me that there is life after AFIT.

Table of Contents

List of Figures

List of Tables

Abstract

This study investigated the stress-strain response and failure modes of Graphite/Polyetheretherketone (Gr/PEEK) tension specimens containing a central elliptical hole. Both experiments and finite element numerical analyses were conducted.

Gr/PEEK is a thermoplastic matrix, graphite fiber reinforced composite material. Its material properties are inherently nonlinear. An expansion of the database on this material was desired, to investigate the effects of hole geometry and the resulting stress concentration on failure loads and stress-strain behavior of tensile coupons.

Test specimens included seven stacking sequences and three hole geometries. The stacking sequences, or layups, tested were $[0_{16}]$, $[90_{16}]$, $[0/90]_{4S}$, $[\pm45]_{4S}$, $[\pm45_2/0/\pm45]_S$, $[(\pm45/0)_2/\pm45]_S$, and $[0/\pm45/90]_{2S}$. The hole geometries consisted of 1.016 cm x 0.508 cm (0.4" x 0.2") ellipse, 0.508 cm x 1.016 cm (0.2" x 0.4") ellipse, and 1.016 cm (0.4") diameter circle. The circle was tested for comparison both with the ellipses and previous studies. Three specimens were tested for each combination of layup and hole geometry. Tests were conducted under quasi-static loading conditions at room temperature. Strains were recorded from gages next to the hole and midway between the hole and tab.

Numerical analysis utilized a nonlinear finite element computer program. This program assumes a state of plane stress; three-dimensional effects are thus ignored. Linear elastic relations form the basis of the analysis, but are applied incrementally, to allow for nonlinear material properties. Data from basic material property tests is included in the input file. Piecewise cubic spline interpolation functions are employed to represent these material properties. The program utilizes a strain energy failure criterion to determine failure of elements in the mesh. Due to symmetry of the coupons and load only one-quarter of the specimen was modelled. One basic mesh was developed for each hole geometry, and then applied to the different layups. Progression of predicted damage or failed elements was noted for comparison with actual failure modes. Element stress-strain data was recorded for comparison also.

Analytical stress-strain response agreed well overall with experimental data. Analysis overpredicted the stiffness of the material in some cases, but underpredicted it in others. Divergence of the analytical curves from experiment was noted in some cases. The analysis could not model abrupt or sudden failures, but predicted failure patterns very well in all other cases.

A STUDY OF GRAPHITE PEEK COMPOSITE WITH CENTRAL ELLIPTICAL HOLES UNDER TENSION

I. Introduction

Database expansion of material properties, response, and behavior of established composite materials promotes vital industrial advancements in safety, durability, and life-cycle cost reduction, thereby fulfilling industry requirements for premier structural materials.

Fiber reinforced resin composites typically exhibit lower weight, greater strength-to-weight ratios, and greater stiffness-to-weight ratios than more traditional aerospace structural materials [1]. This combination of strength and lower weight have made composites ideally suited as component materials in aircraft and spacecraft. A variety of material systems exist and are employed in different applications in this arena. Two widely used systems utilize carbon or graphite fibers in either thermoset or thermoplastic resin-based matrices. Thermosets exhibit an irreversible reaction to the application of heat, and do not soften or flow. Thermoplastics, on the other hand, soften and flow when exposed to heat and pressure, with no chemical reaction occurring [2]. This is a reversible process.

Gr/PEEK is a relatively recent thermoplastic matrix composite which offers several advantages over the well-established thermoset composite, Graphite/Epoxy (Gr/Ep). Although the database for Gr/PEEK properties and response is less extensive than for Gr/Ep, Gr/PEEK has demonstrated higher elastic moduli, greater after impact strength (damage tolerance) and higher fracture toughness, reduced tendency to delaminate, as well as lower moisture absorption and good outgassing properties [3, 4, 5]. PEEK can be stored at room temperature and has an unlimited shelf life, whereas epoxy must be refrigerated and has a limited shelf life [2]. Gr/PEEK thus provides improved performance, especially in areas prone to foreign object damage (FOD) and in space applications.

Although these advantages exist, cost and other considerations have limited somewhat the use of Gr/PEEK and thermoplastics in general. Thermoplastics offer lower

fabrication costs, but higher material and overall costs than thermosets. They require less time to process but use higher temperatures and pressures [2]. As an example of current utilization of the two types of composites, the YF-22 utilized 13% thermoplastic and 10% thermoset materials, while the production F-22 will contain only 4% thermoplastic and 22% thermosets [6]. The thermoplastics will be employed primarily in areas prone to FOD, such as belly skins and access panels.

Thus, the use of composites is balanced against many often conflicting design requirements: cost, strength, stiffness, toughness, weight limitations, fatigue resistance, and temperature and other environmental conditions [7]. A single material system will rarely satisfy all of these requirements; thus, several systems may be used on an aircraft, in addition to more traditional materials such as aluminum or titanium.

Composites in general exhibit nonlinear stress-strain relationships, and Gr/PEEK is certainly no exception [8]. Past AFIT research has highlighted the importance of accounting for the non linearity of the material properties of Gr/PEEK in analysis. This research has investigated Gr/PEEK with central circular holes under tension, with eccentric circular holes under tension, with circular holes at elevated temperature under tension, and with central circular holes under compression [9, 10, 11, 12]. The analysis program PLNRS has been shown to produce good failure progression information and overall material response predictions, and is used in this study.

A. Purpose

The purpose of this thesis is to determine, both analytically and experimentally, the initiation and progression of tensile failure, stress-strain response of the material, and the ultimate failure load of Gr/PEEK with a central elliptical hole. Two configurations of ellipses are studied, both 1.016 x 0.508 cm (0.2" x 0.4"), but oriented longitudinally or transversely. In other words, one ellipse has its semi-major axis aligned with the applied load, whereas the other has its semi-major axis perpendicular to the load. A circular hole of 1.016 cm (0.4") diameter is also considered, for comparison both with the elliptical holes and with previous studies. All tests are at room temperature. A total of seven different stacking sequences or ply layups are considered: $[0°_{16}]$, $[90°_{16}]$, $[0°/90°]_{4s}$, $[\pm45°]_{4s}$, $[0°/\pm45°/90°]_{2s}$ (quasi-isotropic; the material properties are the same in all directions), $[\pm45°_2/0°/\pm45°]_s$, and $[(\pm45°/0°)_2/\pm45°]_s$.

The objectives of this study are to:

1) Investigate the stress-strain response and failure patterns of each laminate for the three different concentric holes. The material response and progression of failure will be predicted using finite element techniques.

2) Add to the existing database on Gr/PEEK, specifically on the stress concentration effects of the different hole geometries on the various ply layups.

3) Compare the experimental and analytical results.

B. Background

Composite materials actually date back thousands of years. One of the earliest known composite building materials was bricks made from a combination of straw, mud, and dung around 800 B.C.; a development which made possible the construction of stronger, more durable structures than previously possible [13]. Around the same era, the Mongols constructed bows utilizing a combination of wood, animal tendons, and silk, resulting in greater strength and resilience than was possible using wood alone [13]. More recently, the invention of reinforced concrete has had a profound effect on construction, permitting the design of large buildings, including skyscrapers.

Advanced fibrous composite materials include a variety of materials constructed from load-carrying fibers and matrix materials. Some of the advantages of composites have already been cited. The composites can additionally be tailored to a specific use, optimizing both strength and weight, as well as other design factors such as service life, resistance to the environment, and ease of maintenance [14]. These materials have become commonplace in sports equipment, and are found in tennis racquets, golf clubs, and bicycles, among others [15].

Fiber reinforced composites include both continuous/oriented, continuous/random, and discontinuous/random material forms [16]. This describes whether the fibers run the length of the object or are chopped into short lengths, and whether they are oriented in a specific direction or combination of directions or are randomly oriented. The continuous/oriented form is more common in aerospace applications, due to its greater strength and versatility. Typical constructions employ panels or laminates made from many plies, stacked in a predetermined sequence. Each ply contains fibers which are parallel; when combined in different sequences, the laminate takes on properties different from an individual lamina. Laminates can also be made from weaves, where fibers are woven in two or more directions as in cloth.

Chapter II of this report covers some of the theory involved in undertaking a study of this nature. More information is provided there regarding the nature, properties, and behavior of fiber reinforced composites.

Both fracture mechanics and the finite element method can be applied to predict the response, strength, and stress state of a composite material. This study utilizes a nonlinear finite element program, PLNRS, developed by Dr. R.S. Sandhu of Wright Laboratories, W ight-Patterson AFB, Ohio. This program has been utilized in previous AFIT studies involving Gr/PEEK and found to produce generally good results [9, 10, 11, 12]. The analytical portion of this thesis is discussed in detail in Chapter III.

As stated in the objectives, experiments were conducted to measure the stress-strain response, ultimate failure load, and observe the failure mode of the composite specimens. Chapter IV discusses the experimental portion of this thesis.

Experimentation and analysis formed the bulk of the work undertaken in this research. The results of these experiments and analyses are presented in detail and compared in Chapter V.

Conclusions drawn from the results and comparison are presented in Chapter VI, along with some suggestions for future research in this area. Supplemental material of potential interest to future researchers is included in the Appendices.

II. Theory

Composite materials may be studied from various viewpoints including elasticity, fracture mechanics, and laminated plate theory [17]. This chapter covers the theories used in this study to describe stress, strain, and failure in laminated composites. These theories include mechanics of composite materials, linear finite element theory, nonlinear constitutive relationships, and the strain energy failure criterion for composite laminates.

Mechanics of composite materials includes both macromechanics and micromechanics, although greater attention is given here to macromechanics. Macromechanics treats composites as homogeneous materials having uniform properties [18]. It deals with the overall material response of a laminated composite. Micromechanics deals with the constituent elements of the composite and the individual behavior and properties of the fibers, matrix, and the interface between the two [19].

Since the mathematics used in the analysis program PLNRS is primarily based on linear finite element theory, this topic is covered for better understanding of the program. The method by which the program accounts for the nonlinear behavior of the composite is through nonlinear constitutive relationships, which is also covered. Finally, the failure criteria by which the program determines element failure is included.

A. Mechanics of Composite Materials

Composite materials are a heterogeneous combination of two or more materials. Fiber-reinforced composites are composed of a principal load carrying element, in this case continuous graphite fibers, and a matrix material which bonds the fibers together, transferring the load from one fiber to the surrounding fibers, protecting against the environment and ensuring that the proper fiber alignment is maintained [16]. The fibers tend to dominate the composite's strength, stiffness, and weight characteristics [2]. The matrix contributes primarily to temperature performance and environmental properties such as damage tolerance and moisture and solvent resistance [2]. These two materials exhibit a defined interface between each other, but both contribute to the composite's performance.

When a composite specimen is tested to failure, damage initiates and progresses at a micromechanical level. Failure can occur due to matrix cracking (micro-cracking), fiber failure, failure of the interface between laminas, failure of the interface between fibers and matrix, or a combination of these [20]. The overall response of a given composite can be characterized at a macromechanical level, and the strength and behavior of a specimen modelled and predicted using basic material properties. Thus, the progression of internal damage and mode of failure can be understood through micromechanics, while the material properties and response are explained through macromechanics.

1. Micromechanics. The Graphite/PEEK in this study consists of Hercules AS-4 high strength graphite fibers combined with the PEEK thermoplastic matrix, designated as an Aromatic Polymer Composite, APC-2. The fibers are of the continuous/oriented form. The matrix consists of closely interwoven long chained or linear molecules, or polymers. These chains are often referred to as crystalline, although theoretically they are semi-crystalline at the molecular level; the chains remain parallel throughout the curing and cooling process [2]. The PEEK material chemically bonds with the graphite fibers to accomplish this.

The fibers are parallel within a given lamina, with a number of laminae stacked together in a desired sequence. Each lamina or ply within the laminate can be aligned at a different orientation from the axis of the specimen. In actual design and production, the stacking sequence is chosen to optimize the material properties of the laminate for a given use and laoding condition. The laminates in this study include unidirectional, cross-ply, and multi-directional layups; all are symmetric about the mid-plane. The symmetry helps to ensure uniform response, and also minimize warpage and internal stresses.

2. Macromechanics. As already stated, macromechanics treats the composite as a homogeneous material, where the components act together as a single material having measureable material properties. Basic material properties tests provide the moduli used to characterize the composite in the macromechanical view.

As noted previously, Gr/PEEK exhibits nonlinearity in its material properties; i.e., the stress-strain response under tension, compression, and shear are not linear functions. The initial moduli are not the same as the moduli at some higher load or stress value. This is simply a characteristic of the material system. However, linear finite element theory can be applied to this problem, if one takes an incremental approach. Within a small increment, the material properties can be taken as linear. The properties are then iterated on between increments to account for the nonlinearities. Linear strain-

displacement relationships may thus be utilized in the analysis, with the resulting linear stress-strain equations given by:

$$d\sigma_i = C_{ij}(\varepsilon_j)d\varepsilon_j \qquad i, j = 1, 2, ..., 6 \qquad (1)$$

where C_{ij} is the 6x6 stiffness matrix, consisting of 36 terms [21]. Details of the ensuing assumptions and manipulations may be found in [12] and [21]. Due to matrix symmetry and an assumption of plane stress, the 6x6 matrix may be considerably simplified and reduced to a 3x3 matrix. Further, the constant terms can be expressed in terms of the engineering moduli of the material. A transformation is introduced to express the stresses or strains in the material axis system as stresses or strains in the global or coordinate axis system. The result is an equation which relates stress to strain in an arbitrary axis system. Applied to each individual lamina, this equation is:

$$\{d\sigma_i\}_k = \left[\overline{Q}_{ij}(\varepsilon_j)\right]_k \{d\varepsilon_j\}_k \qquad i, j = 1, 2, 6 \qquad (2)$$

where the subscript k ranges from 1 to the total number of plies in the laminate, and the $\overline{Q}_{ij}$'s form the transformed reduced stiffness matrix. The laminate behavior is then the sum of the individual lamina behaviors.

The assumption of plane stress ignores any interlaminar stresses. These stresses could result in delamination of a composite if present and of sufficient magnitude. Past testing has shown that the z-component of stress will generally be much less than the x and y-components, and so it is neglected [12].

B. Stress Concentration

The state of stress near a hole or other discontinuity will not be the same as that some distance away, in what is termed the farfield region. The farfield region is defined as the area greater than two hole diameters away from the hole. The stress field is assumed uniform in the farfield region. The discontinuity causes a stress concentration; the degree of concentration depends on the size and shape of the discontinuity [22].

Peterson [23] gives the stress concentration factors K_t for various hole shapes in isotropic material. A more composite-oriented approach is taken in [16], yielding the following equation for K_t:

$$K_{t\infty}=1+\left[\sqrt{2\left(\sqrt{\frac{E11}{E22}}-\nu 12\right)+\frac{E11}{G12}}\right]\left(\frac{a}{b}\right) \qquad (3)$$

where a and b are the semi-axes of the ellipse; for a circular hole a = b. This equation is valid for unidirectional laminates of infinite width. A correction may be applied to obtain the value for a finite-width laminate [17]. The stress concentration factor thus becomes:

$$K_t=\frac{K_{t\infty}\left[3\left(1-\frac{2R}{w}\right)\right]}{2+\left(1-\frac{2R}{w}\right)^3} \qquad (4)$$

where R is the hole radius for a circular hole and w is the laminate width. The semi-axis in the width direction was used for the elliptical holes in place of R; the validity of doing this is not entirely certain [17]. Figure 1 depicts the three hole geometries and the theoretical stress concentration factors from both isotropic and composite approaches.

C. Linear Finite Element Theory

The finite element method (FEM) is a numerical procedure used to analyze the response of a physical object or structure under some load condition [19, 24]. A closed analytical solution for the types of problems addressed using FEM usually does not exist. FEM relies on the use of computers to perform numerical calculations, and itself rarely produces an exact solution to the problem. The FEM approach is to discretize the object of interest into a finite number of interconnected nodal points, which form elements. Boundary conditions are set, and the appropriate stress-strain relationships are applied. A number of iterations are typically required to produce a result.

Dr. Sandhu's PLNRS program is used to analytically model the stress-strain response, initiation of failure, and failure progression of the specimens in this study. The details of the analysis program have been adequately covered in the literature, so this report will cover only the major aspects of how the program works [8, 25, 26, 27, 28]. The program uses piecewise cubic spline interpolation functions to represent the material properties, or stress-strain data, including uniaxial tension, compression, Poisson's ratios along and transverse to the fiber direction, and shear data. The functions maintain

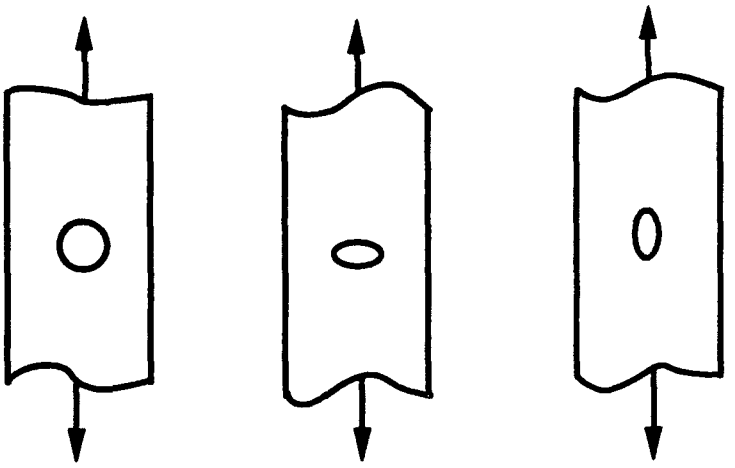

Isotropic:	**3.0**	**3.7**	**1.78**
Composite:	**5.85**	**10.83**	**3.74**

Figure 1. Stress Concentration Factors

continuity over the first derivative and provide smoothness to the stress-strain curves. Tangent moduli can easily be obtained by differentiating the cubic spline curves.

D. Nonlinear Constitutive Relationships

It is assumed that the strain increment is a function of the existing strain state and the stress increment, and that the strain increment is proportional to the stress increment. Under these assumptions, the incremental constitutive relations for a generalized state of plane stress can be written as [25]:

$$d\varepsilon_i = S_{ij} d\sigma_j \quad (i, j = 1, 2, 6) \qquad (5)$$

where $d\varepsilon_1$ = normal strain increment in the fiber direction
$d\varepsilon_2$ = normal strain increment in the transverse direction
$d\varepsilon_6$ = shear strain increment
$d\sigma_1$ = normal stress increment in the fiber direction
$d\sigma_2$ = normal strain increment in the transverse direction
$d\sigma_6$ = shear stress increment

The program uses the uniaxial stress state data to calculate the biaxial stress state. Incremental stresses are found from given incremental strains and a calculated stiffness matrix. These values are transformed from the material to the coordinate axes on a ply by ply basis.

The stresses are assumed to be uniform tl rough each ply. The strain is constant through the thickness; the plies deform in the same manner, without voids appearing or delamination occuring. Average compliance properties during the $n+1^{th}$ increment are used to solve for the strains. These values are not known when the $n+1^{th}$ increment is applied, so elastic properties at the end of the n^{th} increment are used to compute strain and stress increments in the plies. The stress and strain increments are summed, and the average elastic properties are then found. Each iteration must converge to a preset tolerance before the next increment is computed. Wham [12] presents a more thorough treatment of this with detailed mathemetical development.

The stress-strain data obtained from uniaxial tests are included in the input files in tabular form. The data includes the initial moduli. Appendix B contains the data input file format, and describes the various entries, including the material property data.

E. Strain Energy Failure Criterion

The program incrementally applies load or displacement, and computes the stresses and strains for each element in the mesh. A lamina subjected to continually increasing incremental tensile load will eventually reach a stress state where it can carry no additional load. The lamina reaches its ultimate strength at this point and fails. To determine that state, PLNRS uses a failure criterion which is a function of both stress and strain. It has been asserted that a strain-based approach yields more accurate results when analyzing the failure of a composite [29]. A detailed explanation of the strain-energy criterion used in this study and its development has been given by Sandhu in [25, 28]; the essentials follow.

This criterion is based upon energies under simple load conditions being independent parameters. For a generalized stress state, this criterion is given by:

$$\sum_{i=1}^{3}\sum_{j=1}^{3} K_{ij}\left[\int_{\hat{\varepsilon}_{ij}} \sigma_{ij} d\varepsilon_{ij}\right]^{m_{ij}} = 1 \qquad (6)$$

where ε_{ij} are the current strain components, and K_{ij} are the material characteristics [25]. The m_{ij} are parameters defining the shape of the failure surface in the strain energy space. They are adjustable to fit the experimental data, for biaxial tests. Since biaxial test data is unavailable for this study, they are taken to be equal and have values equal to unity. The criterion thus reduces to a linear relationship of strain energy ratios.

The program applies the failure criterion to each element after each increment of loading. When the equality in Equation (6) is met, the element has failed. The program distinguishes between longitudinal, transverse, and shear failures. These can occur alone or in combination. An element which has failed in the transverse direction may still carry load in the longitudinal direction.

When an element has failed, the loads it was carrying must be passed to the surrounding elements. This is referred to as unloading of the failed element. The surrounding elements will then experience an increased stress state. There are several ways in which a failed element can be unloaded [12, 28]. This study employed gradual unloading of the failed elements. This involved setting all the moduli of the affected element to their initial values but with minus signs, and continuing the loading. This

increased the loads on surrounding elements, and more elements would usually fail with successive load increments.

In the case of a uniform specimen having a central discontinuity, it is expected that the failure will initiate at or near this discontinuity, where the load-carrying area is the smallest, and the local stress the greatest [22]. Failure at any other location may point to a flaw in the model used in the analysis. (This was the case with an initial analysis run; the model initially failed at the tab, and was subsequently found to have erroneous boundary conditions applied to it.)

III Numerical Analysis

As previously mentioned, the Wright Lab finite element analysis program PLNRS was used in this study. A finite element model was thus required for use in the program. This model consisted of a mesh of interconnected nodal points, forming discrete elements. Appropriate boundary conditions had to be included, and the program run until adequate data was obtained.

A. Finite Element Models

A finite element model should capture the state of stress, boundary conditions, displacements, and strains present in a structure or specimen. It should also be sufficiently refined so as to provide adequate resolution in areas of interest. However, it needs to be less refined in other areas, to reduce model complexity and limit computer run times and memory requirements [30]. Due to the size and configuration of the specimens of this study, it was impractical to model the entire object. Fortunately, the symmetry of the specimen and load made it possible to model just one-quarter of the specimen. This resulted in a model with sufficient resolution in the region around the hole. Three basic models were developed; one for each hole geometry.

In all cases, the first step was to generate a mesh for a circular hole using the Wright Lab algorithm GENCIR, written by Dr. Sandhu. This program requires the width of the model, the number of divisions of the quarter circle, and the number of divisions between the hole and the edge of the specimen. It then generates the nodes and connections, forming quadrilateral elements. These elements are formed into concentric circles, leaving much larger elements in the final ring which connects the outer boundaries of the specimen. From this run, one can adjust the circular mesh lines and "grade" the mesh to more evenly fit the space. Once the region near the hole is completed, the program can be run again, and a second region added to cover the length of the specimen. This region was modelled with a much coarser mesh, as it was of less interest in this study. Figure 2 depicts the basic circular hole mesh, showing the detail of the region near the hole.

In the case of the ellipses, a separate algorithm was developed by the author, based on GENCIR, and called GENELP. The code for this routine is included in Appendix C. This routine read the data for a circular case, and then recomputed the nodal

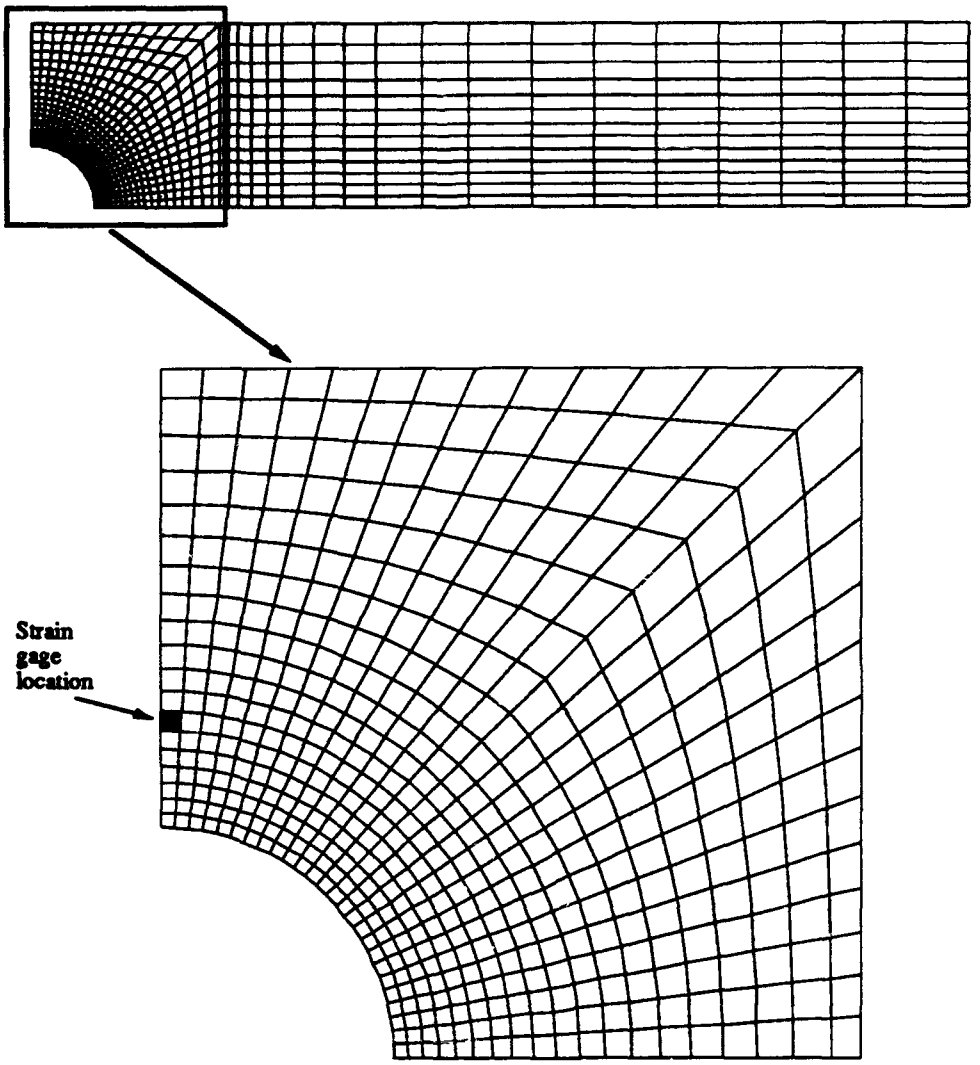

Figure 2. Finite Element Mesh, Circular Hole

coordinates based on the input ratio of the semi-major and semi-minor axes of the ellipse. The result was a mesh of concentric ellipses around the elliptical hole, but with a large gap between the outer elliptical ring and the specimen boundaries. Due to time constraints, this area was filled by selecting nodal points by hand. (Had enough time existed, the author had intended to incorporate a scheme to automatically grade the ellipses, as GENCIR does.) A few triangular elements had to be added using this approach, and the mesh near the boundaries of the specimen became much coarser than near the hole. As with the circular hole, the region in the farfield was modelled with rectangles of increasing size, in a coarse mesh. Figures 3 and 4 present the two elliptical hole meshes.

The three basic meshes were complete; at this point they only modelled a unidirectional layup. The basic mesh files were then used to create the individual models for each ply layup. The GENCIR program has an option allowing the user to specify the appropriate variables; the program generates the complete data for the mesh. For the ellipses, a second algorithm called STACK was written which took the existing file and added additional elements needed for the input number of ply orientations in the laminate. These elements were stacked on top of each other. The STACK code is listed in Appendix D.

Individual models were made by specifying element thickness and fiber direction, and adding stacked elements for the multi-directional layups. Appendix B explains the input file format and content in detail. Plies of the same orientation were modelled as one thickness. For unidirectional laminates, thickness was 0.21336 cm (0.084"), which corresponds to the thickness of 16 plies. For multidirectional laminates, each direction had its own thickness. The nodes were modelled as going through the entire thickness of the laminate. The element numbering of the stacked elements progressed through the different layers, so that more than one element could share the same nodal connections, but have a different thickness and orientation. Thus, in a quasi-isotropic laminate, each set of unidirectional plies was modelled as 0.05334 cm (0.021") thick . There were four such sets; each set modelled four plies at the same orientation, for a total of 16 plies. The number of elements thus increased with the number of directions in the layup. The number of elements in the various models are shown in Table 1.

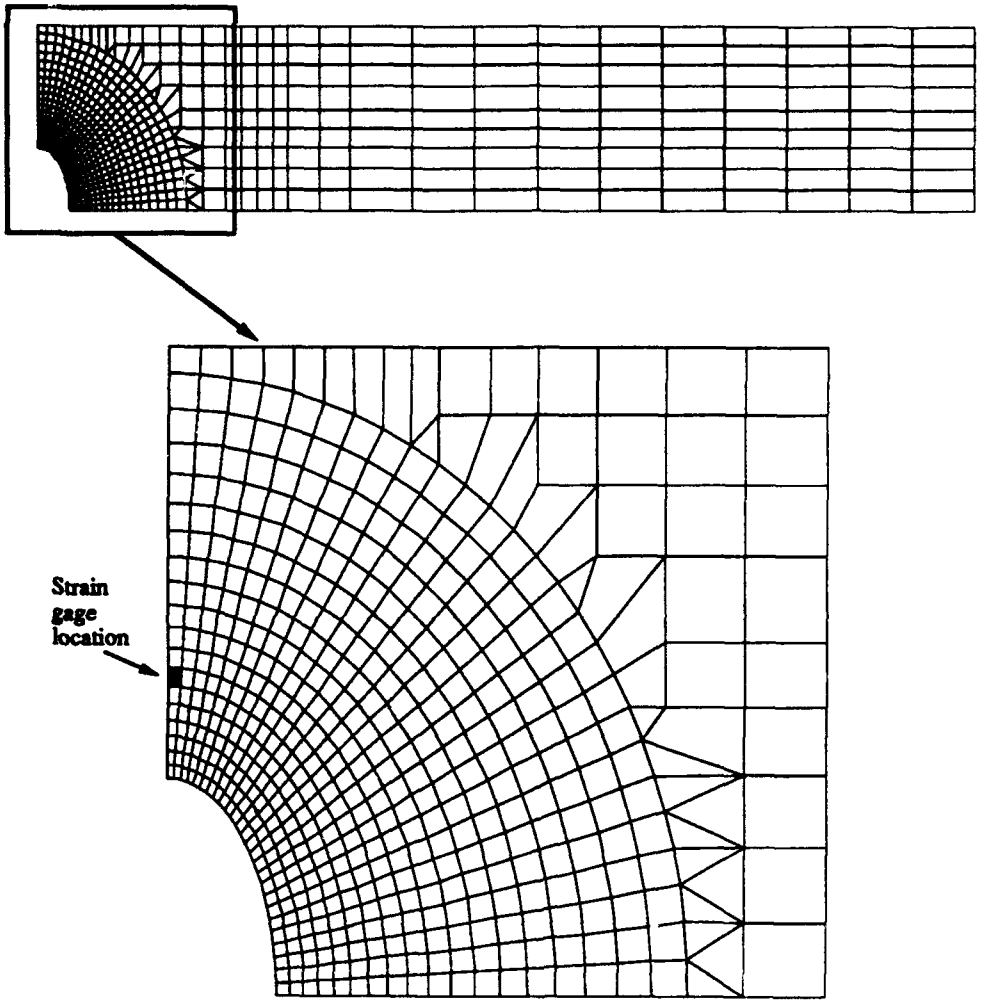

Figure 3. Finite Element Mesh, Transverse Ellipse

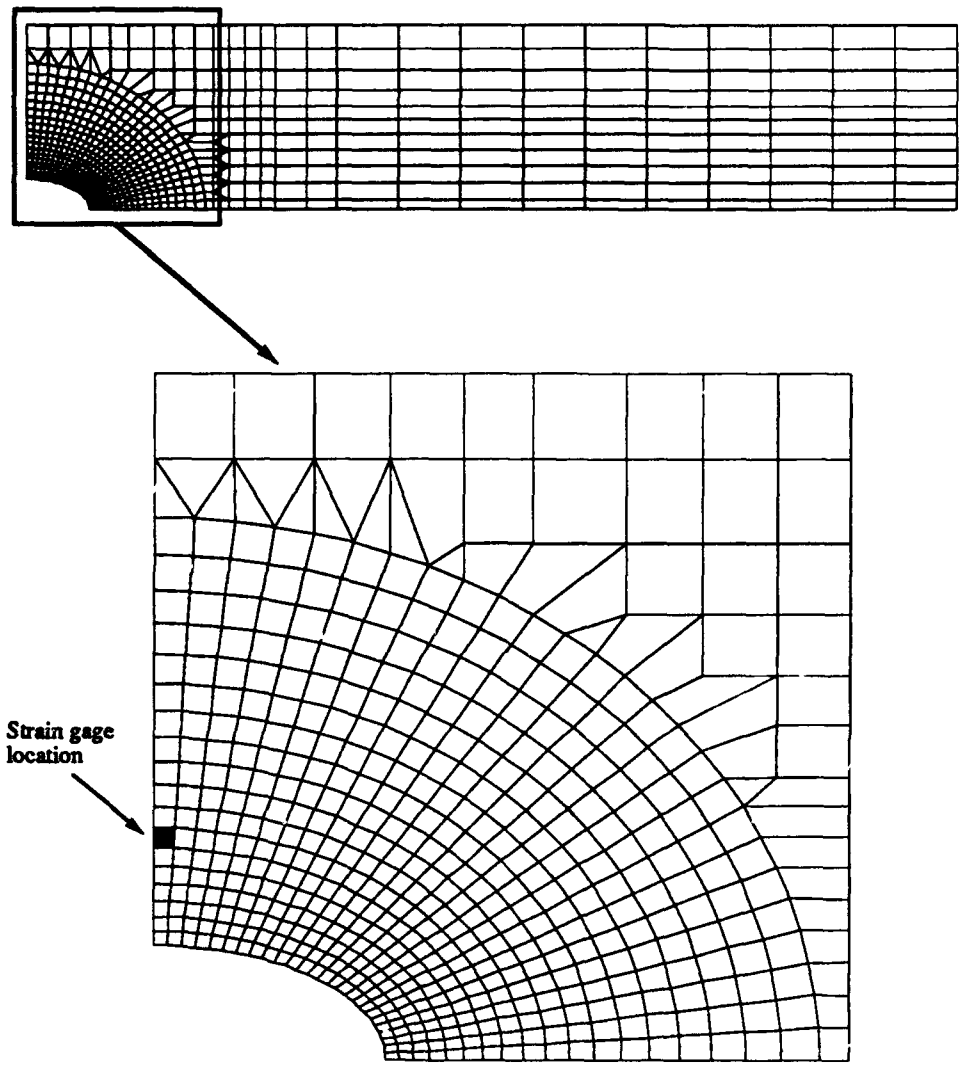

Figure 4. Finite Element Mesh, Longitudinal Ellipse

Table 1. Number of Elements in Finite Element Models

Hole Geometry	No. of Ply Directions	Number of Elements
circular	1	728
transverse ellipse	1	664
longitudinal ellipse	1	704
circular	2	1456
transverse ellipse	2	1328
longitudinal ellipse	2	1408
circular	3	2184
transverse ellipse	3	1992
longitudinal ellipse	3	2112
circular	4	2912
transverse ellipse	4	2656
longitudinal ellipse	4	2816

B. Boundary Conditions

The symmetry of the model dictated the type of boundary conditions to be applied. The nodes along the y-axis (normal to the load) were free to move in the y-direction, but constrained from motion in the x-direction. This maintained the continuity of the material. Likewise, nodes along the x-axis were free to move in the x-direction but constrained in the y-direction. Load was applied at the end nodes in the x-direction. The program was provided with an initial displacement of these nodes, and computed the corresponding load. Each increment increased the displacement and hence the load applied. Figure 5 shows the boundary conditions as applied to the model.

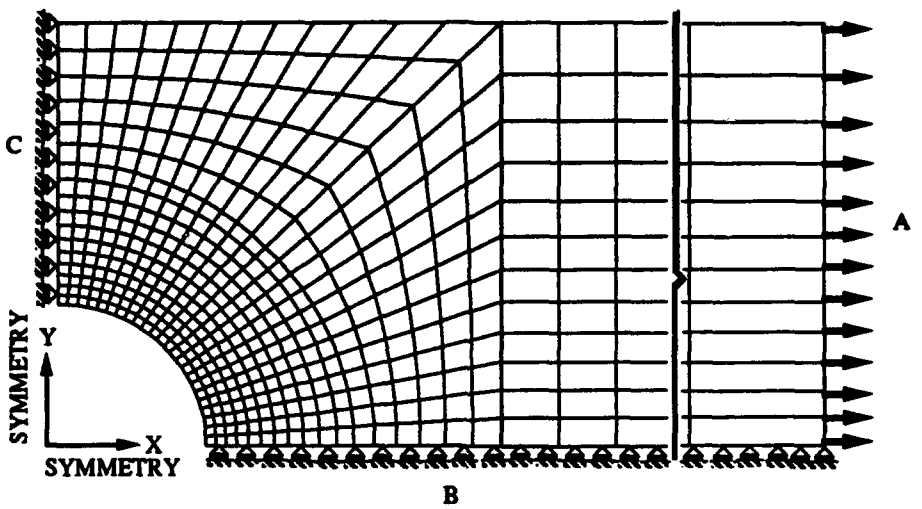

Figure 5. F.E. Mesh Boundary Conditions

C. Convergence Study

Wham [12] conducted a convergence study on the circular hole using a mesh very similar to that used in the present study. He ran a case using isotropic material data and obtained very good correlation with thepublished value in Peterson [23]. Due to time limitations this case was not considered, but the composite case was run instead.

An initial run was made on the 0-degree models to ensure that the meshes were adequately refined. The analytical stress concentrations were determined indirectly: since the element at the edge of the hole had constraints applied to one side, the stresses from nearby unconstrained elements were obtained. The distances from the edge of the hole to the element centroids was also obtained. The stresses were then plotted against the distances, and various curve fits tried until the best fit was found. In all cases an exponential fit worked best. From this curve fit the stress at the hole edge was extrapolated. Results are presented in Table 2.

Table 2. Stress Concentration Factor Comparison

	Stress Concentration Factor, K_t		
		Theoretical	
Hole Geometry	Isotropic	Composite	Analytical
Circle	3.0	5.85	5.54
Transverse Ellipse	3.7	10.83	8.05
Longitudinal Ellipse	1.78	3.74	3.28

The circular hole agrees within 5.3% of theory. The transverse and longitudinal ellipses agree within 25.7% and 12.3% of theory, respectively. The greater discrepancy in these cases may be due to the coarseness of portions of the elliptical hole meshes, as well as the approach taken in reducing the theoretical values to the finite-width case. Again, time became a factor, and the meshes were taken to be adequate for use.

D. Program Execution

The mesh files were created on an Apple Macintosh IIx computer linked to a Vax system. Once the mesh itself was complete, control cards and material data cards were added. A graphics program was used to view the mesh and double check for obvious errors, such as misconnected nodes. Wham's material property data was used in the analysis [12]. His study was the most recent conducted at AFIT involving Gr/PEEK. The author felt confident in using this data, as the same batch of material was used to make the specimens for this study, the same construction and curing procedure followed, and the same void content and fiber volume fraction specified.

The files were ready to run at this point, and were transferred to a Cray 2, where they were submitted as batch files. Preset values in the input file control cards limited the number of increments to compute and allowable run time. The program itself was modified so as to output data only for elements as they failed, as well the element corresponding to the location of the strain gage near the hole on the experimental specimens. The program generated a number of files as output: element stresses, strains, and energy levels, and applied loads, all in the basic output file; data for strain contours in a separate file; and a restart file, containing the data in the output file for the last increment, as well as the current moduli and iteration data. The latter permitted the user to continue a run from the point where it had terminated, in the event not enough data had been collected. The output files were then transferred back to the Vax system.

Due to the number of cases to run and the time limitations imposed, the author chose to limit the analysis runs. The experimental failure loads were used as reference values, and the analyses run to approximately 10% above these values. This choice meant that few analysis runs resulted in a prediction of laminate failure. The intent was then to look for the trends of laminate damage predicted analytically. Thus, analysis provided both some insight into predicted failure modes or damage zones , and stress-strain response of each layup/hole geometry combination.

IV. Experimentation

The discussion of experimentation begins with a description of the tensile specimens, strain gage locations, and test equipment used. The test procedures are covered, including data acquisition and processing. The actual testing results are given in Chapter V.

A. Test Specimens

Test specimens were all 25.4 cm (10.0 in) in length and 3.048 cm (1.2 in) in width. Figure 6 shows the test specimen geometry and dimensions. These specimens were cut from larger panels; Appendix A contains the Test Plan submitted to Wright Lab, which provides the specifications used to construct the panels. Each panel was sized so as to allow for saw cut widths and leave some trim area around the entire panel. The basic panels were layed up by hand from 30.48 cm (12 in) wide prepreg tape supplied by ICI. Since thermoplastic composites have no tack to the surface, each successive ply had to be spot soldered at the corners. The panels were then vacuum bagged and cured in an autoclave at aprroximately 400°C (750°F) and 1.4 MPa (200 psi). A thermocouple was attached to the panel to monitor the actual composite temperature; once the panel reached the cure temperature, the cure cycle was initiated.

Following curing, an edge on each panel was bevelled slightly, to visually verify the proper ply layup. The panels were then subjected to C-scan to check for voids or other flaws. Void content was less than 1% for all panels, as specified in the Test Plan. No significant flaws were discovered. Resin content analyses were also conducted. Resin content varied from 28-33.4% by weight. The fiber volume fraction V_f was determined from the resin content w_r and the fiber and resin densities, ρ_f and ρ_r, using the following relationship:

$$V_f = \frac{\rho_r(100 - w_r)}{\rho_r w_r + \rho_r(100 - w_r)} \qquad (7)$$

with w_r in percent weight and ρ_f and ρ_r in g/cm^3 [2]. For this study, $\rho_f = 1.76$ and $\rho_r = 1.32$, yielding fiber volume fractions from 59.9 to 65.9%.

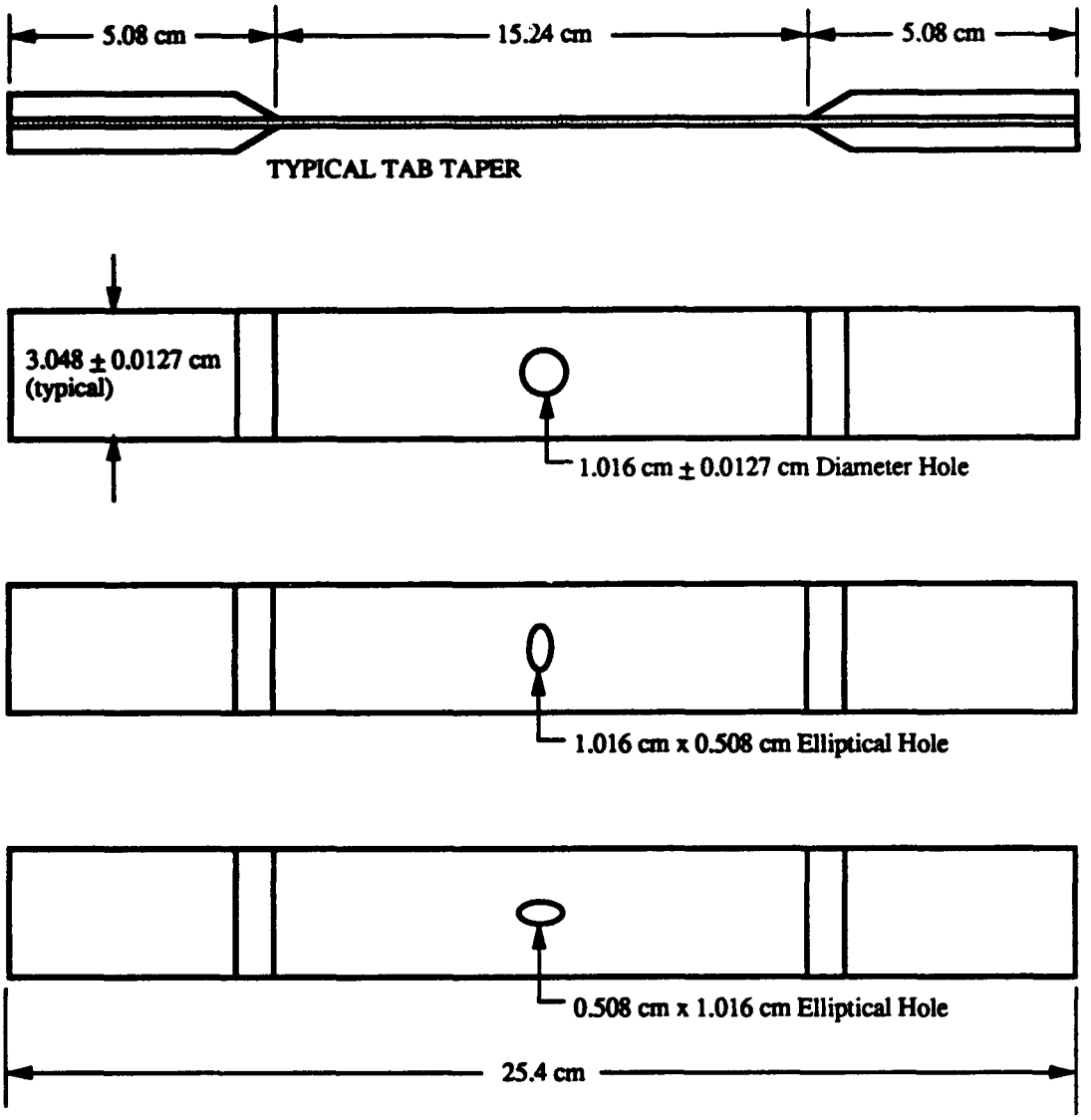

Figure 6. Specimen Geometry

A border strip of material around the entire panel was removed, to eliminate this possibly resin-rich area. The holes were then cut using a water jet cutter, following drilling of a pilot hole. One panel had to be replaced when the water jet reflected off the underlying metal grid and damaged the underside of the specimens. With the holes cut, the specimens could be cut from the panel using a diamond blade saw. This order was followed to ensure that the holes were in the center of each specimen.

It should be noted that due to an error in the Test Plan, the circular holes were initially cut to one-half the desired diameter. This was not discovered until the specimens had been cut from the panels. Once cut out, there was no way to ensure that the waterjet would be perfectly centered, so test holes were drilled out on several of the unusable setup specimens using carbide reamers. There appeared to be only slight damage to the outermost ply, on the underside. It was decided that the possibility of minor damage to some specimens was preferable to the possibility of eccentricity of the hole. Therefore, the reamers were used to expand the holes to the desired size. These specimens were carefully inspected for visible damage to the hole area following reaming. No delamination was evident, and only very minor surface damage was observed on a few specimens, confined to the outermost ply.

The thickness and width of each specimen was carefully measured in several locations and recorded. Glass/Epoxy tabs were applied at both ends. Specimens were then ready for the application of strain gages. Figure 7 is a photo of a set of "set-up" specimens, made from the damaged panel, but not used in testing. This photo shows what the specimens looked like prior to attachment of strain gages.

B. Strain Gages

Two types of strain gages were applied to the specimens; two CEA-03-125UR-350 gages were applied at a farfield location, approximately four hole diameters away from the hole along the axis of the specimen. (A minimum distance of two hole diameters away would have been adequate to be considered farfield in this study. The additional distance merely helped to ensure a uniform stress field in the region of these gages.) These are three-element rosettes arranged at 0, 90, and 45 degrees. They were placed on the top and bottom on the same end of the specimen. These gages measured the overall state of strain of the specimen. One WA-03-030-WR-120 gage was placed near the hole edge, between the hole and side of the specimen. This is a very small stacked three-element rosette, arranged at 0, 90, and 45 degrees. The stacked gage

Figure 7. Testing Specimens

measured the local strain near the hole, expected to be greater than the overall strain on the specimen. Figure 8 graphically presents the gage placement information with exact dimensions.

Due to the layout of the stacked rosette and the desire to place the gage as close to the hole as possible, it was not possible to align the gage elements as desired. Figure 9 depicts the orientation of this gage with respect to the specimen axes. The element which would normally be at the 45 degree position, leg A, was actually aligned transversely, or at 90 degrees. Leg C would ideally have aligned with the y-axis instead, and leg B with the x-axis. This resulted in a transformation being required to extract the strains in the desired directions (the x- and y-directions, specifically). Note that this equation utilizes the engineering shear strains, not the tensorial shear strains. The transformation equation is:

$$\begin{Bmatrix} \varepsilon_x \\ \varepsilon_y \\ \gamma_{xy} \end{Bmatrix} = \begin{bmatrix} m^2 & n^2 & mn \\ n^2 & m^2 & -mn \\ -2mn & 2mn & m-n \end{bmatrix} \begin{Bmatrix} \varepsilon_B \\ \varepsilon_C \\ \gamma_{BC} \end{Bmatrix} \qquad (8)$$

where $m = \cos\theta$ and $n = \sin\theta$ [31]. Since $\theta = 45°$, $m^2 = n^2 = mn = 0.5$; $(m-n) = 0$. Further, since $\varepsilon_y = \varepsilon_A$, and ε_A, ε_B, and ε_C were known, it was possible to solve for γ_{xy}:

$$\gamma_{xy} = -\varepsilon_B + \varepsilon_C \qquad (9)$$

Also, γ_{BC} could be found directly from:

$$\gamma_{BC} = \varepsilon_B + \varepsilon_C - 2\varepsilon_y \qquad (10)$$

From this, ε_x could be determined as follows:

$$\varepsilon_x = 0.5(\varepsilon_B + \varepsilon_C + \gamma_{BC}) \qquad (11)$$

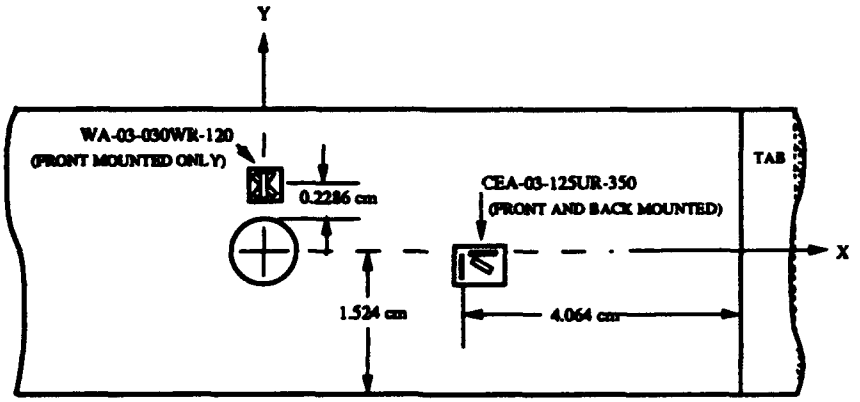

Figure 8. Strain Gage Placement

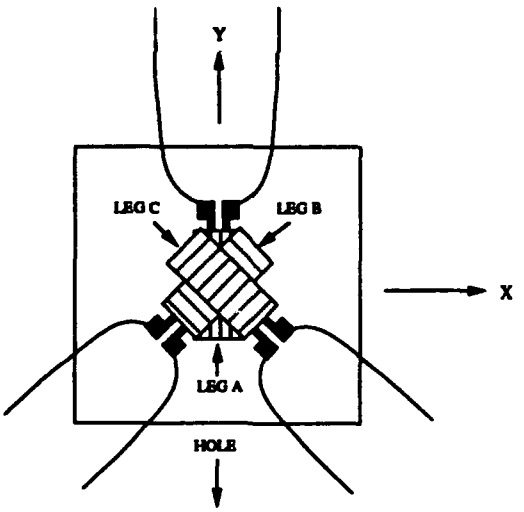

Figure 9. Stacked Strain Rosette Geometry

C. Test Procedure

All testing was conducted at ambient room temperature conditions, which ranged between approximately 21°C and 27°C (70-80°F). Test coupons were visually inspected prior to testing, and strain gage leads carefully identified.

The coupons were loaded into the grips of a Sintech Model 20/D test apparatus, as shown in Figure 10. The specimen was visually aligned using a guide armature on the upper grip fixture, and the grip was closed onto the tab with a pressure of 6.895 MPa (1000 psi). The strain gage leads were then attached to a terminal strip in a specific order. A current was applied to the gages; as load was applied, the resistance of the gages changed. The load cell and strain gage data went into a signal conditioner and was passed through an amplifier to a computer, where the resistance changes were converted into strains, using the equation:

$$\varepsilon = \frac{1}{GF}\left(\frac{\Delta R}{R}\right) \tag{12}$$

where GF = gage factor

R = resistance of gage.

The inputs and data acquisition program were all zeroed prior to gripping with the lower grip. Testing was conducted at a constant cross-head speed of 0.127 cm/min (0.05 in/min). A display of load vs displacement was monitored during testing. Sample rate was selected by the acquisition program operator for each run. Sample rates resulting in approximately 60-90 data points were preferred. A process of trial and error was used to select the optimum sample rate; previous studies [10, 12] were used as a guideline, but in some cases the sample rates chosen were found to result in too much data. Most tests were sampled at 1 or 2 samples per second; values of 1 sample per two seconds and even 1 sample every ten seconds were used in specific cases. Observations were recorded to aid in post-test analysis.

Failure was determined by the combination of a sudden, characteristic bang and a sudden, dramatic drop in applied load. The test conductor terminated the test run at that instant, and the grips were immediately stopped in place. The rapid termination of the tests left many specimens still in one piece, although they were failed. Detailed descriptions of the failure characteristics of each layup follow in the next chapter.

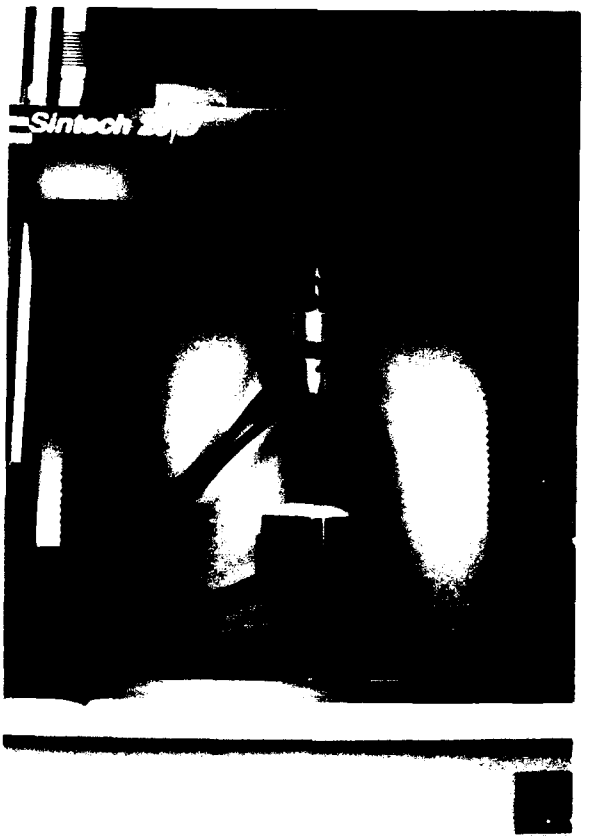

Figure 10. Test Equipment with Specimen

The recorded data were processed and printed, and the data files were then put on floppy disk in ASCII format. The printouts were used for initial review of the tests. The files on disk were later reduced and used to present test data graphically.

A major concern of the author was to verify that the load applied was concentric, so that the stress state of the specimen matched that modelled analytically, and to reduce three-dimensional effects. The first group of tests showed a trend toward higher strain on the front side of the specimens, suggesting eccentric loading. The gages on the next specimens were connected in reversed order to check this. (That is, the gage on front was connected as the gage on the rear.) If load was truly eccentric, these test runs should have recorded the rear strains being higher. They did not, and so it was determined that specimen imperfections must be responsible for the difference. In fact, later tests did have a mismatch in the other order. Visual inspections of untested specimens did reveal some visible warping from end to end, and even some slight twist longitudinally in some specimens, reinforcing this conclusion.

D. Post-Failure Analysis

Post-failure analysis of the specimens has been limited to visual and optical microscope inspection of areas of interest. This inspection has been focused primarily on the failure surfaces, where the most information is available. Time limitations prevented the author from conducting further inspections using a scanning electron microscope (SEM). This method may have provided additional insight into the micromechanics of the failures.

An entire set of ±45 degree specimens had been prepared and tested to 90 and 95% of the failure loads of the respective cases, for damage progression studies. It had been thought that these could be studied using the SEM. The sectioning method of cutting a small portion of the specimen using a diamond coated wafering blade obscured the fibers on the cut surfaces, with the result that only a surface inspection using the optical microscope was possible. This essentially restricted the progression of failure study to exterior visible damage, such as edge delamination and outer lamina or surface cracking. Little information is thus provided regarding experimental damage progression.

V. Results

This section presents the results of the experiments, providing stress-strain plots, observations made during testing, and descriptions of the failure surfaces. The results of the numerical analyses are also presented, and compared with the experiments both in terms of stress-strain response, and prediction of the failure modes. It will be seen that the analytical solutions model the material response very well, but can predict the failure mode only in certain cases. In other cases, they predict a damage zone which may correlate with experimental failures.

A. Stress Calculations

Experimental nominal stress values were obtained from the applied load data, and converted to stresses using the nominal pre-test cross-sectional area of the individual specimen. The farfield strains were measured directly on the top and bottom surface, at the same location. The data from the two gages were averaged. The near-hole strains were obtained by the transformation equations presented in the preceding chapter (Eqs. 9-11). Analytical stresses were obtained from the applied load, presented in the computer program output file, and the theoretical cross-sectional area. The program output included the strains at the element corresponding to the gage location. There is a minor difference between the actual gage location and the centroid of the element, where the strains are actually computed, but this should be negligible given the fineness of the mesh in this vicinity.

B. Experimental and Analytical Results

Table 3 presents the average experimental failure loads for the various layup and hole geometry combinations. Three specimens were tested for each combination of layup and hole geometry. Following the table, details of the results are presented by layup, with all three hole geometries included for each. Photos of failed specimens are included in each section. Damage predicted by the finite element models at various load levels is presented. Stress-strain data is presented in plots containing both experimental and analytical results. Plots include the response in the load direction (ε_x) and normal or

transverse to it (ε_y). Figure 11 presents the strain designations related to the specimen geometry. Positive strains denote elongation while negative values apply to contraction.

Table 3. Experimental Failure Loads

Layup	Hole Geometry	Average Failure Load, N (lb)
$[0_{16}]$	Circle	24021 (5398)
	Transverse Ellipse	23959 (5384)
	Longitudinal Ellipse	39997 (8988)
$[90_{16}]$	Circle	2982 (670)
	Transverse Ellipse	2715 (610)
	Longitudinal Ellipse	4481 (1007)
$[0/90]_{4s}$	Circle	19647 (4415)
	Transverse Ellipse	19282 (4333)
	Longitudinal Ellipse	29437 (6615)
$[\pm 45]_{4s}$	Circle	10698 (2404)
	Transverse Ellipse	9154 (2057)
	Longitudinal Ellipse	17738 (3986)
$[\pm 45_2/0/\pm 45]_s$	Circle	13034 (2929)
	Transverse Ellipse	12656 (2844)
	Longitudinal Ellipse	16643 (3740)
$[\pm 45/0/\pm 45/0/\pm 45]_s$	Circle	18294 (4111)
	Transverse Ellipse	17960 (4036)
	Longitudinal Ellipse	24902 (5596)
$[0/\pm 45/90]_{2s}$	Circle	18610 (4182)
	Transverse Ellipse	17017 (3824)
	Longitudinal Ellipse	26589 (5975)

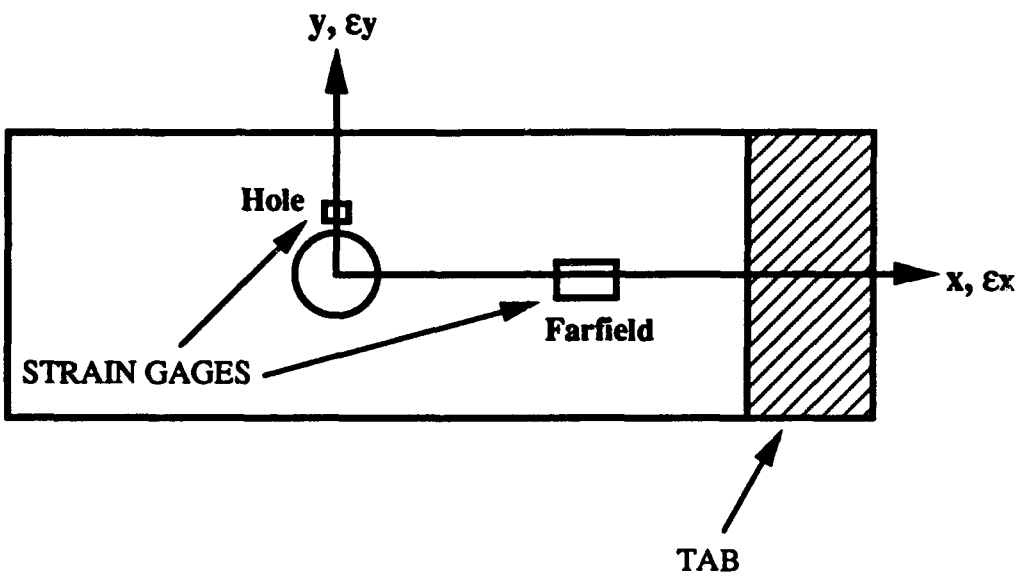

Figure 11. Strain Designation Related to Specimen Geometry

In all stress-strain plots presented, the experimental farfield strains have been averaged from the two gages. The strains recorded by the two farfield gages differed by fairly small amounts in all cases. These differences were not large enough to cause concern or to imply eccentric loading. They may be due to minor warpage of specimens during curing or other minor specimen imperfections.

All stresses are normal stresses, i.e., stresses in the load direction. Experimental stresses were not measured directly, but derived from the recorded load and measured pre-test cross-sectional area of each specimen. Analytical stresses were likewise obtained from load and cross-sectional area.

1. $[0^{\circ}_{16}]$ Layup. Failure of these specimens was characterized by longitudinal splitting, originating at the hole edge on either side of the hole, and extending into the tab areas. The splits occur both in complete pairs running the full length of the specimen on both sides of the hole and in single pairs running only half of the specimen length, in opposite directions . These splits are difficult to see without bending the specimen laterally or looking with an optical microscope.

The failures were very sudden with no forewarning, and were accompanied by a sudden and large drop in applied load. This load drop point corresponded to the formation of the splits. Once the splits formed, there was no longer a specimen containing a hole, but rather two small strips under tension. Thus, the load at which splits formed is considered the failure load. Figure 12 depicts typical failed samples. The splits have been highlighted with a silver pen. Figure 13 is an optical microscope photograph showing a close-up view of a typical split where it emanates from the hole edge. There was no visible delamination, and minimal necking was observed only in the case of the longitudinal ellipse.

The analytical solution is unable to model failures of an abrupt nature, and so failed to accurately predict the failure load or mode. The first element always failed below the experimental specimen failure load; 8% low for the circle, 27% low for the transverse ellipse, and 14% low for the longitudinal ellipse. The amount of damage predicted at the experimental failure loads varies somewhat, from a few failed elements to ten or fifteen. Figure 14 depicts the failed elements corresponding to experimental failure loads.

As seen in Figure 15, the circular hole stress-strain data is in good agreement with analysis for ε_x. ε_y data agrees well initially, but experimental strains follow a different, very nonlinear path which diverges dramatically from the analytical curve. This may be due to interlaminar stresses and/or free edge effects, which the program does

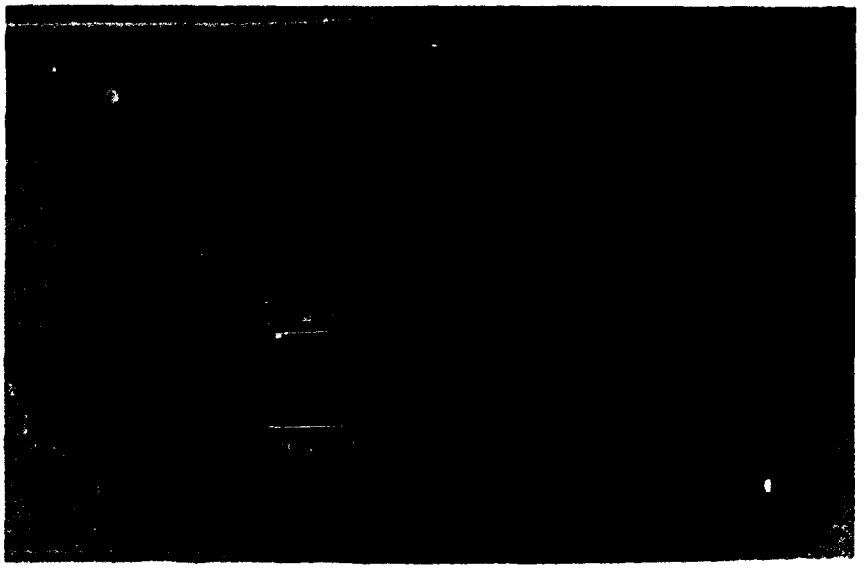

Figure 12. Failed 0-degree Specimens

Figure 13. Split in 0-degree Specimen, 50x Magnification

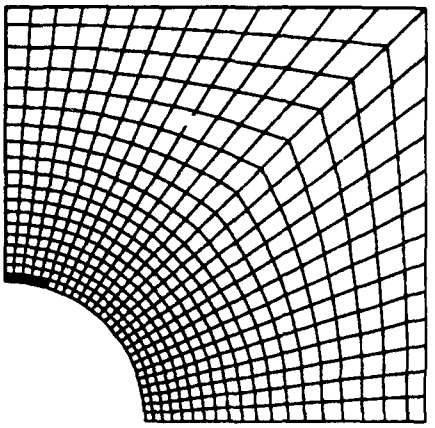

Circular Hole

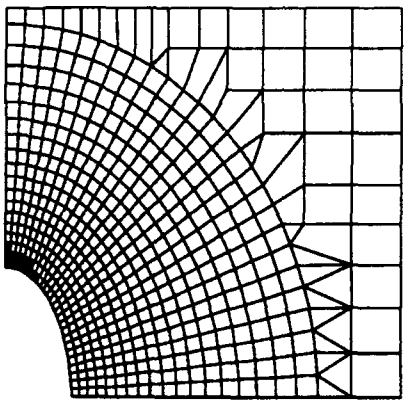

Transverse Ellipse

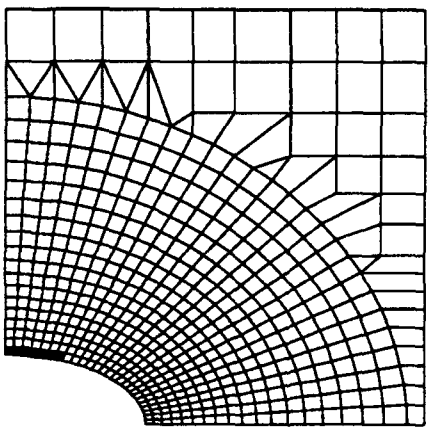

Longitudinal Ellipse

Key

- 10% below exp. failure
- Exp. failure load
- 10% above exp. failure

Figure 14. 0-Degree Analytical Damage Zones

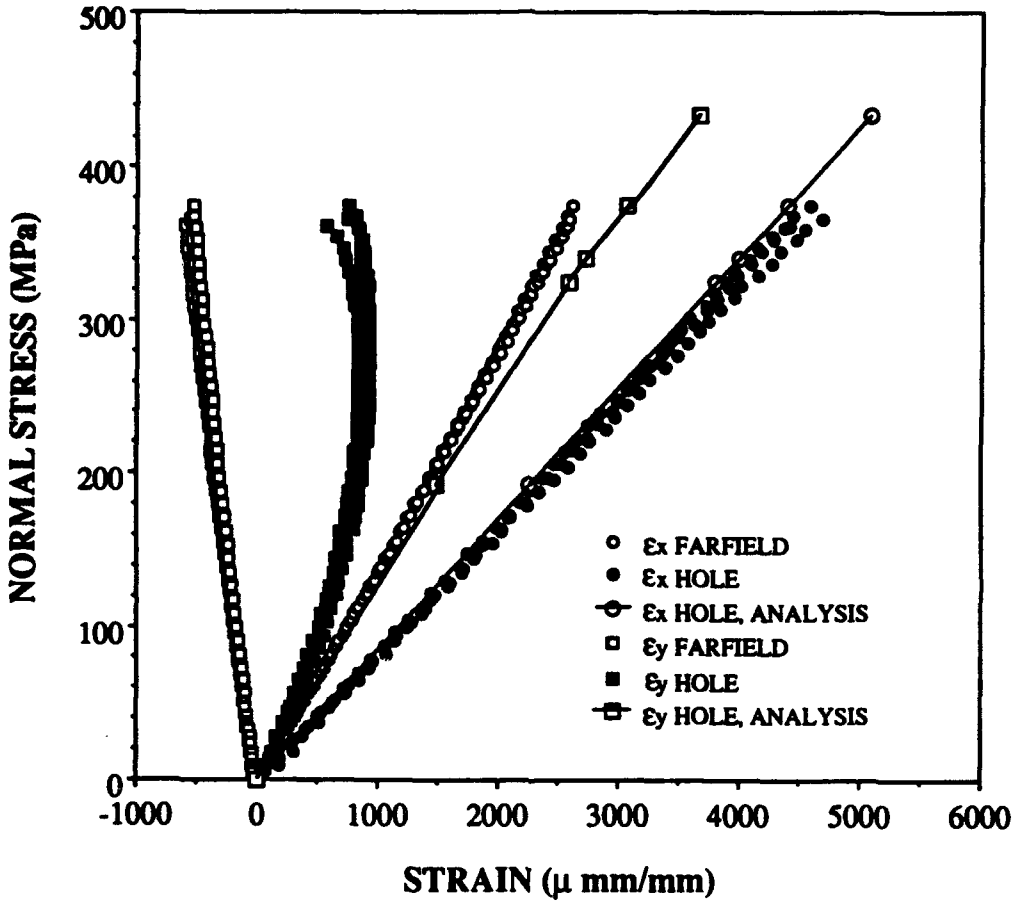

Figure 15. 0-Degree, Circular Hole

not account for. Certainly some phenomenon is not being captured by the analysis.

Figure 16 presents the results for the transversely oriented ellipse. There is wider scatter to the experimental data, but still good agreement with analysis in ε_x. The ε_y data diverge from analysis as in the first case. Note that the experimental curve breaks sharply in the negative direction, implying some sudden effect.

Figure 17 applies to the longitudinal ellipse. Again, strains in the x-direction agree closely , while strains in the y-direction diverge; however, the analytical and experimental curves are closer than for the other two hole geometries. This suggests that whatever is responsible for the difference is magnified with the higher stress concentration.

2. [90°$_{16}$] Layup. These specimens failed at the hole parallel to the fiber direction, that is, across the width of the specimen. This was another case of a sudden failure with little or no forewarning. Light cracks were heard just prior to failure for some specimens, but not all. The transverse ellipse failed directly across the hole. The circular holes failed directly across or slightly offset from one side of the hole to the other. The longitudinal ellipse did not break evenly, but failed from different locations on either side of the hole. Figure 18 is a photo of typical failed specimens. The failure surface was not along a plane in the z-direction when viewed from the side, but involved some variation in the x-direction. There was no visible delamination or necking of any of the test specimens.

It is the author's opinion that imperfections in the specimens have a greater influence on the material behavior in the case of the longitudinal ellipse, where the stress concentration is much lower. The other two hole geometries involve stress concentrations nearly twice as high, and so the effects of imperfections are less noticeable. Figure 19 is an optical microscope close-up view of an untested hole edge. While the holes appear very smooth and continuous to the unaided eye, this photo clearly shows the rough, uneven nature of the hole at the microscopic level, at least on the outer ply. The longitudinal ellipses may thus have failed at a locally narrowed section of the hole.

The analytical solution was again unable to predict the true failure mode. The first element failures occured 33% low for the circle, 43% low for the transverse ellipse, and 26% low for the longitudianl ellipse. The damage zone predicted at the actual failure loads originated at the top edge of the hole, and extended up a number of rows into the mesh. Figure 20 depicts these damage zones for the three cases.

Figure 21 presents the stress-strain results for the circular hole. This time there is a notable difference between experiment and analysis for the ε_x data. Analysis predicts a

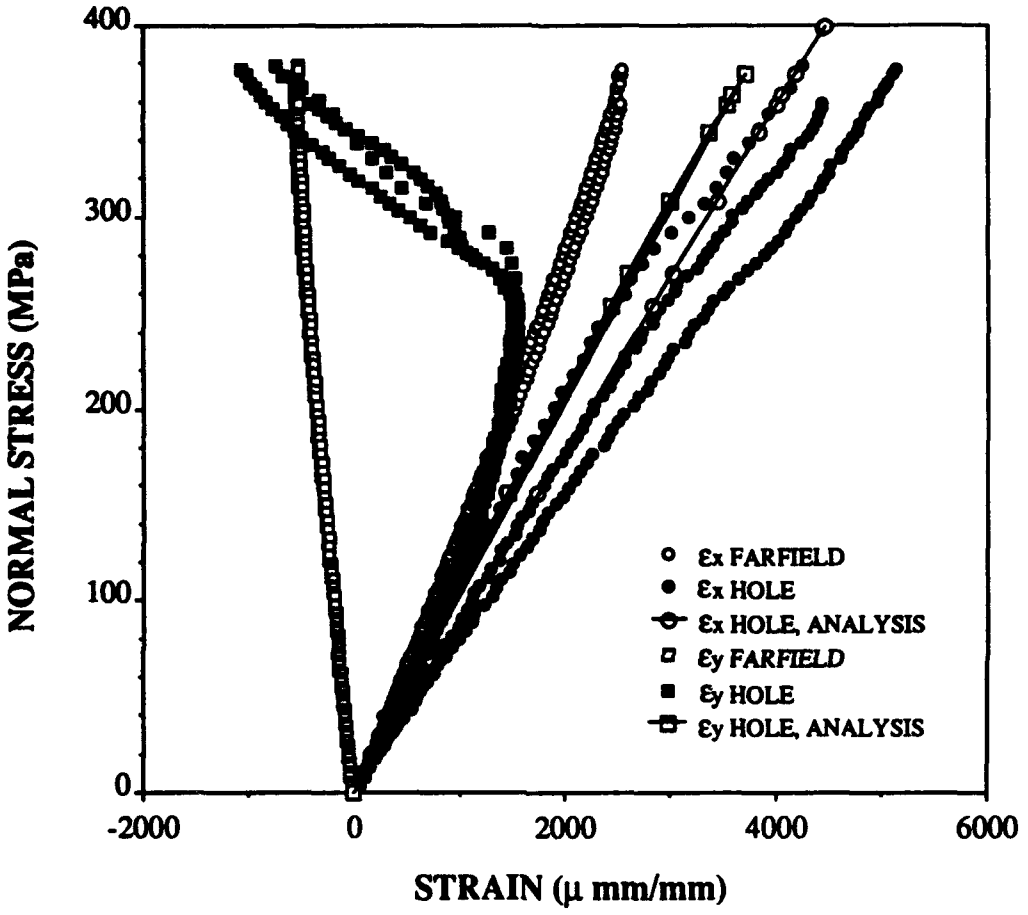

Figure 16. 0-Degree, Transverse Ellipse

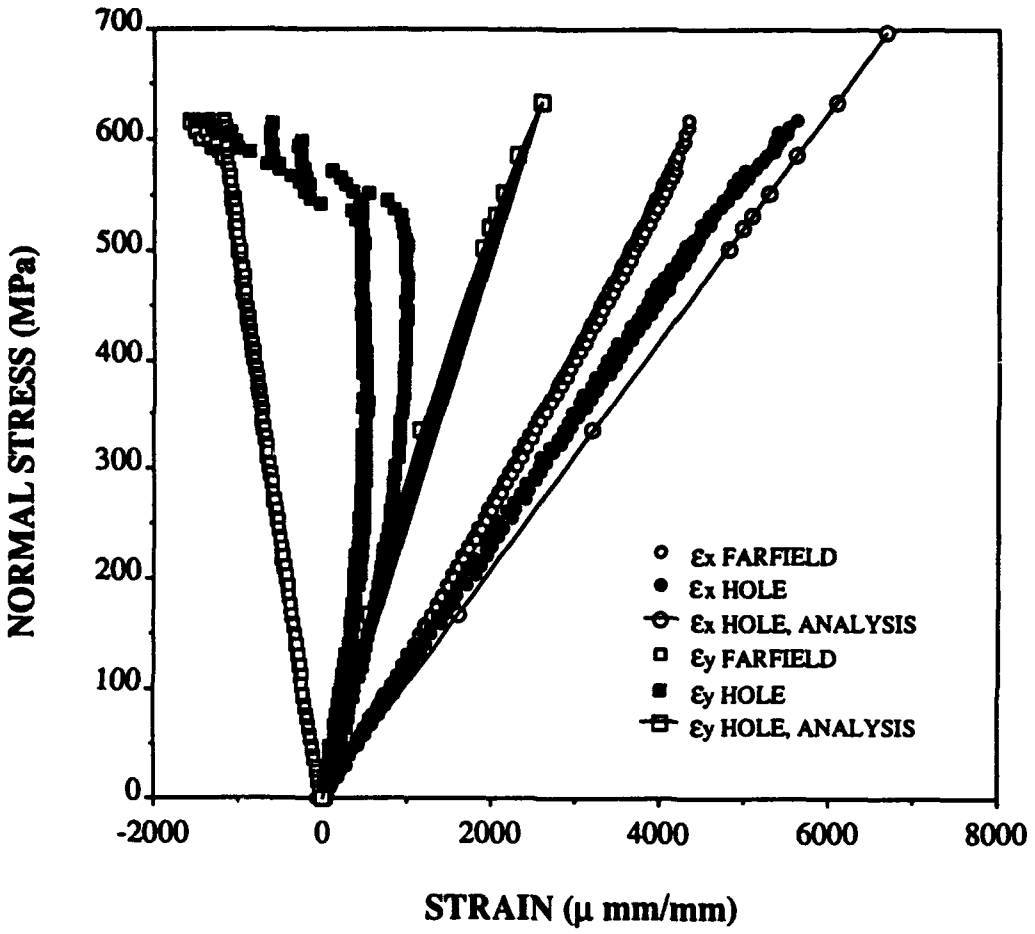

Figure 17. 0-Degree, Longitudinal Ellipse

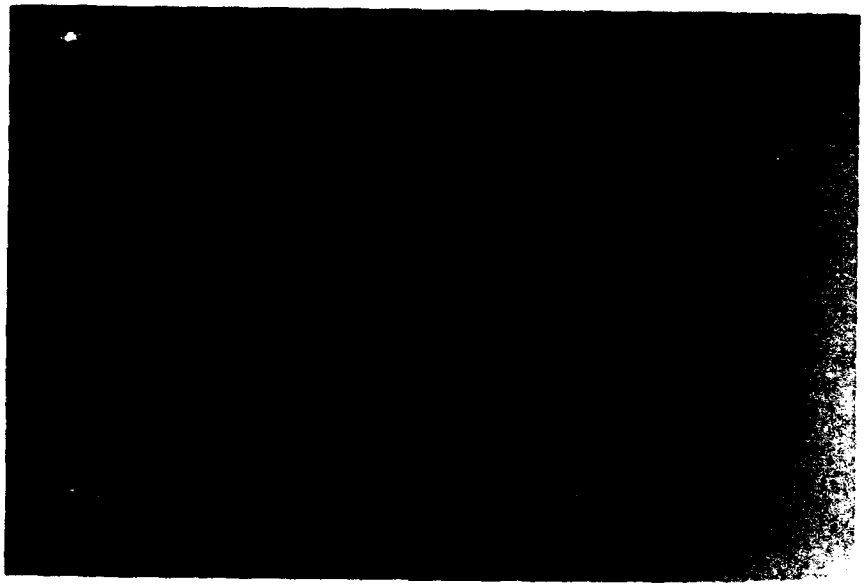

Figure 18. Failed 90-degree Specimens

Figure 19. Hole Edge, 50x Magnification

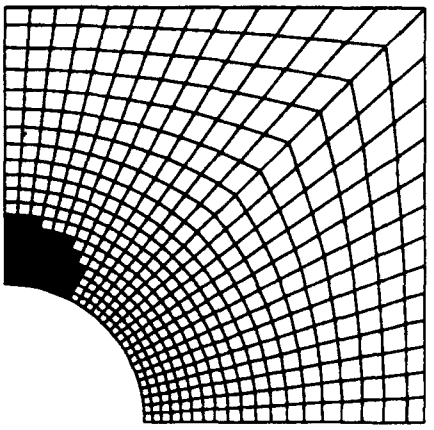

Circular Hole

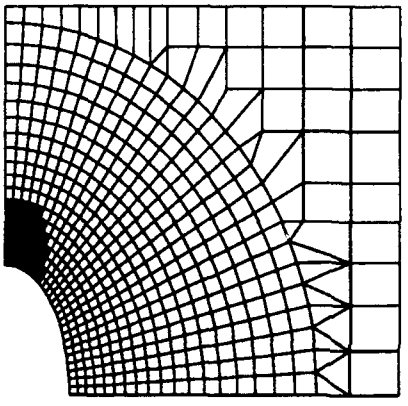

Transverse Ellipse

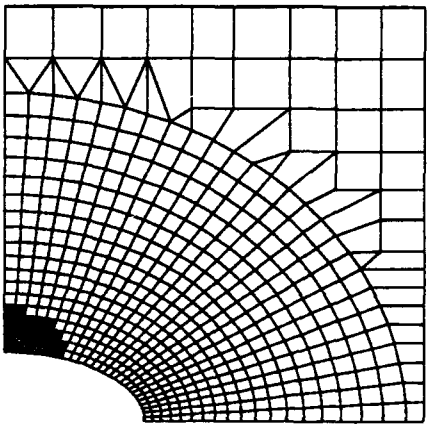

Longitudinal Ellipse

Key

- 10% below exp. failure
- Exp. failure load
- 10% above exp. failure

Figure 20. 90-Degree Analytical Damage Zones

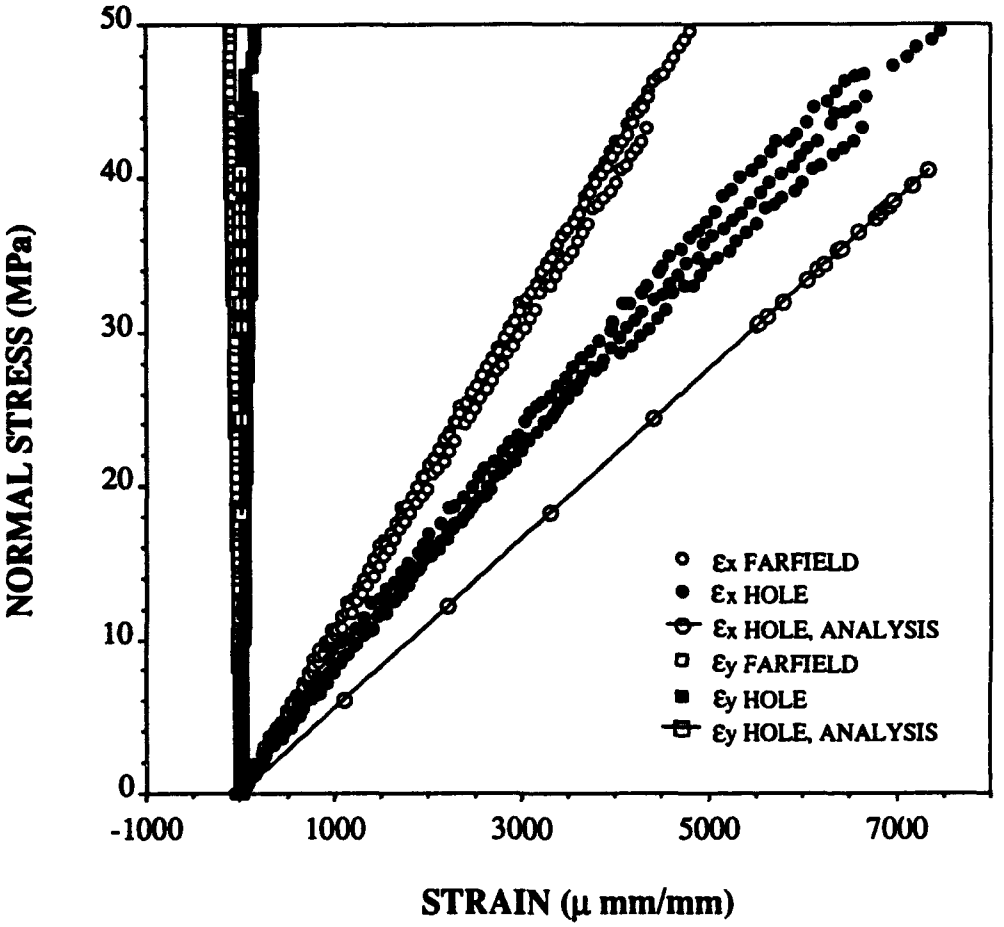

Figure 21. 90-Degree, Circular Hole

more flexible response, as seen from the greater strains at given stress levels. Strains in the y-direction are much smaller than in the x-direction, both analytically and experimentally, which makes sense, since this layup's greatest strength is in the y-direction.

Figure 22 depicts the transverse ellipse data. The results are very similar to the circular case, with actual specimen response again stiffer than predicted. The longitudinal ellipse results are shown in Figure 23, and agree quite well. As a note, one of the longitudinal ellipses failed at both tabs. It was observed to have a slight twist along the loading axis, probably from the curing cycle of the original panel. This may have caused an eccentric load condition resulting in higher stresses at the tabs.

3. $[0/90]_{4s}$ Layup. The cross-ply specimens failed across the width of the specimen at the hole, just as the 90-degree specimens did. They had a rough or jagged failure surface, unlike the clean break on the 90's. The ends of many zero degree fibers could be seen with the unaided eye. Some narrow strips of zero degree fibers remained intact on the outer surfaces of some specimens, even though the specimens had failed. Cracking was heard in some cases, around half to three-quarters of the failure load for the longitudinal ellipses, or just prior to failure for the transverse ellipse and circle. Figure 24 depicts a typical failed specimen for each hole configuration. There was slight delamination on some specimens, *in the immediate vicinity of the failure; no necking* was observed.

The analytical damage prediction corresponding to actual failure loads varies with hole geometry, but in all cases damage is predicted in both the zero and ninety degree plies. A greater amount of damage is predicted for the ninety-degree plies. For the circular hole, damage is confined to the region at the top of the hole, extending only two or three rows into the mesh. For both ellipse cases, damage extends further into the mesh, particularly in the 90-degree plies, but also deviates from the observed failure pattern. As can be seen in Figure 25, the damage zone has begun to follow a 45-degree or sharper angle into the 90-degree plies, whereas the actual failures were in the 90-degree direction. There is no information available as to the internal damage of the test specimens.

Figure 26 presents the stress-strain response for the circular hole. There is very good correlation between analysis and experiment for both ε_x and ε_y at the hole.

Figure 27 shows the transverse ellipse results, while Figure 28 gives the longitudinal ellipse results. Both are very similar to the circular case. All three geometries demonstrate low experimental data scatter.

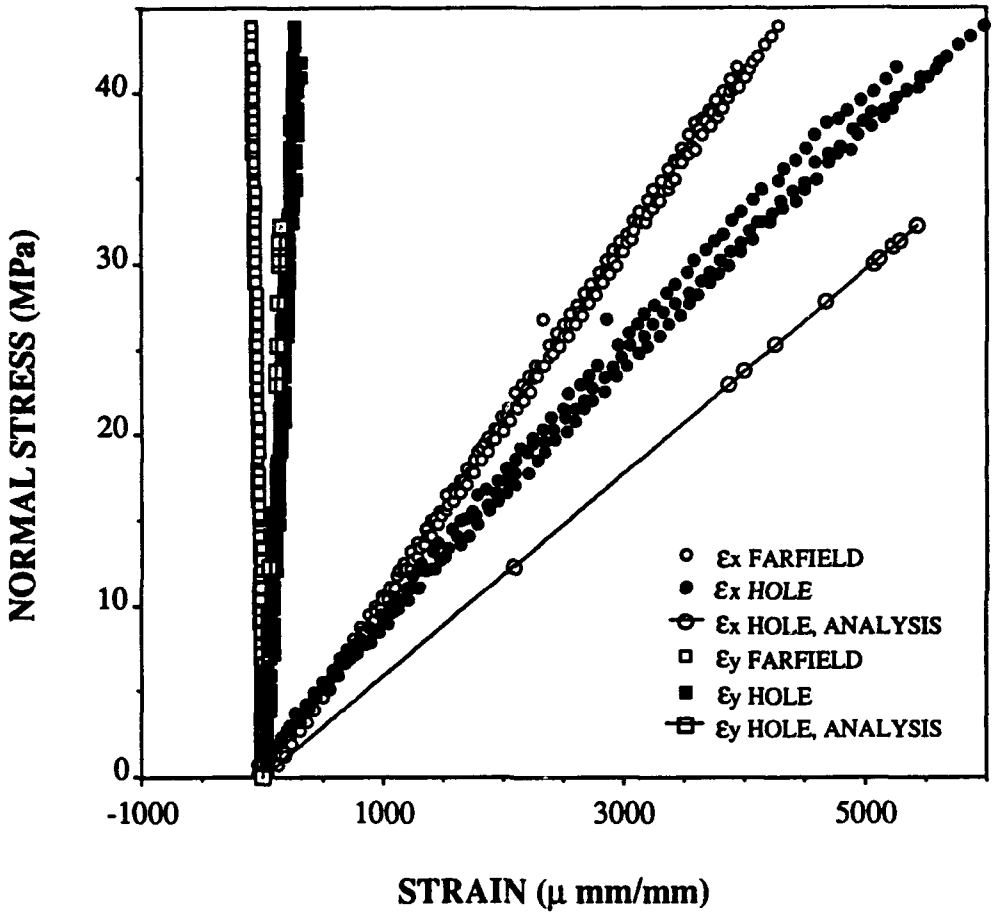

Figure 22. 90-Degree, Transverse Ellipse

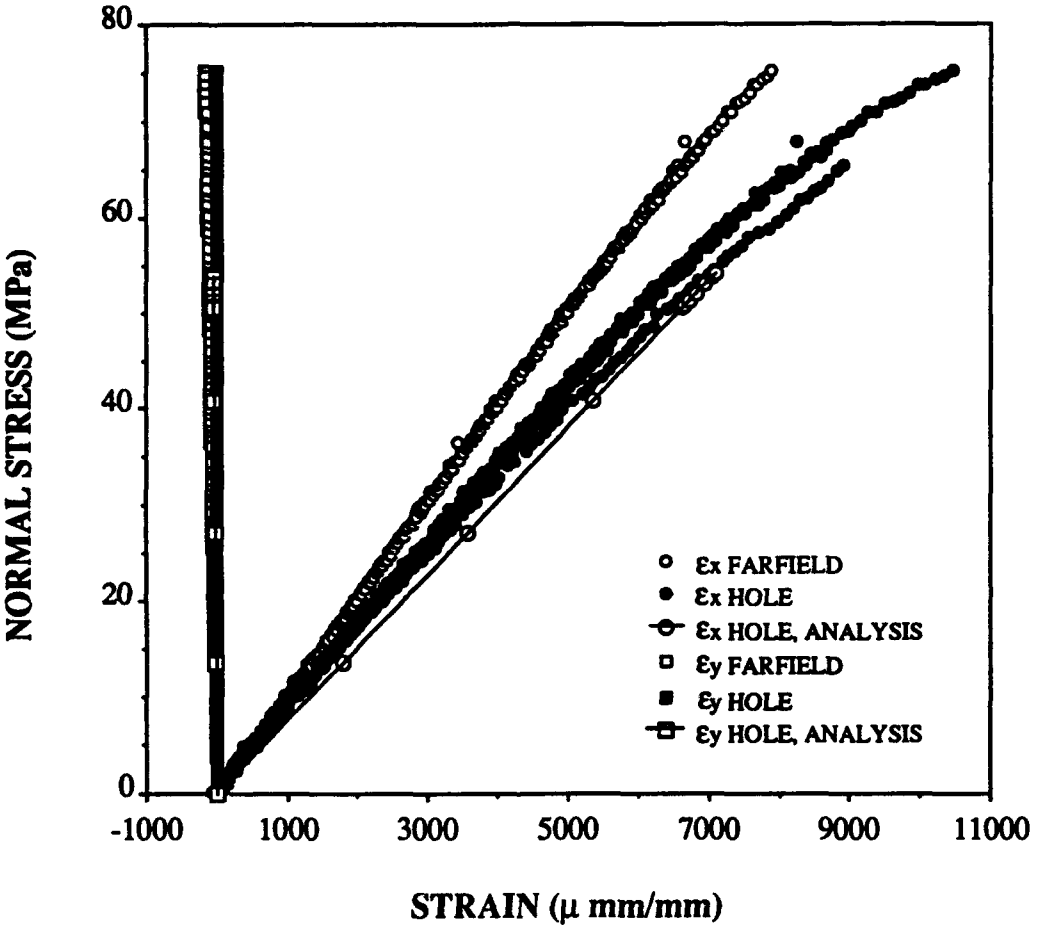

Figure 23. 90-Degree, Longitudinal Ellipse

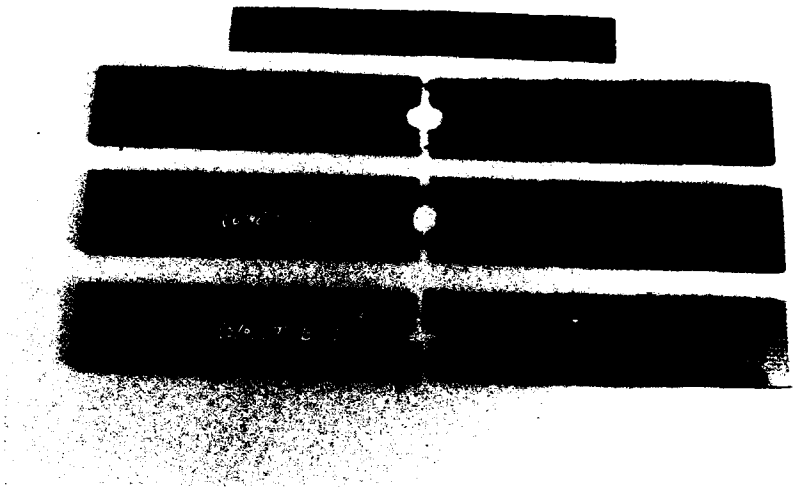

Figure 24. Failed 0/90 Specimens

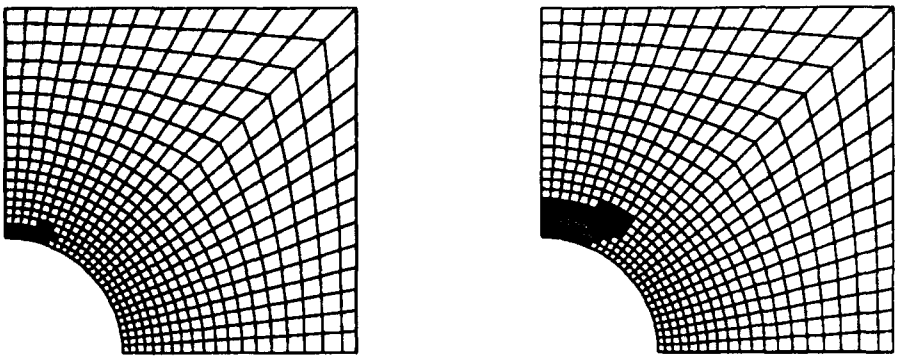

Circular Hole

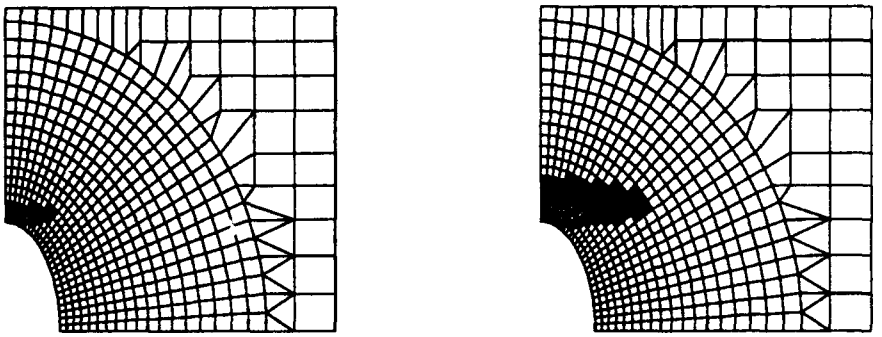

Transverse Ellipse

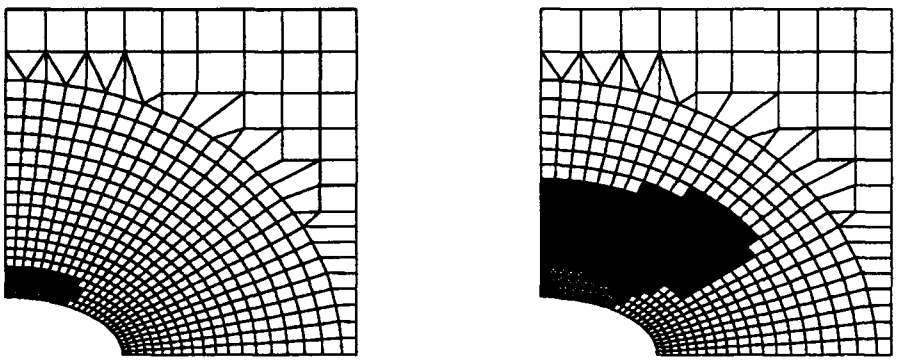

Longitudinal Ellipse

0-degree plies

90-degree plies

Key

- 10% below exp. failure
- Exp. failure load
- 10% above exp. failure

Figure 25. 0/90 Analytical Damage Zones

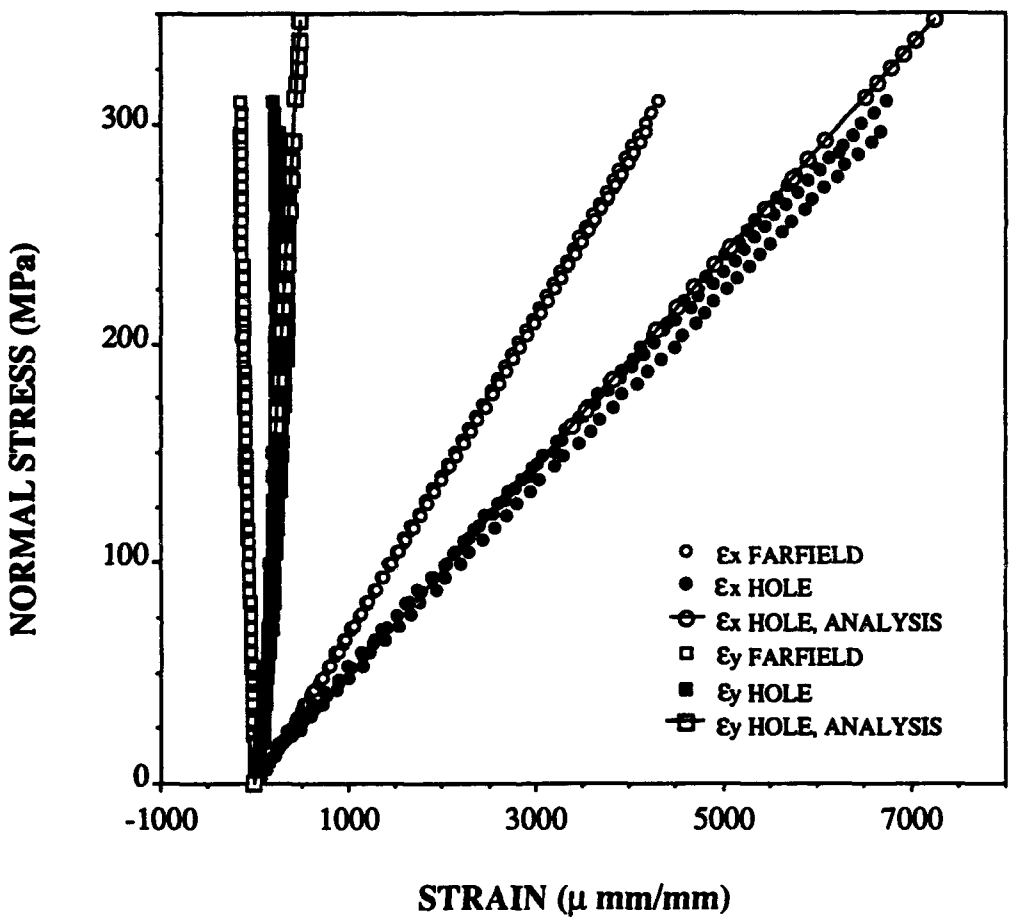

Figure 26. 0/90, Circular Hole

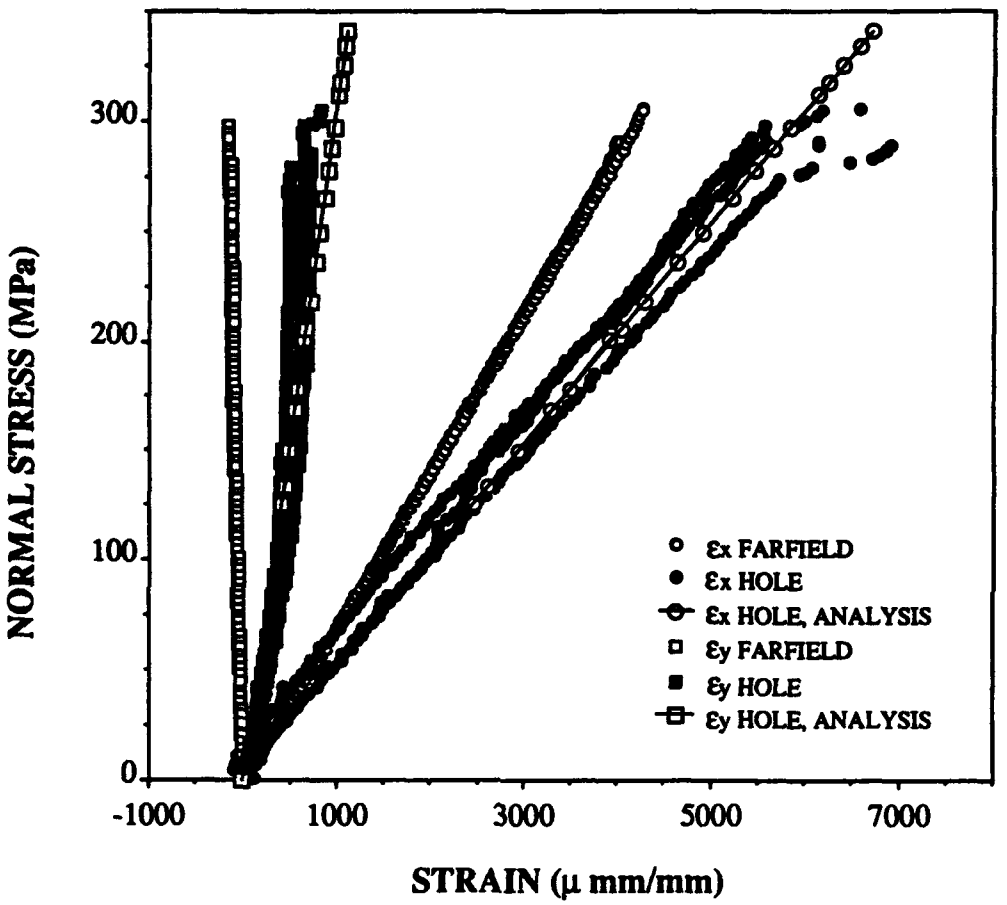

Figure 27. 0/90, Transverse Ellipse

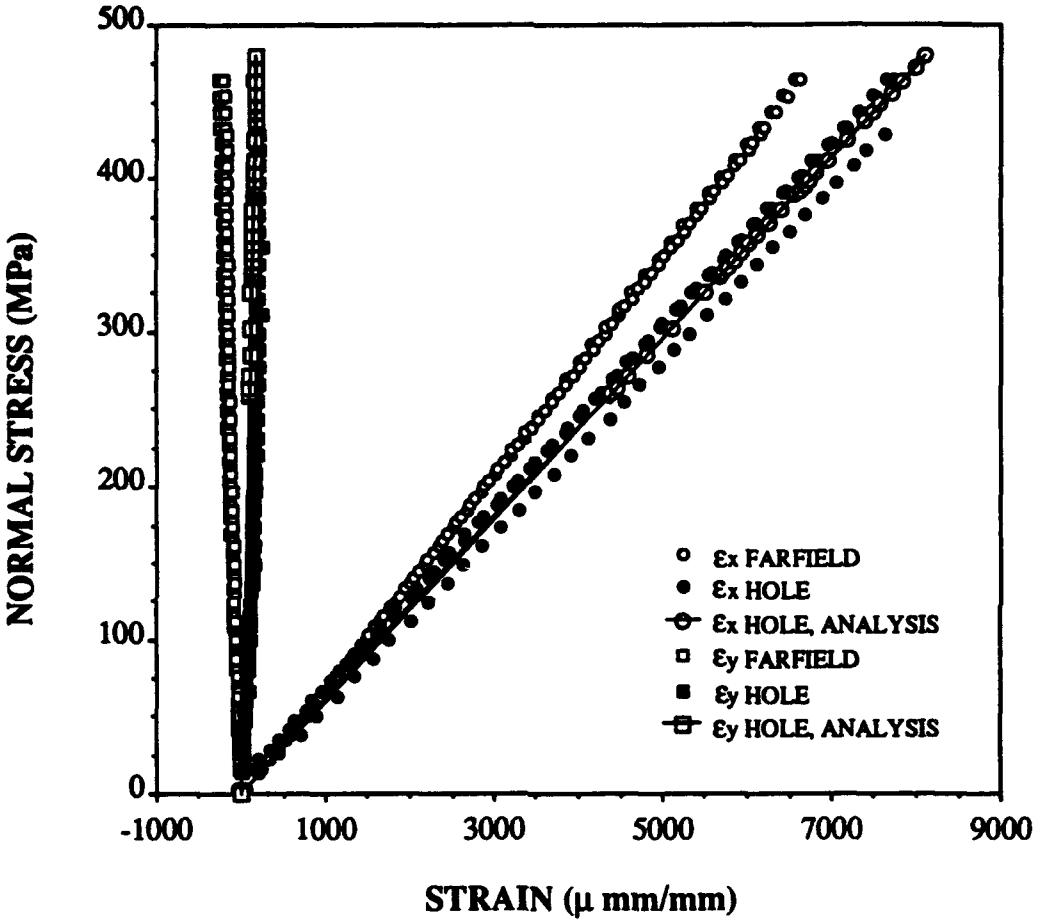

Figure 28. 0/90, Longitudinal Ellipse

4. $[\pm 45]_{4s}$ Layup Tests of these specimens were characterized by long test runs, noticeable necking along much of the specimen length, very nonlinear load-displacement curves, and scissoring of the fibers. Light cracking or tinking noises were heard starting around half of the ultimate failure load, and continuing intermittently up to failure. Test runs took between 20 and 30 minutes, due to the extreme amount of deformation and displacement; the load increased very slowly at the constant crosshead speed used. Due to the large displacements, the strain gage data quickly saturated the data input system, thus producing valid data for only part of the load cycle. Future studies involving this ply layup should consider reducing the amplification applied to the strain gages to the smallest setting available, to avoid this problem. Failure loads were obtained, however, as this phenomenon did not affect the load transducer.

Scissoring is a term indicating that the fibers attempt to align themselves with the load. As the applied load is increased, the angle between the fibers will decrease. This is shown graphically in Figure 29.

Figure 30 is a photo of the typical failure modes of each hole geometry. The failed specimens tended to exhibit a failure originating at the hole edges in the width direction, and then splitting at a + or -45-degree angle some distance between the hole and specimen edge. The longitudinal ellipses did not all have the width-wise failure, but failed with strictly + or -45 degree splits. In all cases, the internal plies failed in the fiber directions, producing alternating + and -45-degree angle surfaces.

There was a varying amount of delamination observed, both on the outside edge of the specimens and on the edges of the holes. Very obvious necking occured; in the area around the hole and center third of the specimen for the circular hole and transverse ellipse, and extending part way into the tab area on the longitudinal ellipse.

The anaysis predicted the failure modes quite well for this layup, as can be seen in Figure 31. The analytical failure load for the circular hole fell within the range of experimental values, while it ran approximately 20% high for the transverse ellipse and 20-25% low for the longitudinal ellipse. Analytical failure of the mesh elements was dominated by shear, which explains the preponderance of + and -45-degree failure surfaces.

Figure 32 depicts the stress-strain data for the circular hole; Figure 33 for the transverse ellipse. The results for the two cases are very similar. The analytical curves correlate very well with the experimental data. The experimental strain adjacent to the hole diverges from the analytical prediction well past the halfway point, revealing greater

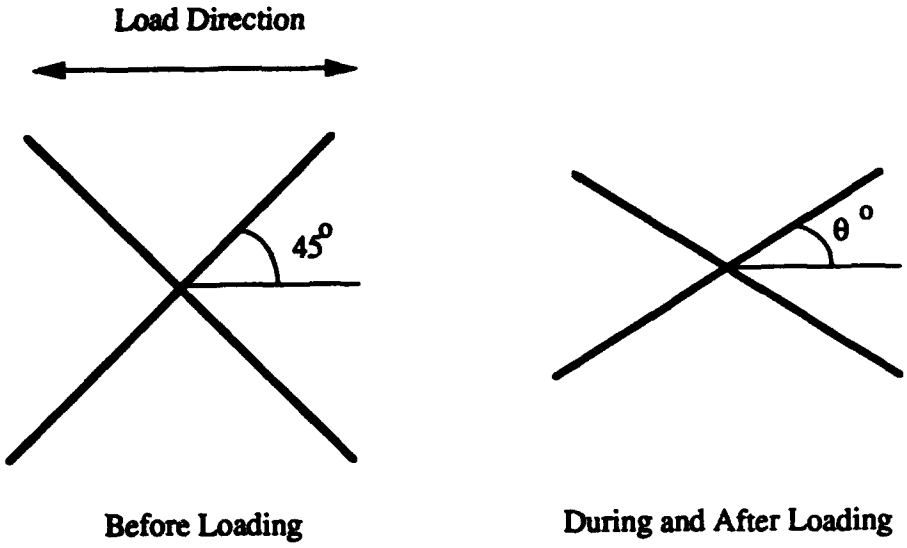

Figure 29. Scissoring of Fibers

Figure 30. Failed +/- 45 Specimens

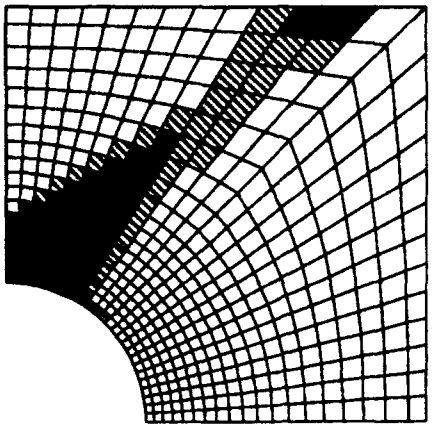

Circular Hole

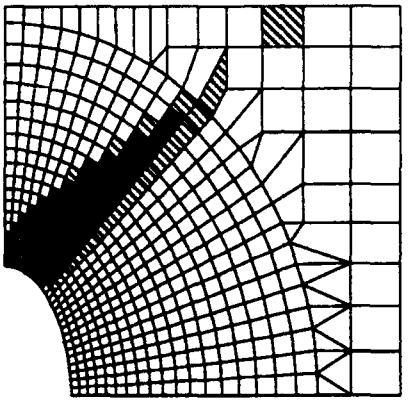

Transverse Ellipse

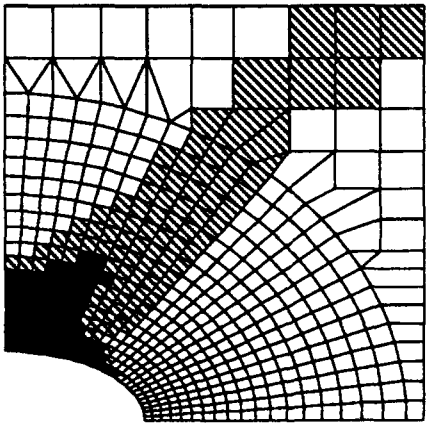

Longitudinal Ellipse

Key

- 20% below model failure
- 10% below model failure
- Near model failure
- Model Failure

Figure 31. ±45° Analytical Damage Zones

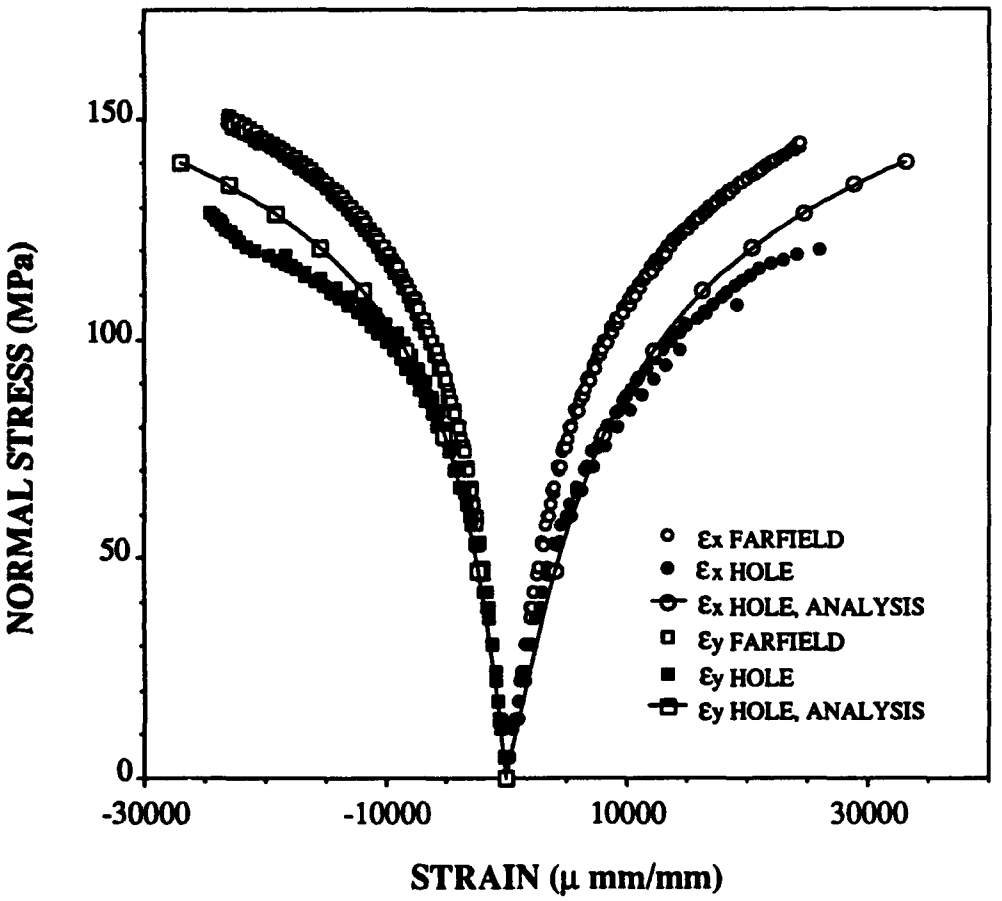

Figure 32. +/-45, Circular Hole

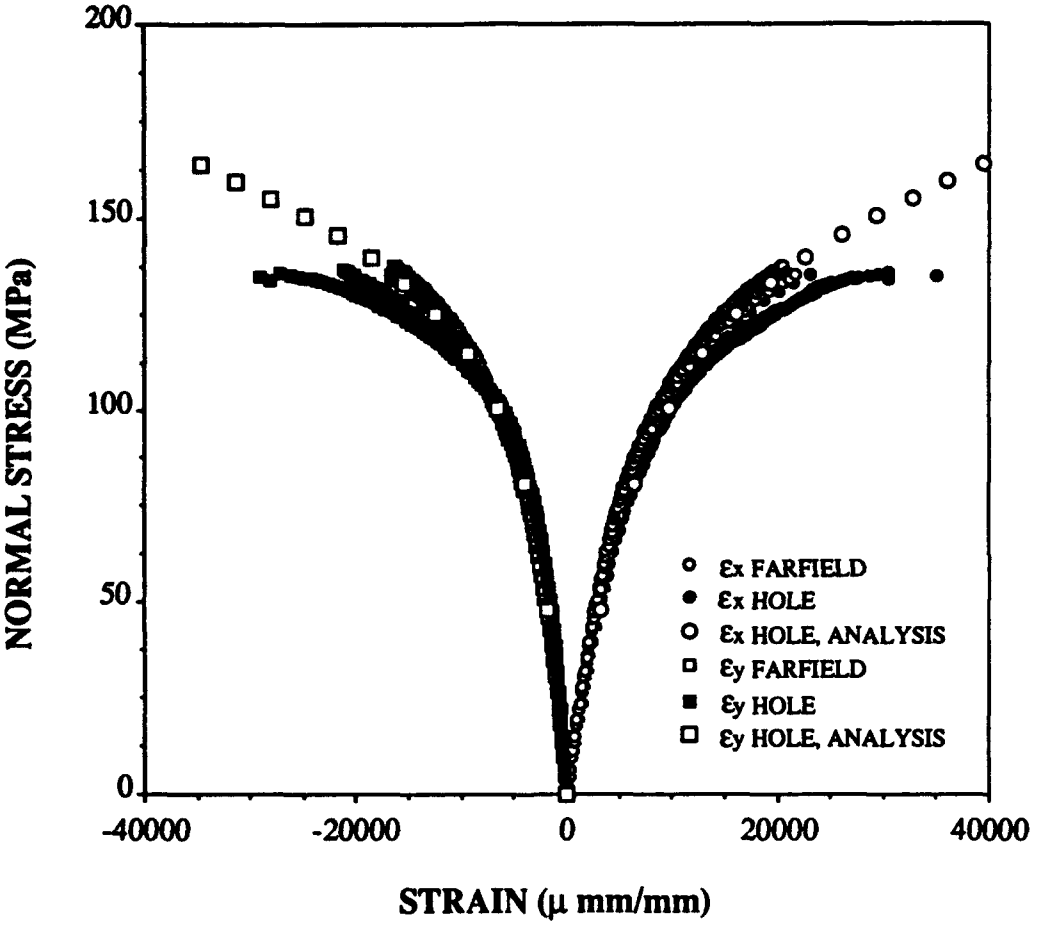

Figure 33. +/-45, Transverse Ellipse

than predicted strains. The analysis thus predicted a stiffer response than was actually measured.

The longitudinal ellipse case is presented in Figure 34. Here, the farfield strains follow the predicted curve for the near hole strains; the actual strains near the hole agree initially, but are considerably larger than predicted above 100 MPa of stress. Following testing, the tabs on this group of specimens were observed to have partially delaminated. It is possible that the stress field applied was no longer uniform once this delamination began, and this may account for the greater divergence of experiment from analysis in this case.

5. $[\pm 45_2/0/\pm 45]_s$ Layup This ply layup consistently failed along + or -45-degree lines extending from the hole edge out to the edge of the specimen. Figure 35 is a photo of one of each hole geometry after testing. The longitudinal ellipse case resulted in a much wider damage zone, with numerous parallel splits. The other two cases yielded single splits on either side of the hole. These specimens did not pull completely apart upon completion of testing. Some delamination was observed in the region of the failure lines, especially at the hole edges. There was some necking and lateral distortion of the specimens. By lateral distortion, the author means that there is a bend around the middle of the specimen; the x-axis no longer passes through the centerline of the specimen at all points. This layup is listed as 0/45 on the figures.

Figure 36 depicts the analytical damage prediction for the actual failure loads of the three hole geometries. Minimal or no damage was predicted for the ±45-degree plies, as can be seen. The zero-degree plies in the circular hole case have essentially failed at a 45-degree angle according to the analysis. The damage zone has not extended so far into the 0-degree plies for the transverse or the longitudinal ellipse The damage zone did extend at a 45-degree angle, when the analysis was run further (to approximately 25% above actual failure loads). Some elements failed in shear in the analyses, but not so overwhelmingly as in the ±45 layup.

The circular hole results agree closely with analysis for both ε_x and ε_y. Figure 37 presents the two sets of data graphically. Just below 200 MPa applied stress, both experimental curves undergo a sudden reduction in slope. This trend is consistent among all three specimens. This may indicate that some internal ply failure or damage has occured.

The transverse ellipse specimens did not show this same response, but maintained roughly constant slopes to the stress-strain curves. There is a jump in transverse strain, just below the 200 MPa stress level, but without the sudden slope change of the previous

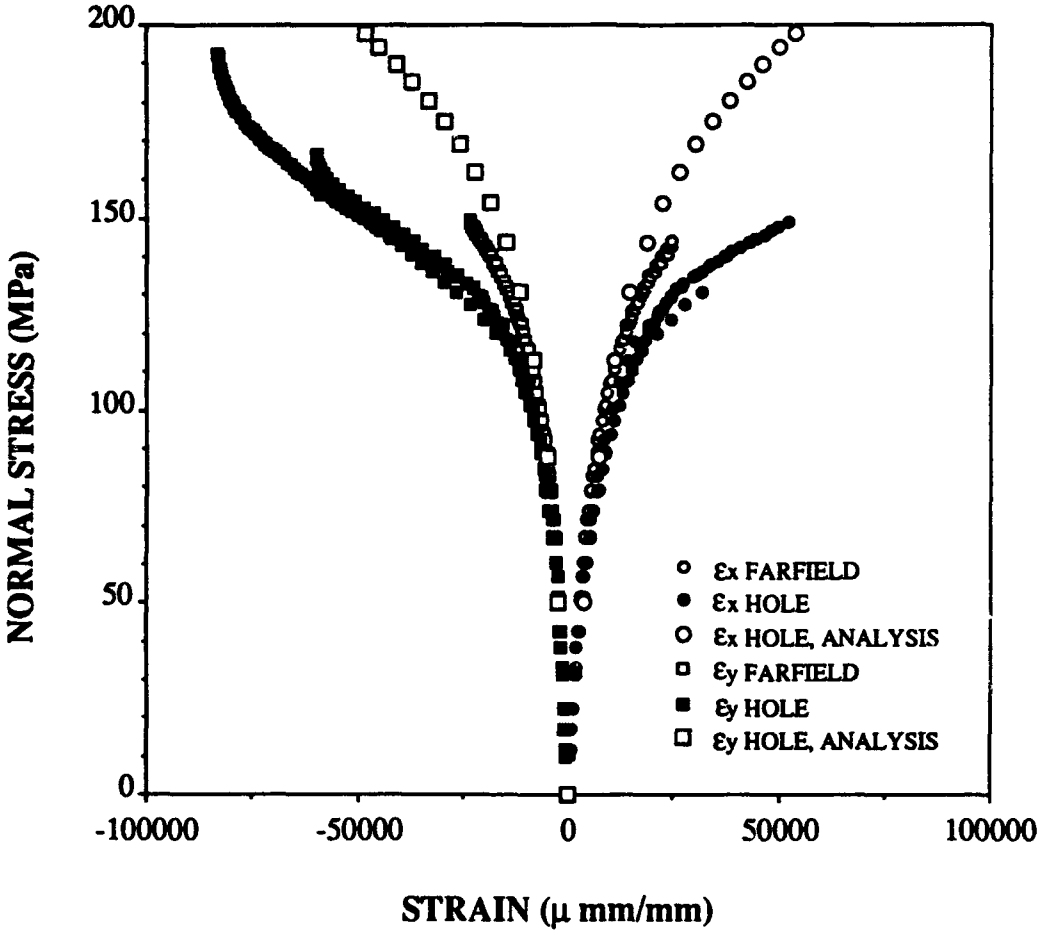

Figure 34. +/-45, Longitudinal Ellipse

Figure 35. Failed 0/45 Specimens

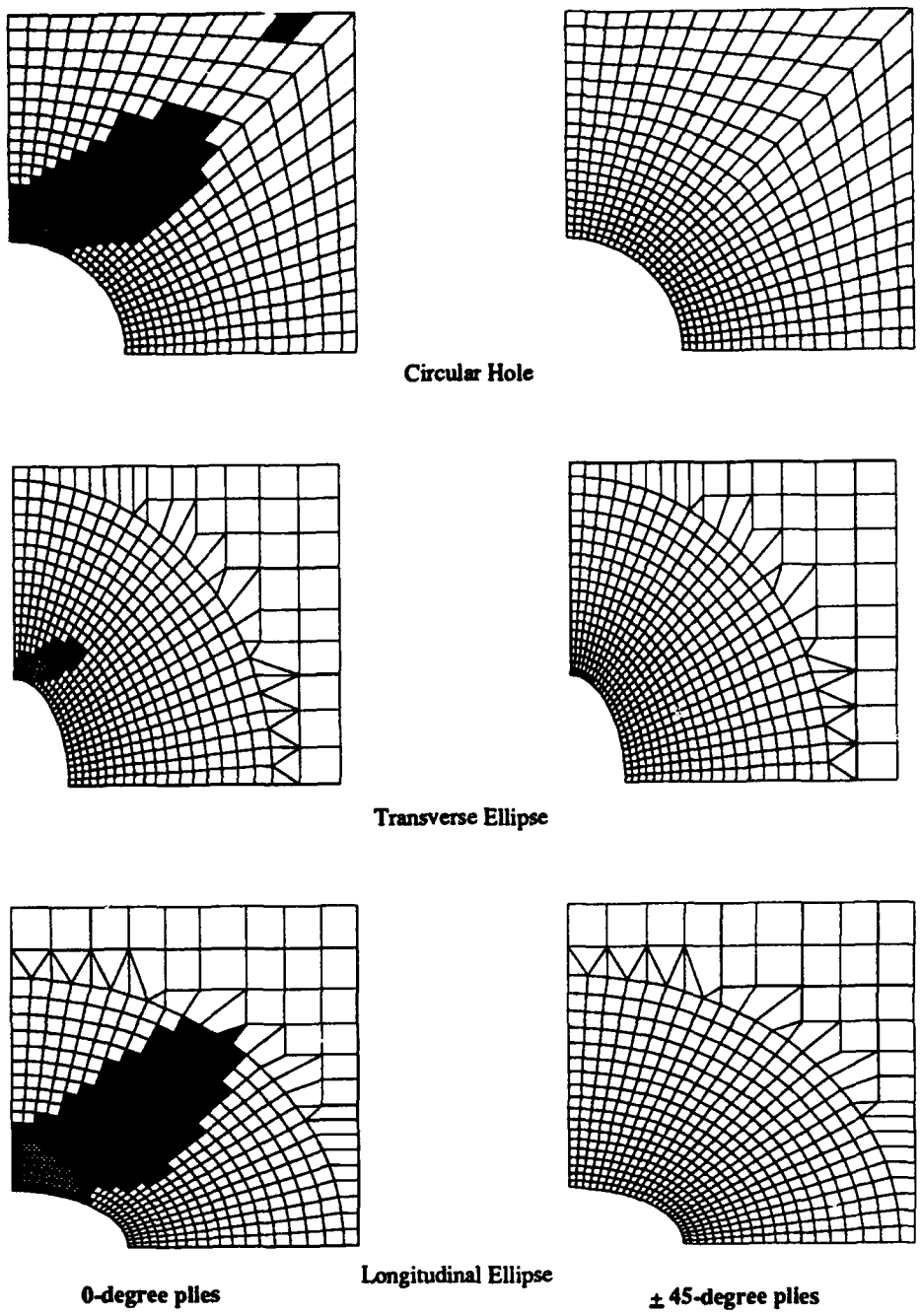

Figure 36. 0/45 Analytical Damage Zones

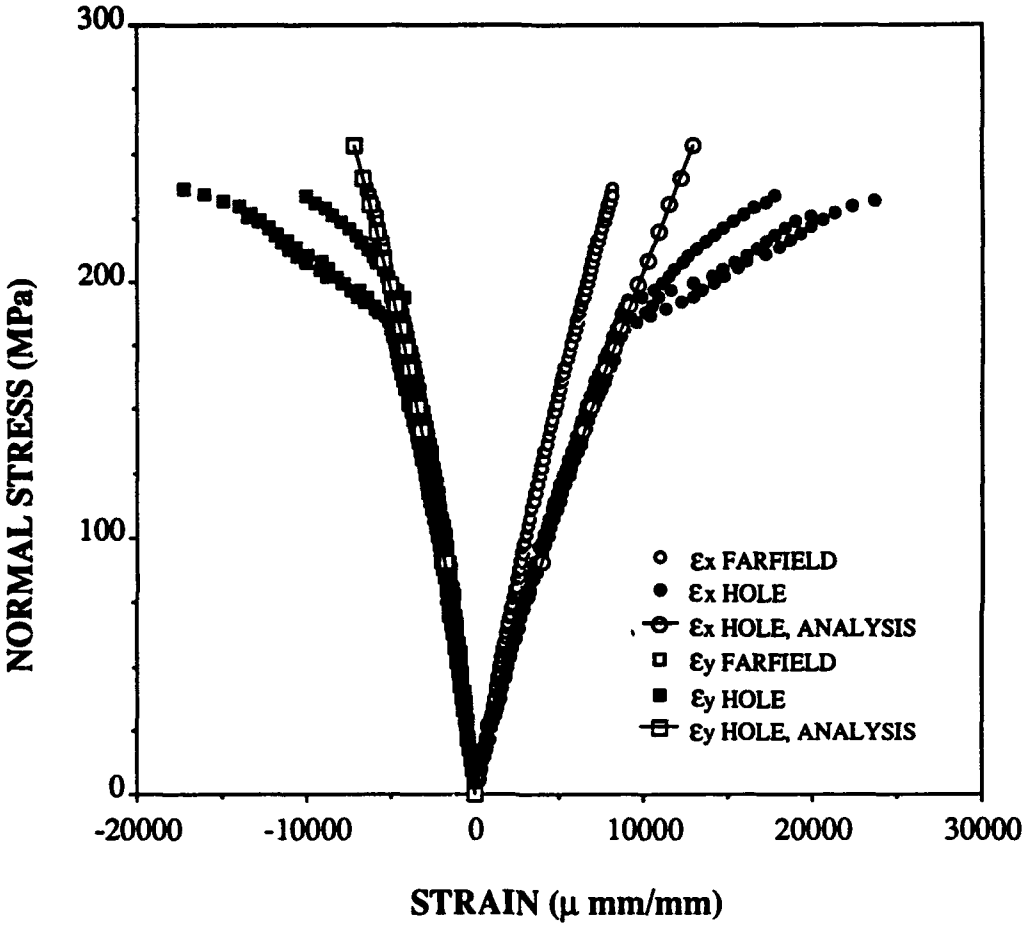

Figure 37. 0/45, Circular Hole

case. Figure 38 depicts this information. Again, there is good correlation of analytical and experimental data. There is also slighlty more scatter to the experimental data than for the circle.

The longitudinal ellipse tests reveal less linear curves than the other two cases, as seen in Figure 39. The analytical data agrees initially, but predicts fairly linear response, and diverges from the experimental data between 150 and 200 MPa stress level. This divergence is in the direction of greater stiffness than was actually the case.

6. $[(\pm 45/0)_2/\pm 45]_S$ Layup The failure mode of this layup is virtually identical to that of the $[\pm 45_2/0/\pm 45]_S$ specimens. Figure 40 shows the failed test specimens. These specimens evidenced greater delamination than the previous layup, but less necking. Some but not all experienced lateral distortion. Again, there is very good agreement between analysis and experiment, though the strains in the y-direction tend to less linear behavior than predicted. All specimen failures were preceded by audible cracking, within 1000 lb of failure load or less. This layup is called $0_2/45$ on the figures.

Figure 41 shows that the analysis predicted a fairly small damage zone at the actual failure loads of all three hole geometries, primarily in the zero-degree plies. The damage in the ±45-degree plies was only a few elements, if any at all.

Figure 42 presents the circular hole data. There is good agreement of analysis and experiment up to 200-250 MPa stress. Beyond that point, the analysis predicts slightly stiffer response than was measured. The transverse ellipse data is shown in Figure 43. In this case, the analysis predicts slightly greater strains, i.e., the specimens exhibited stiffer response than predicted. Finally, the longitudinal ellipse case is plotted in Figure 44. This last case shows the greatest deviation in predicted ε_y from experiment, although the ε_x data agree very well.

Since the longitudinal ellipse fails at a much higher load than the circle or transverse ellipse, it is possible that the 0-degree plies have lost progressively more load-carrying capability. Thus, more deformation occurs within the angle plies, and the material response becomes less stiff.

7. $[0/\pm 45/90]_{2S}$ (Quasi-Isotropic) Layup. Failure of these specimens occured along + and -45-degree lines from the hole edges, on both sides of the specimen. There was no necking of the specimens observed, although there was some delamination visible at the hole edges and outer edges of the specimens. There was some variation in the failure pattern; some specimens failed along straight lines, while others had failure lines which reversed direction part way into the specimen. The longitudinal ellipse case exhibited initial cracks in the width direction, which abruptly split at + or -45-degree

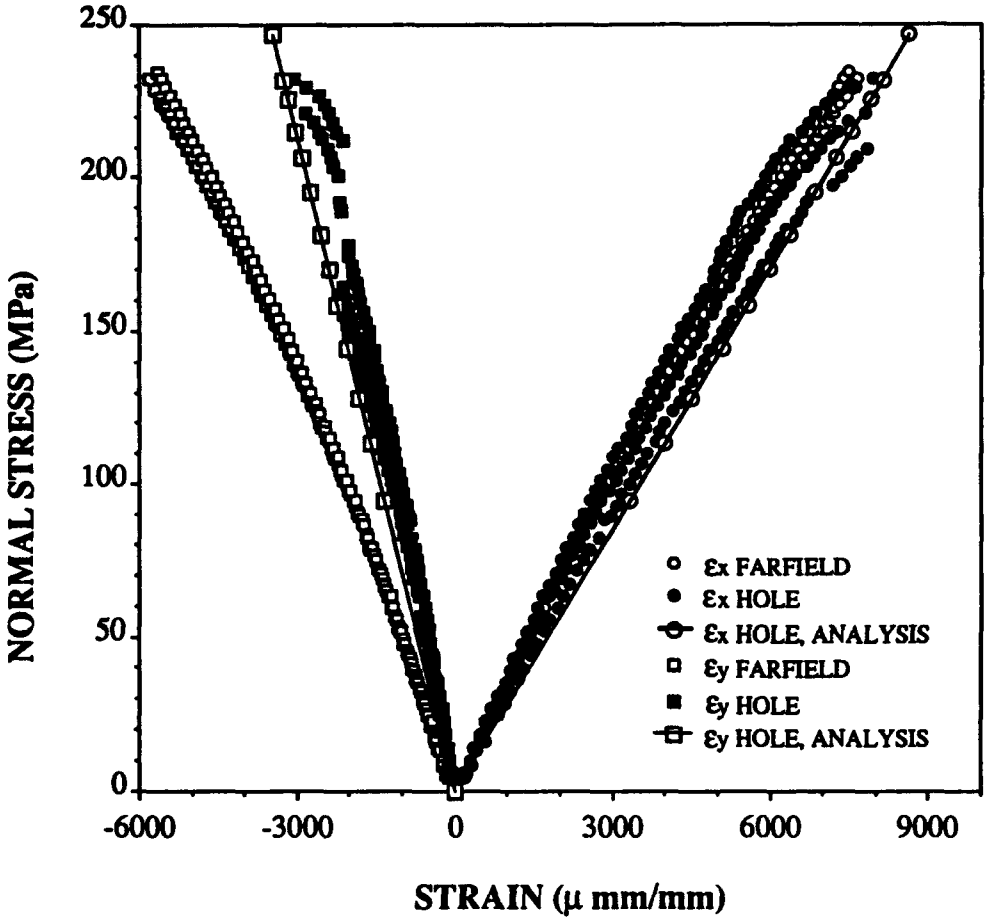

Figure 38. 0/45, Transverse Ellipse

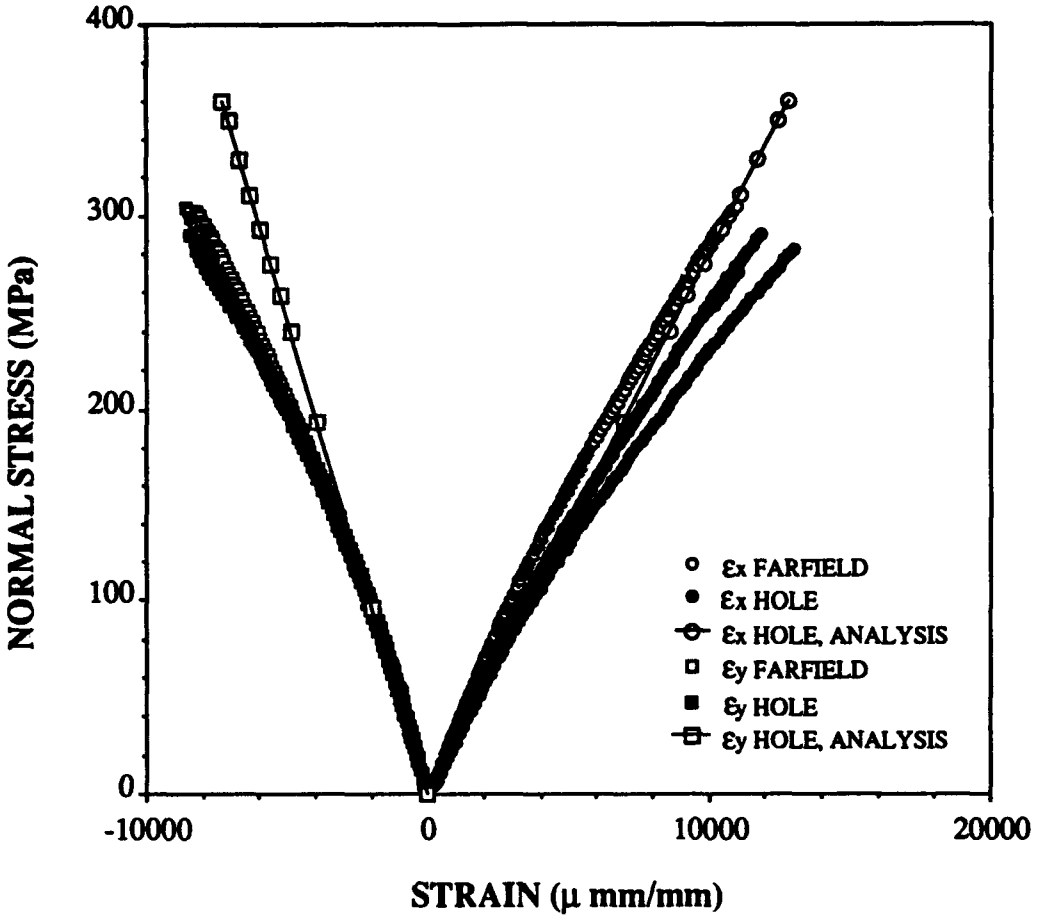

Figure 39. 0/45, Longitudinal Ellipse

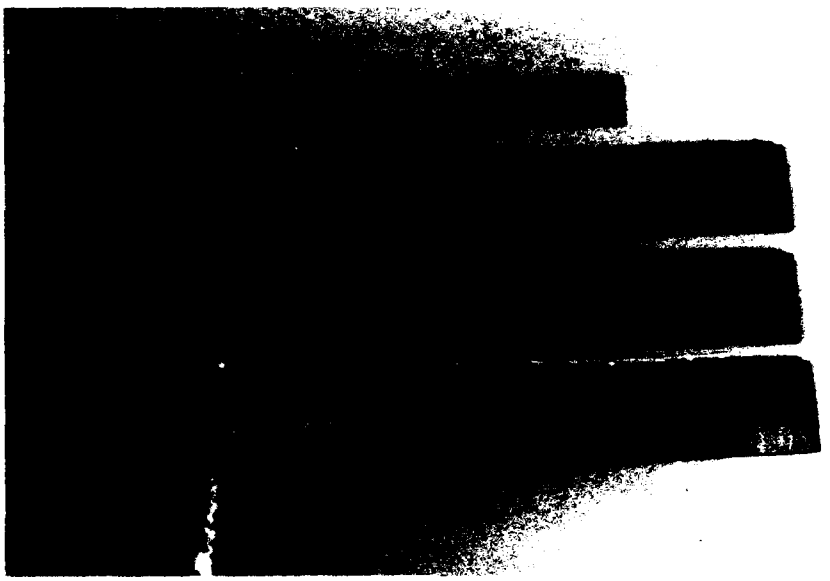

Figure 40. Failed 02/45 Specimens

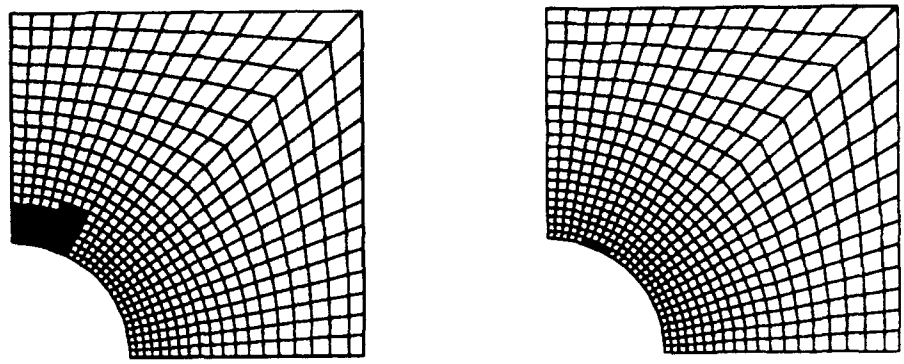

Circular Hole

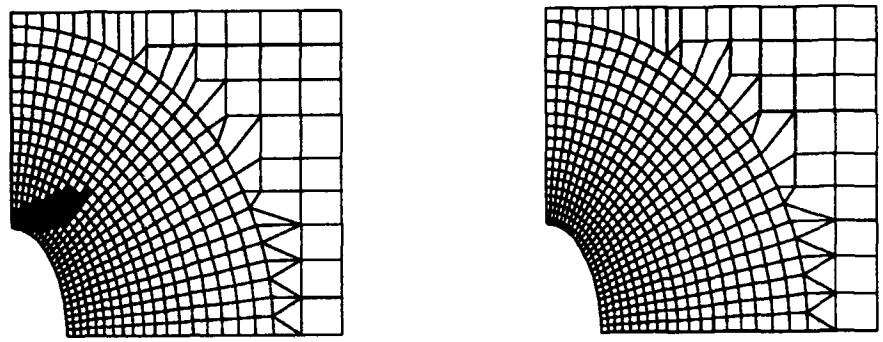

Transverse Ellipse

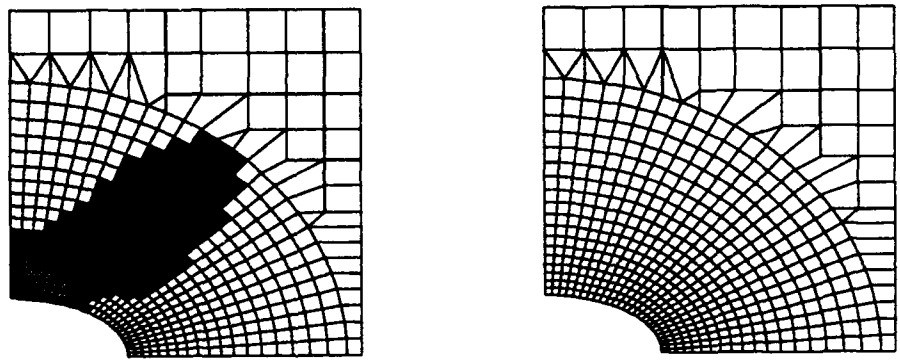

Longitudinal Ellipse

0-degree plies

± 45-degree plies

Key

- 10% below exp. failure
- Exp. failure load
- 10% above exp. failure

Figure 41. 02/45 Analytical Damage Zones

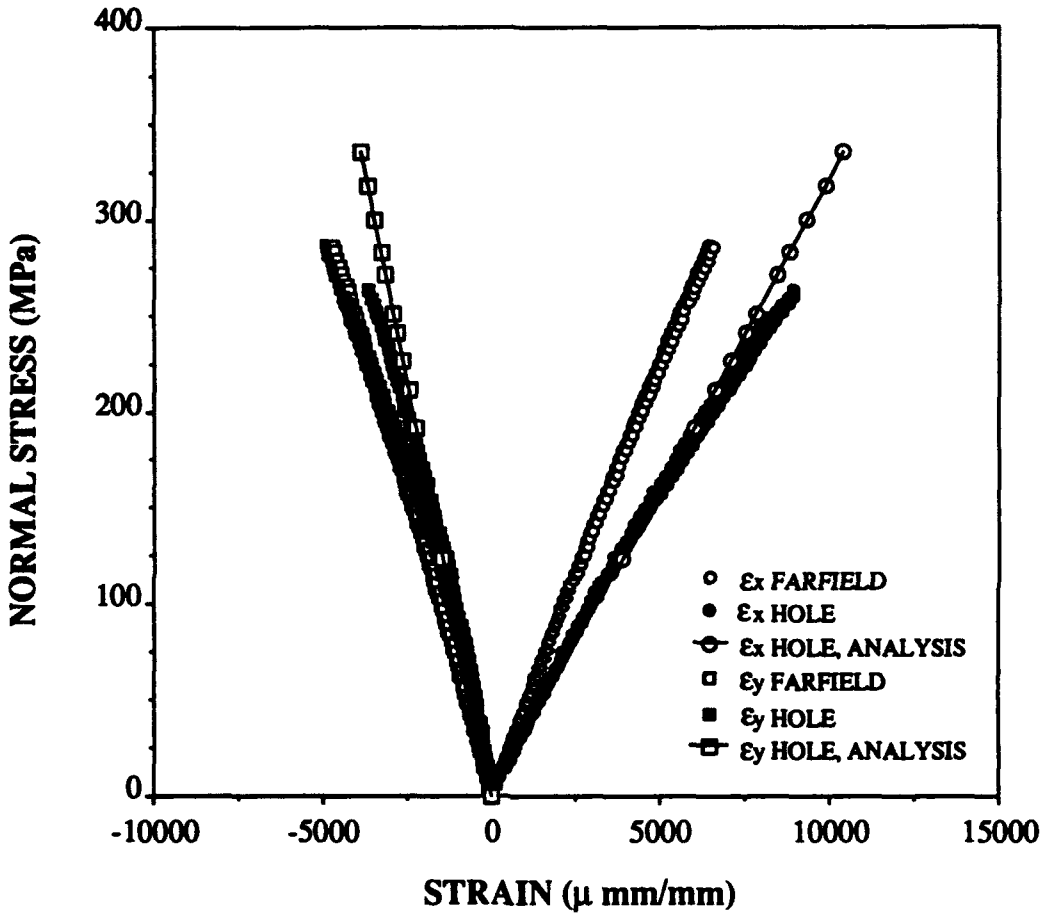

Figure 42. 02/45, Circular Hole

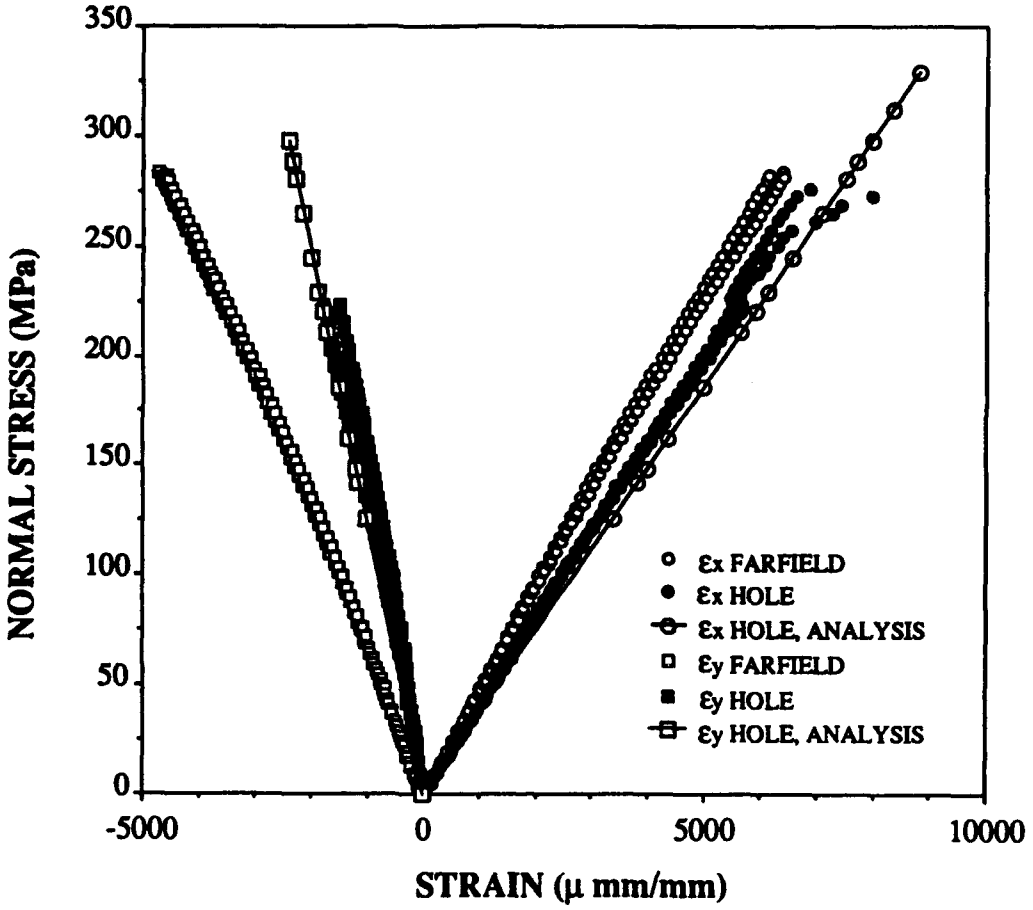

Figure 43. 02/45, Transverse Ellipse

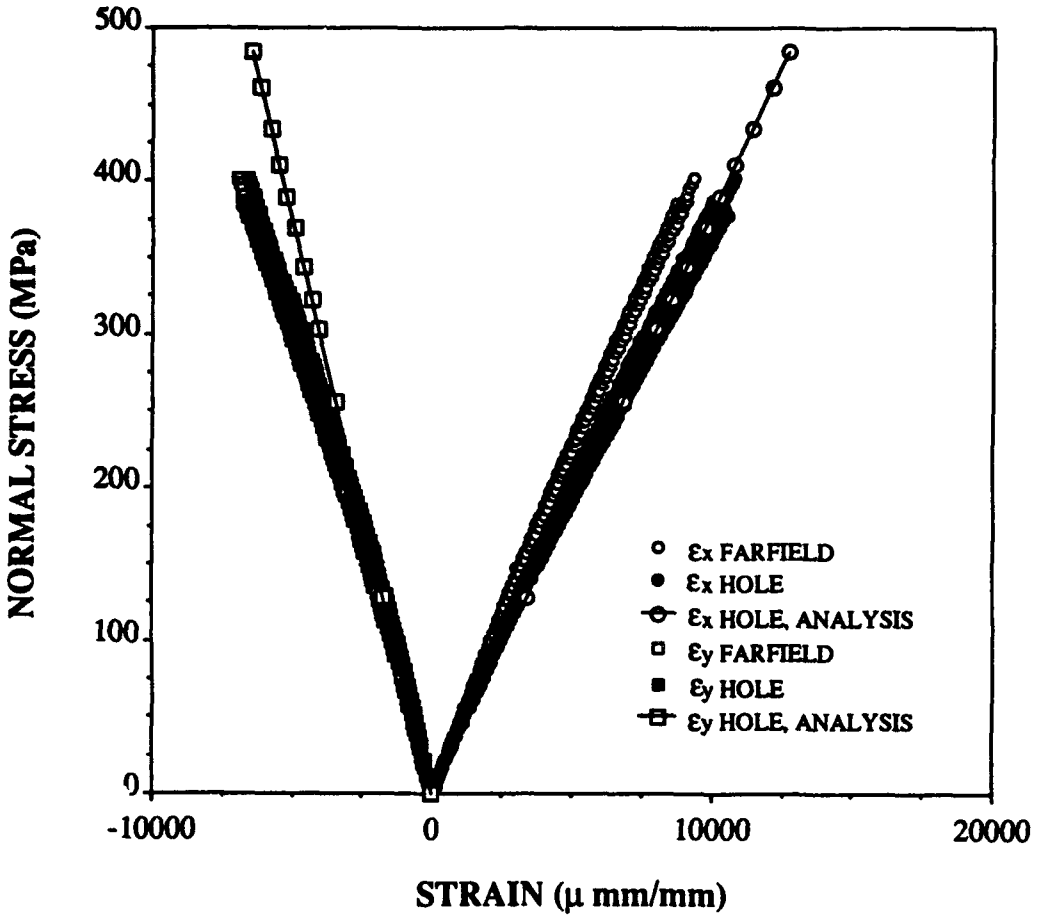

Figure 44. 02/45, Longitudinal Ellipse

angles some distance into the specimen. Figure 45 shows some of the failed test specimens. The figures use the shorthand designation QI for this layup.

Figure 46 depicts the damage predicted for the circular hole case. The damage is greatest in the 90-degreee plies, and extends at a 45-degree angle. The same is essentially true for the transverse ellipse, except that the damage does not extend as far into the plies, as seen in Figure 47. Figure 48 shows the longitudinal ellipse. This time, the 90-degree plies have failed completely.

The circular hole data is presented in Figure 49. There is good agreement between analysis and experiment for the stress-strain response in both x- and y-directions. ϵ_x shows some divergence as the failure load is approached.

Figure 50 depicts the results for the transverse ellipse. There is very good agreement again between analysis and experiment. Once again, there is some divergence in ϵ_x near the failure stress.

The longitudinal ellipse also shows close agreement, as can be seen in Figure 51. There is slightly greater experimental scatter in both curves; the analytical ϵ_x curve falls in the middle of this scatter, while it borders one side of the experimental ϵ_y data.

8. Summary. Figure 52 summarizes graphically the experimental failure modes for the various layups. A circular hole is depicted to represent typical failures for all hole geometries, unless another geometry is specifically shown. This may be compared with Figure 53, the analytically predicted failure modes. As can be seen, the analysis predicts the failures well except for the 0, 90, and 0/90 layups. As previously noted, the analysis program is unable to model failures of an abrupt nature; both the 0 and 90 degree layups experienced this type of failure. However, the stress-strain response was modelled more accurately.

The assumptions made in the analysis regarding plane stress, and the strain energy failure criterion would thus appear to be valid in general for this study. The areas where analysis diverges from experiment may point to the presence of three-dimensional effects such as interlaminar stresses and free edge effects. Where these phenomenon are present in adequate magnitude, the analysis cannot accuately predict either the material response or failure mode of a specimen. Futher comments on possible explanations for discrepancies are provided in the following chapter.

Figure 45. Failed QI Specimens

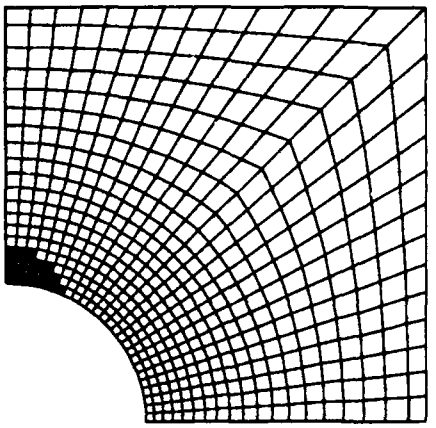

0-degree plies

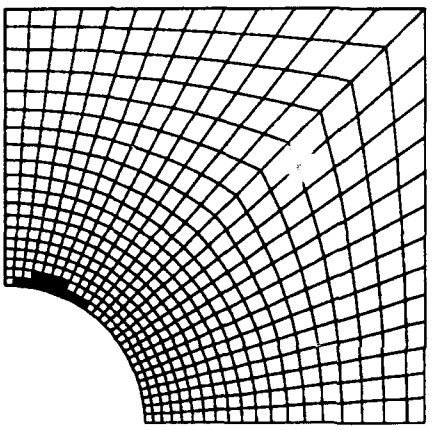

±45-degree plies

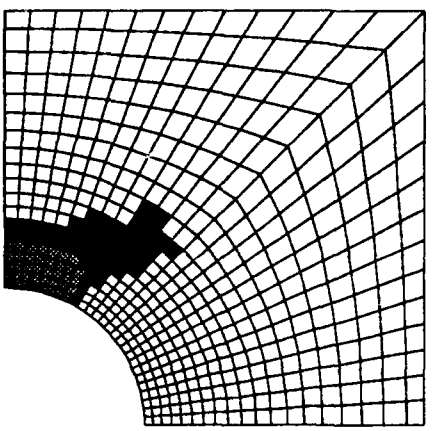

90-degree plies

Key

10% below exp. failure

Exp. failure load

Figure 46. QI Circle Analytical Damage Zones

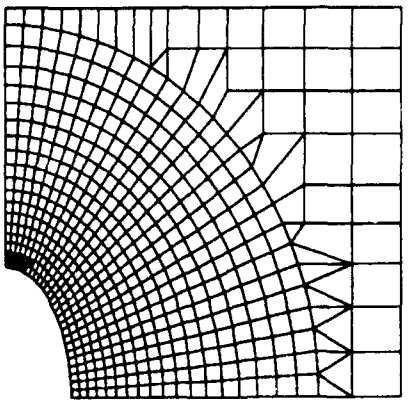

0-degree plies

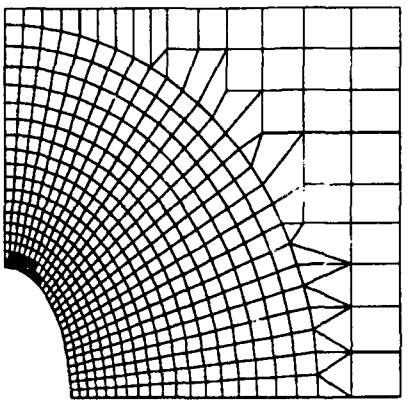

±45-degree plies

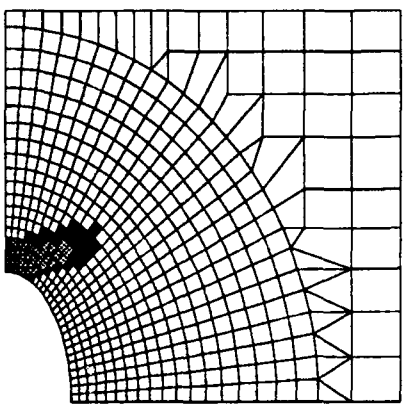

90-degree plies

Key

- 10% below exp. failure
- Exp. failure load

Figure 47. QI Transv. Ellipse Analytical Damage Zones

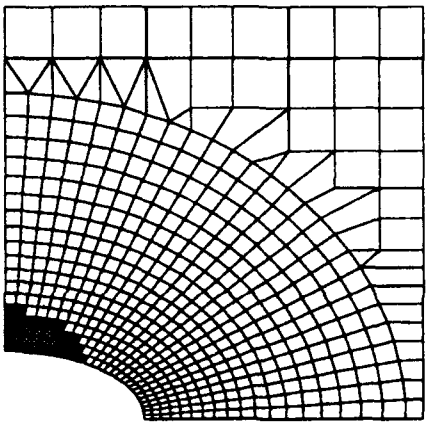

0-degree plies

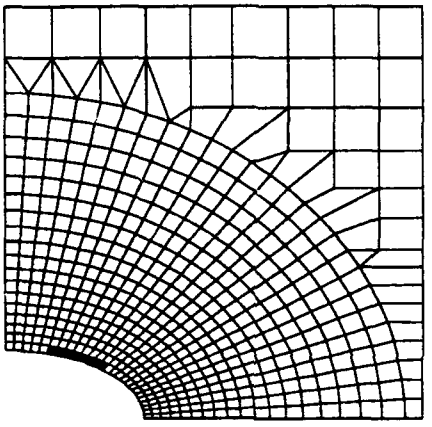

±45-degree plies

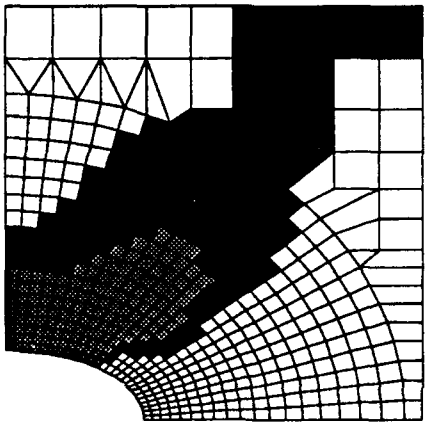

90-degree plies

Figure 48. QI Longitudinal Ellipse Analytical Damage Zones

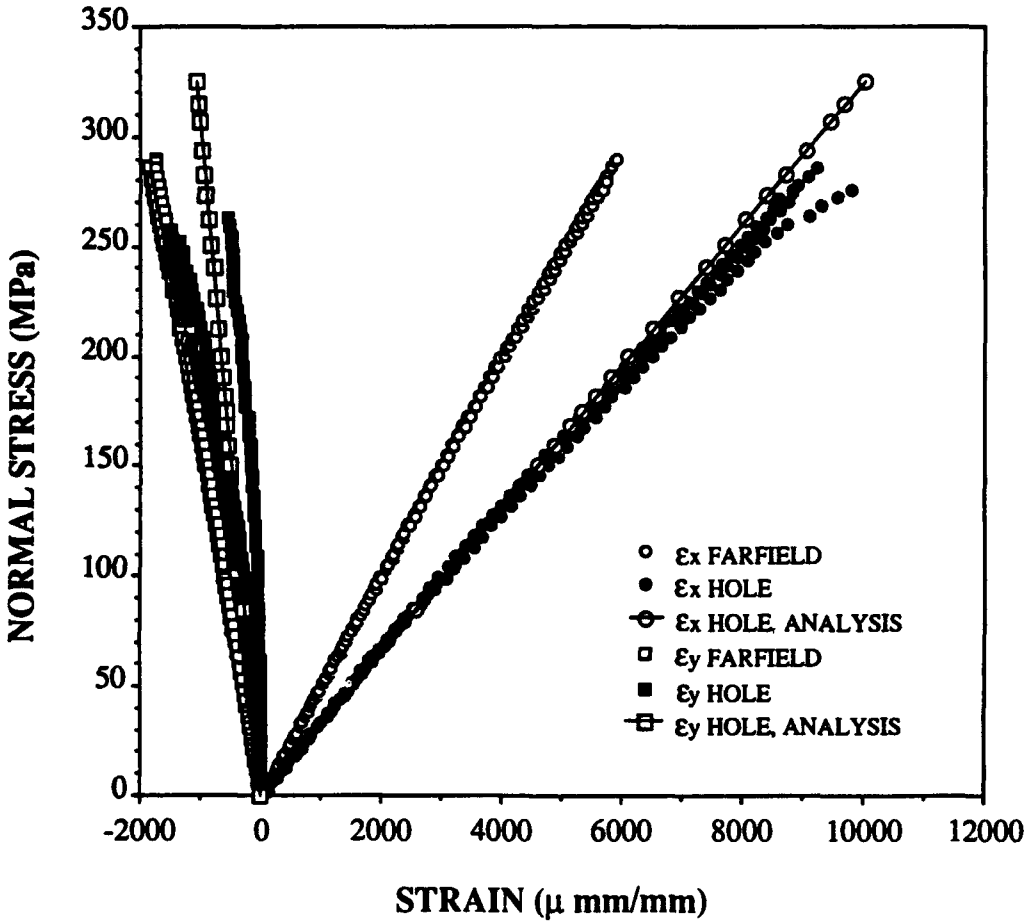

Figure 49. Quasi-Isotropic, Circle

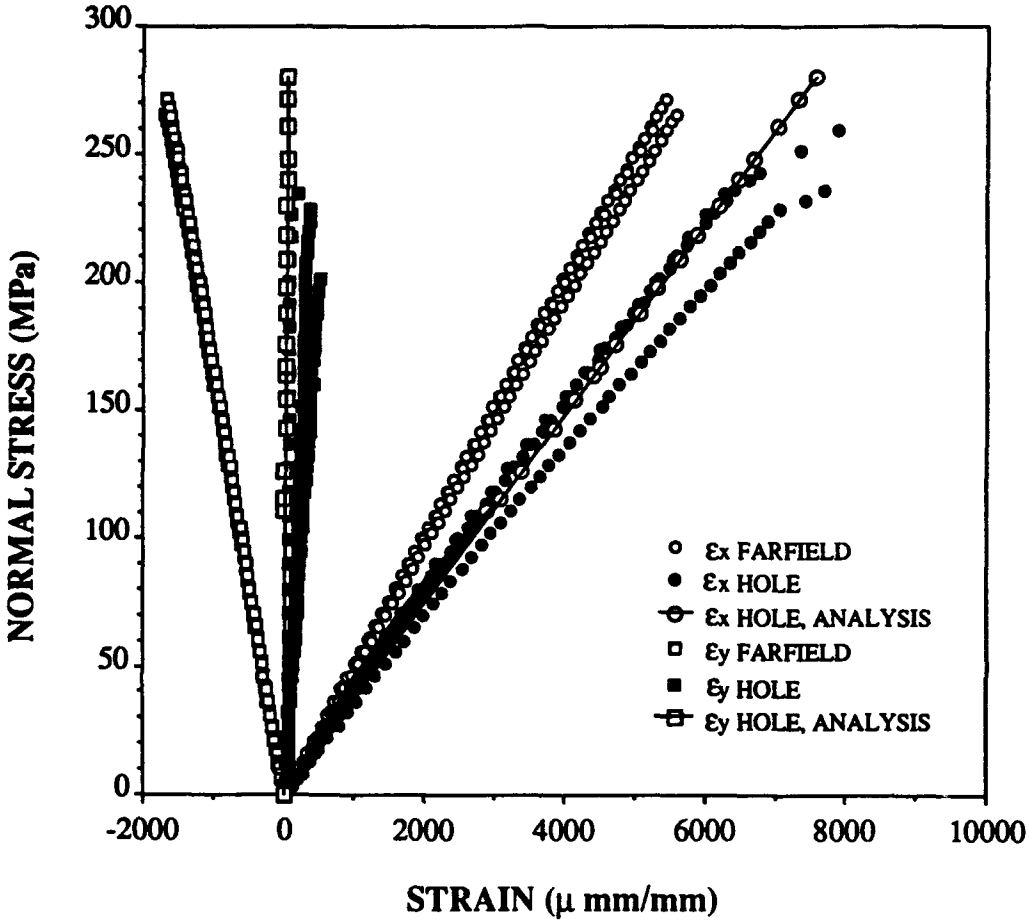

Figure 50. Quasi-Isotropic, Transverse Ellipse

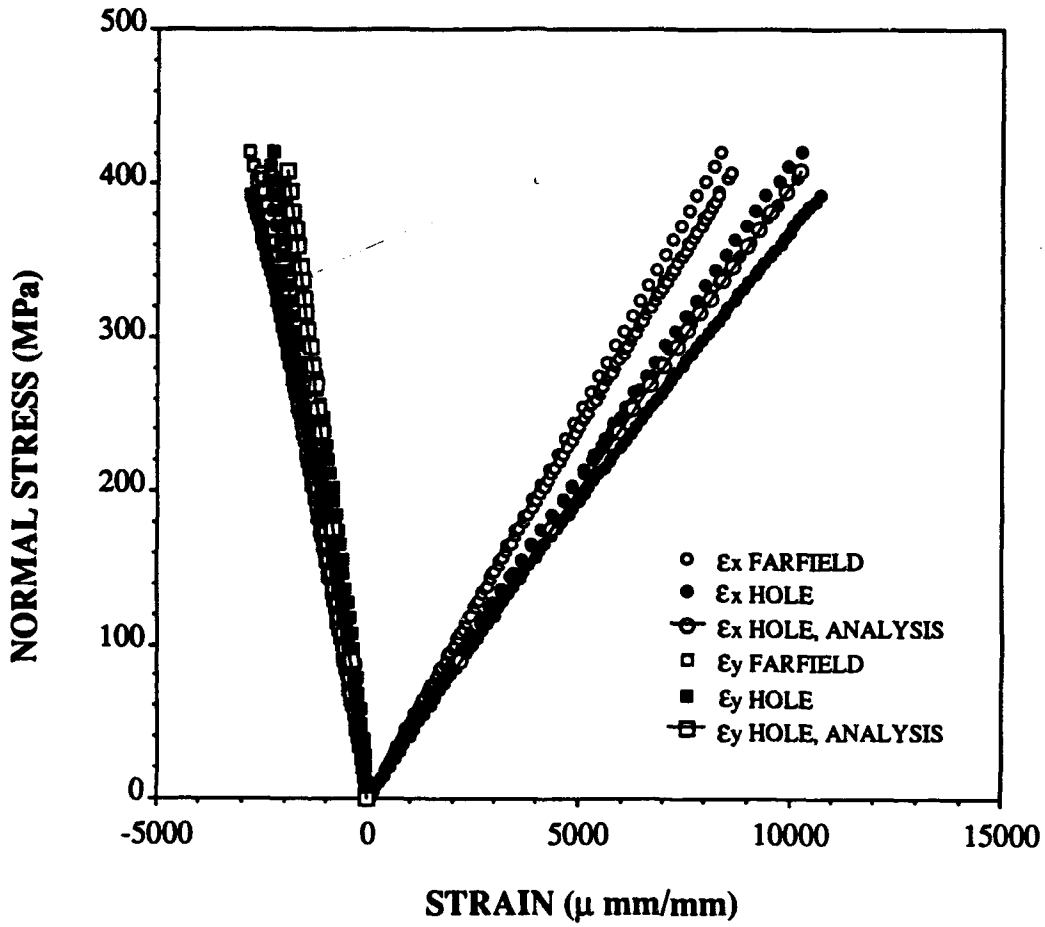

Figure 51. Quasi-Isotropic, Longitudinal Ellipse

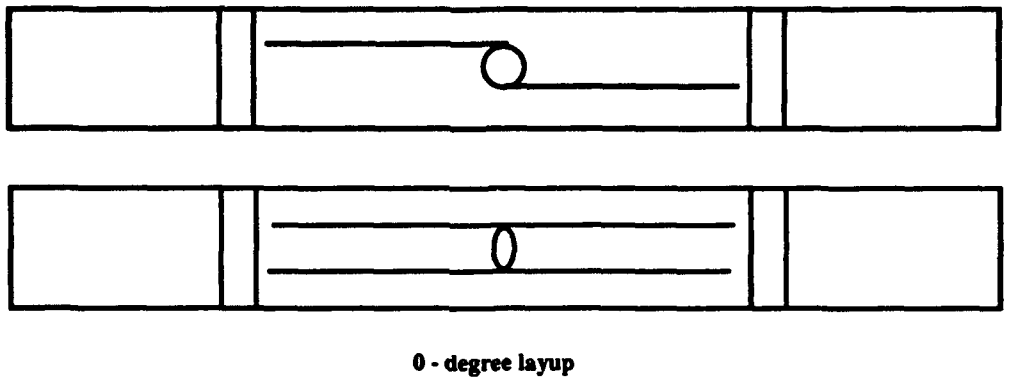

0 - degree layup

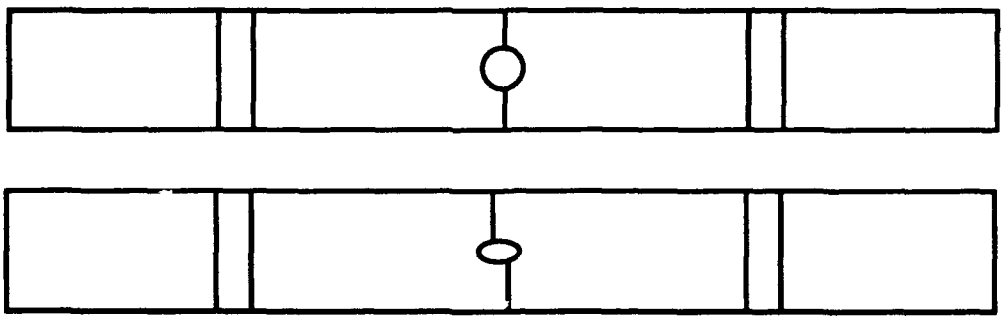

90 - degree layup

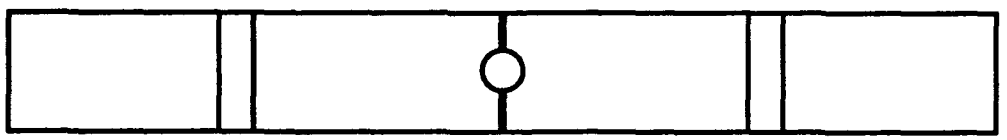

0/90 - layup

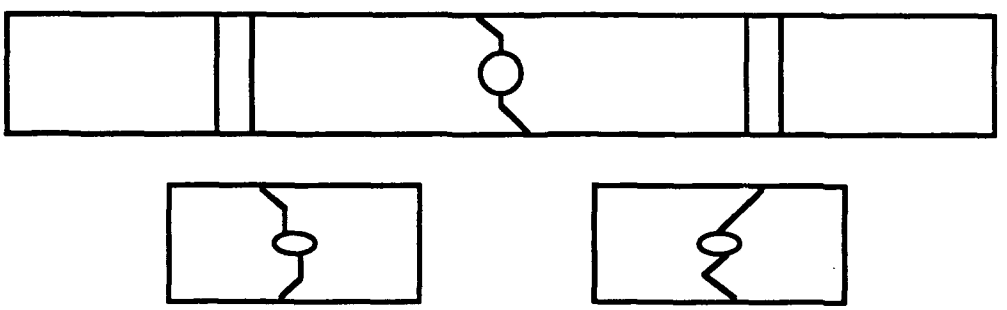

+/- 45 - degree layup

Figure 52. Typical Experimental Failure Modes

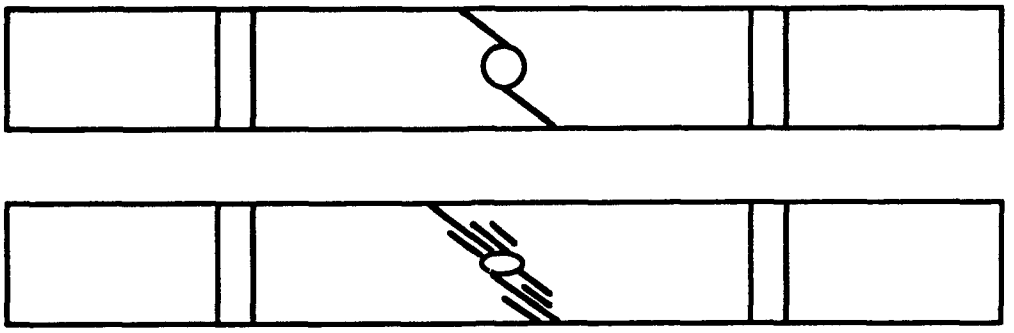

Both 0/+/- 45 layups

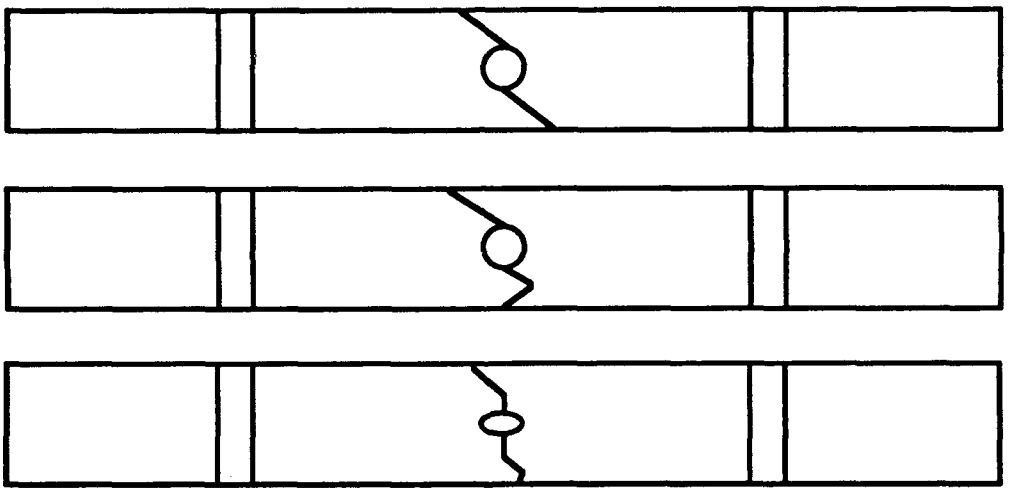

QI layup

Figure 52 (Cont.). Typical Experimental Failure Modes

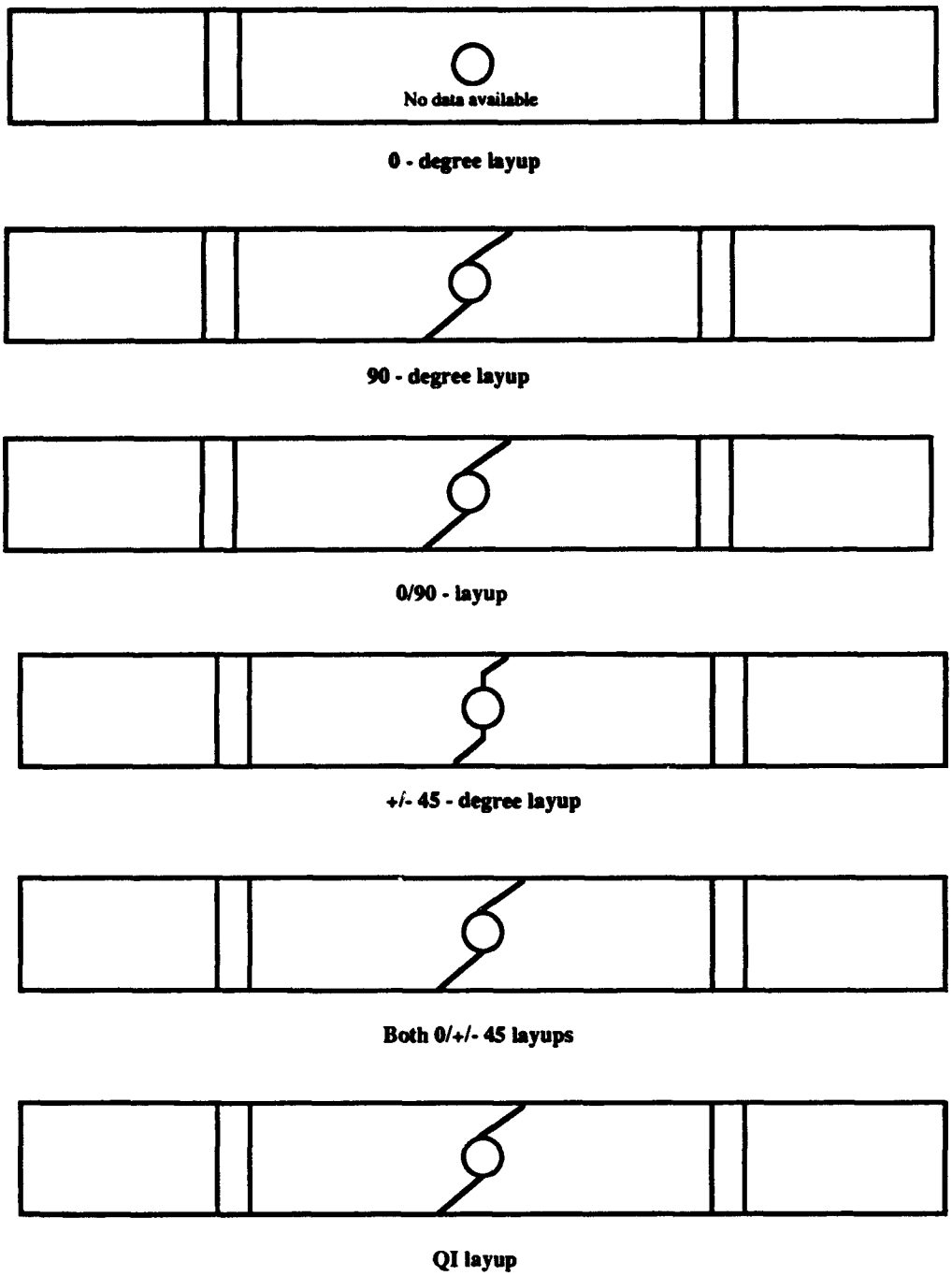

Figure 53. Analytical Failure Modes

VI. Conclusions

This study has investigated the behavior of Gr/PEEK tensile specimens containing central elliptical holes. Testing was conducted on seven different ply layups and three hole geometries, with three specimens for each combination. Results were very consistent, with minimal experimental data scatter. Investigation of failure modes was limited to visual inspection of failure surfaces.

Finite Element analysis was also conducted to predict the specimens' response and failure modes. The analysis program PLNRS demonstrated overall good correlation with experiment in predicting the stress-strain response of the specimens, but in most cases did not itself predict failure even within 10% of the experimental failure load. The program also had mixed results in predicting failure modes. Results were good for the layups including ±45° plies in the stacking sequence. Failures of these layups were characterized by audible noise as damage occured, progressing to failure. The other layups tended toward more sudden failures, with little or no forewarning. The program is unable to accurately model these types of failures.

Four of the layups tested in this study were also used by Martin and Daniels with a concentric circular hole of the same diameter as in this study [9, 10]. The results of this study were compared and found to agree with the general trends, failure modes, and failure loads of the previous studies. Table 4 presents the failure load comparison. This tends to support the decision to use the material property data determined by Wham [12].

Table 4. Circular Hole Failure Load Comparison with Previous Studies

	Average Experimental Failure Loads in N (lb)		
Layup	Martin ‡	Daniels	Present Study
$[0_{16}]$	26700 (6000)	22944 (5156)	24021 (5398)
$[90_{16}]$	3427 (770)	3333 (749)	2982 (670)
$[\pm 45]_{4s}$	11285 (2536)	10404 (2338)	10698 (2404)
$[0/\pm 45/90]_{2s}$	19313 (4340)	18103 (4068)	18610 (4182)

‡ The cross-sectional areas of the specimens were slightly larger than the present study's.

The specimens exhibited the expected relative failure load levels, based upon hole geometry and the associated stress concentration. In other words, the transverse ellipse specimens always failed at the lowest load, followed at some higher load by the circular hole. The longitudinal ellipses failed at much higher loads, consistent with theory.

A number of factors exist which may be responsible for the divergence of analysis and experiment where it occurs. As previously mentioned, the analysis assumed a state of plane stress, ignoring any through-the-thickness stresses, free edge effects, or edge delamination. However, these phenomenon are often present and sometimes significant [32, 33, 34, 35]. Interlaminar matrix cracking and delamination cause a redistribution of load; if this occured, the analysis no longer modelled the actual problem, and may account for some of the discrepancies observed [34]. Certainly if three-dimensional effects were of sufficient magnitude to affect the problem, these effects were unaccounted for by the analysis.

Only one of several available schemes was utilized in unloading the failed elements within the finite element mesh. This method may not be optimum for all of the layups or hole geometries tested. Had time permitted, the author could have rerun select cases using one of these other schemes. It is possible that this could result in the analysis more closely matching the actual failure loads.

The coarseness of portions of the finite element meshes may be a source of error contributing to discrepancies between analysis and experiment. The elliptical meshes in particular contained very coarse regions near the edge of the model, but even the circular mesh could be finer in this region, as evidenced by the failure progression of the ±45 model. This model failed at the edge just prior to the failure from the hole region extending to the edge itself. This indicates too coarse a mesh in that region.

The failure criteria used in the program may be a source of some error as well, although it should be geometry-independent, and has yielded good results in the past.

Minor imperfections in the specimens may have played a part as well. Some of the panels from which the specimens were cut developed a slight warp and/or twist during the curing process. This was observed visually in a few of the specimens, and likely resulted in a somewhat eccentric load distribution throughout the specimens. The specimens were not all perfectly uniform in thickness, either. This could also yield some nonuniformity of load and stress distribution which would then impact the experimental response. It may be that the cases demonstrating greater experimental data scatter are in fact those cases where these imperfections were present.

Another consideration is that the analysis was run using a nominal cross-sectional area for stress determination. The actual areas varied from one specimen to another, rarely equalling this ideal value. Thus, another minor source of error was introduced.

Finally, some of the divergent behavior could be due to gage-related effects. The adhesive attaching the gages to the specimens could be failing in some cases, or damage could be occuring in the region of the gage. Either occurence would affect the data recorded, and lead to erroneous values for strains. This would seem more likely in those cases where the strain data suddenly diverged from its previous trends and changed sign.

There is certainly room then to continue and expand this research. Some changes which would reduce sources of error include refining the finite element meshes further and running isotopic cases in the analysis for comparison. Also, the analyses could be run utilizing alternate unloading schemes. Ultrasonic inspection of failed and percentage-of-failure-load specimens could be undertaken to gain insight into the internal damage of the various configurations.

A more ambitious undertaking would entail accounting for interlaminar stresses and other three-dimensional effects in the analysis, or utilizing another failure criteria for comparison.

In conclusion, this study has investigated the effects of hole geometry on material response and failure loads in Gr/PEEK tensile specimens. Nonlinear analysis using the program PLNRS has shown overall good agreeement with experiment, with some shortcomings. This study will hopefully be a useful addition to the data and knowledge base on Gr/PEEK and advanced composite materials in general.

Appendix A - Test Plan

This appendix contains a copy of the Test Plan submitted to the Wright Lab. Such a plan is required by the lab for any specimen construction and testing. The plan details the specifications to construct the panels and specimens required for experimental testing, as well as the placement of strain gages.

TEST PLAN

Study of Graphite PEEK with Elliptical Holes Under Tension

1. Program Information

a. Organization	WL/FIBCA
b. Project Number	24010366
c. Project Title	"An Investigation of Graphite PEEK with Elliptical Holes Under Tension"
d. Security Classification	Unclassified
e. Project Engineer	Capt Bill Lau
f. Project Advisor	Dr. Anthony Palazotto
g. Project Sponsor	Dr. R. S. Sandhu
h. Instrumentation Engineer	Assigned by FIBT
i. Fabrication Engineer	Assigned by Composites Facility
j. Test Location	WL/FIBEC, Bldg 65, Area B

2. Program Objectives

The objectives of this effort are to correlate the analytical and experimental responses of Graphite PEEK with a central elliptical hole under tension loading.

3. Technical Description

The following paragraphs provide technical details to fabricate specimens required to conduct the investigation.

3.1 Material

The specimens required for this program will be fabricated using AS4 graphite fibers in a Polyetheretherketone (PEEK) matrix.

3.2 Stacking Sequence of Panels

Specimens (of sizes that will be specified in paragraph 3.4) will be cut from panels fabricated of the material system of paragraph 3.1 and will conform to the following stacking sequences:

A	$[0°]_{16}$	16 plies
B	$[0°/90°]_{4S}$	16 plies
C	$[\pm 45°]_{4S}$	16 plies
D	$[(0°/\pm 45°/90°)_2]_S$ (QI)	16 plies
E	$[\pm 45°/0°/\pm 45°/0°/\pm 45°]_S$	16 plies
F	$[\pm 45°_2/0°/\pm 45°]_S$	14 plies

The panels will be uniform in thickness and the average ply thickness will be 0.00525" ±0.0003". The thickness of the fabricated panels (before cutting into specimens) will be measured at locations shown in Figure 1. Any panel which does not comply with the specified thickness will not be used.

3.3 Panels

3.3.1 Size

For the material system described in paragraph 3.1, the size and the number of panels will be in accordance with the following table:

Panel Designation	Size Before Trimming	Size After Trimming	Quantity
A	14.0" x 24.0"	13.0" x 23.0"	1
B	12.0" x 14.0"	11.0" x 13.0"	1
C	12.0" x 38.0"	11.0" x 37.0"	1
D	12.0" x 14.0"	11.0" x 13.0"	1
E	12.0" x 14.0"	11.0" x 13.0"	1
F	12.0" x 14.0"	11.0" x 13.0"	1

3.3.2 Void Content

The void content will not be in excess of one per cent with variations of thickness specified in paragraph 3.2.

3.3.3 Determination of Flaws

All untrimmed panels will be subjected to C-scan to determine flaws before being cut into specimens. The final acceptance or rejection of panels will be made by the project engineer.

3.3.4 Resin Content

Samples will be taken at suitable locations to determine resin content, fiber volume, and void fraction for all of the panels. These results will be compared with optical observations and thickness per ply.

3.4 Specimens

Specimens of the following types will be cut from the panels of paragraphs 3.2 and 3.3.1:

a.	0 T	1.2 inch wide tension specimen with centrally-located hole, either circular or one of two elliptical configurations, with standard tapered tabs (Fig. 2, 3, & 9). **Three of each hole configuration required.**
b.	90 T	1.2 inch wide tension specimen with centrally-located hole, either circular or one of two elliptical configurations, with standard tapered tabs (Fig. 2, 3, & 9). **Three of each hole configuration required.**
c.	(0/90) T	1.2 inch wide tension specimen with centrally-located hole, either circular or one of two elliptical configurations, with standard tapered tabs (Fig. 2, 4, & 9). **Three of each hole configuration required.**
d.	±45 T	1.2 inch wide tension specimen with centrally-located hole, either circular or one of two elliptical configurations, with standard tapered tabs (Fig. 2, 5, & 9). **Nine of each hole configuration required.**
e.	QI T	1.2 inch wide tension specimen with centrally-located hole, either circular or one of two elliptical configurations, with standard tapered tabs (Fig. 2, 6, & 9). **Three of each hole configuration required.**
f.	(0$_2$/±45) T	1.2 inch wide tension specimen with centrally-located hole, either circular or one of two elliptical configurations, with standard tapered tabs (Fig. 2, 7, & 9). **Three of each hole configuration required.**
g.	(0/±45) T	1.2 inch wide tension specimen with centrally-located hole, either circular or one of two elliptical configurations, with standard tapered tabs (Fig. 2, 8, & 9). **Three of each hole configuration required.**

The specimens will conform to the dimensions shown in Figure 2; this figure also provides specifications for the circular hole to be tested, and designates the three hole types. Figure 9 and Table I provide coordinates for the two elliptical holes to be tested. These specimens will be designated as follows:

XX - ZZ - HH - NN

where

XX: Specimen type

ZZ: Panel designation (A,B,C, D, E, or F)

HH: Hole type I, II, or III

NN: Specimen number

3.5 Tabbing Specimens

Tabs for the specimens identified in paragraph 3.4 will be cut from fiber glass fabric 1/16 inch thick (approximately) and bonded to the specimens using standard procedures.

3.6 Instrumentation

The specimens will be instrumented using the appropriate gages etc. as indicated in the following paragraph:

a. A stacked strain gage rosette, WA-03-030WR-120 will be bonded adjacent to the hole on one side only of the specimen. In addition, a far field strain gage rosette, CEA-03-125UR-350 will be bonded at the midpoint between the hole and the tab on both sides of the specimen. Exact locations of the gages will be provided at a later date. No gages are required on 18 of the "d" specimens from Panel C.

3.7 Testing

3.7.1 Ultimate Tensile Strength

To determine the ultimate tensile strength of specimens with three types of holes all specimens will be instrumented with strain gage rosettes near the hole and at a far field location and tested under tension. The three configurations of holes are a 0.4" diameter circle, a 0.4" x 0.2" ellipse, and a 0.2" x 0.4" ellipse, all centrally located. These holes are designated Type I, II, amd III respectively (see Figures 2 & 9 and Table I). **Three specimens of each hole type will be tested for each panel.**

3.7.2 Progression of Failure

To determine the growth of ply failure in the (±45°) layup for all three hole configurations, specimens of this type will be loaded to 90% and 95% of ultimate tensile strength. **A total of six specimens of each hole configuration are required.** The specimens will then be removed from the loading device and investigated using a scanning electron microscope.

3.7.3 Loading and Sampling Rates

All specimens will be loaded at the crosshead speed of 0.05 inches per minute. Sampling rate for the various specimens as follows:

Ply Layup	Sampling Rate
0T	1 sample/sec
90T	4 samples/sec
0/90T	2 samples/sec
±45T	1 sample/sec
QIT	2 samples/sec
0_2/±45T	1 sample/sec
0/±45T	1 sample/sec

3.8 Scrap

The scrap will be saved and identified.

3.9 Report

The results of this study will be compared and contrasted to an analytical study. The final results and discussion will be incorporated into a graduate thesis by the project engineer.

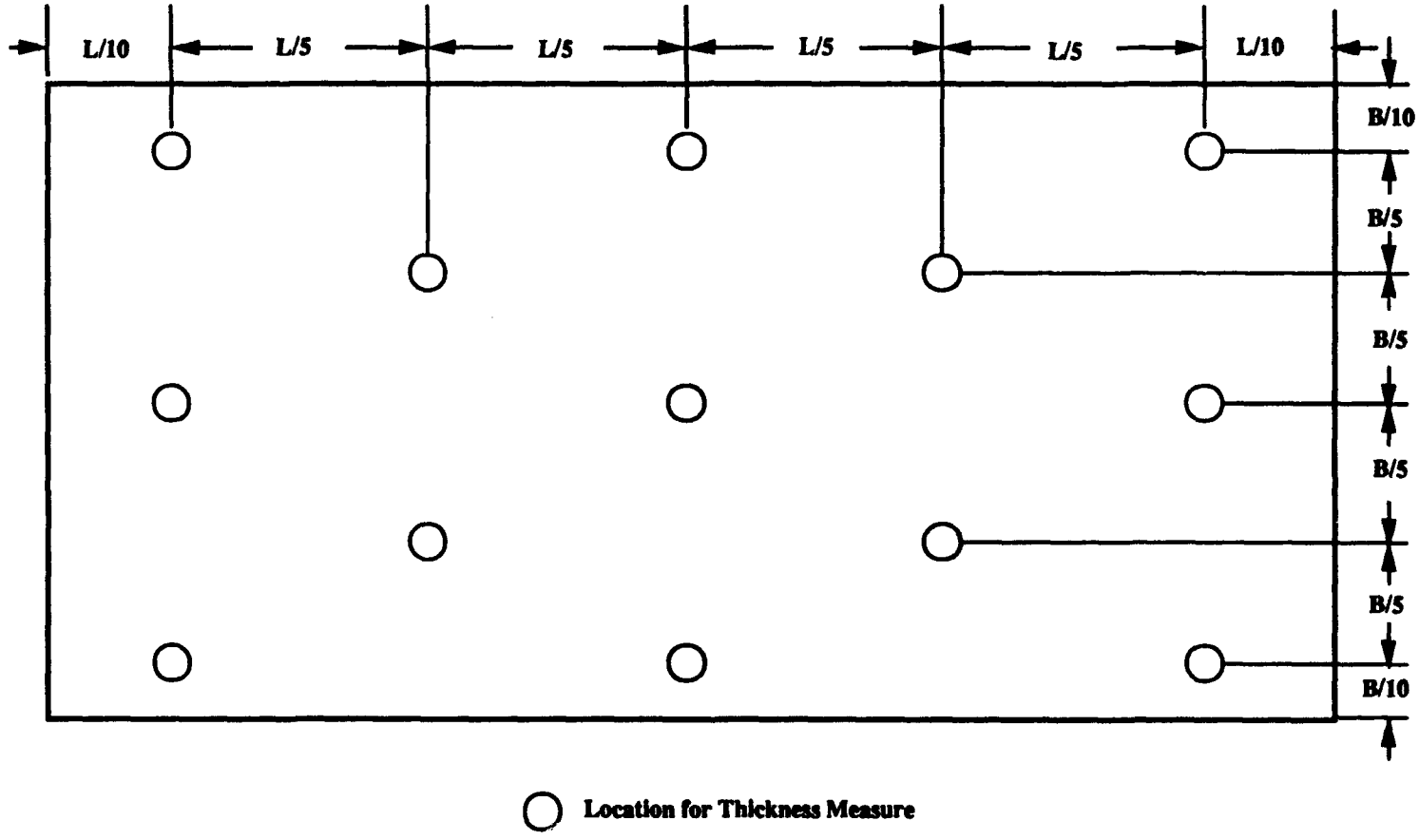

Figure A-1. Thickness Measurement

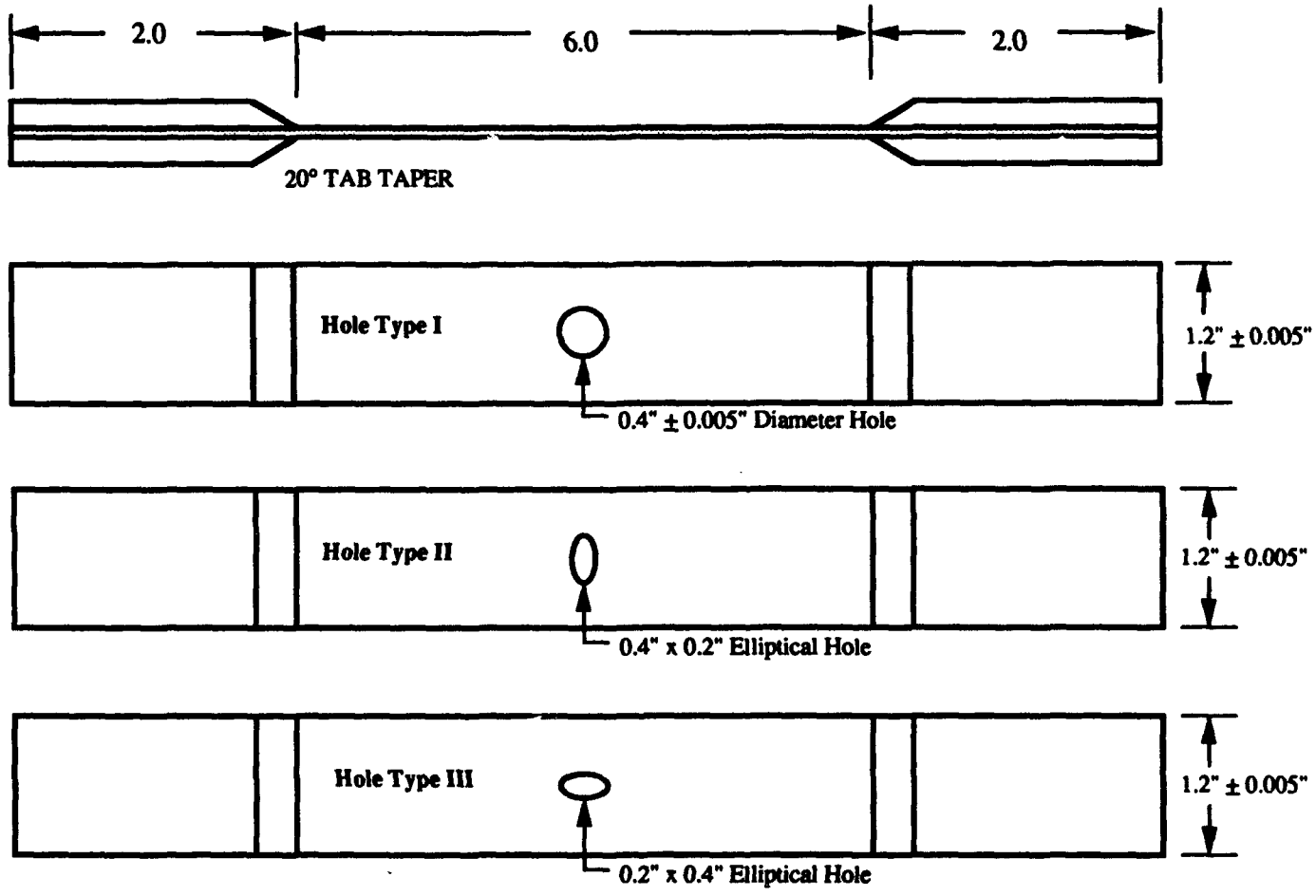

Note: See Figure 9 and Table I for elliptical hole information

Figure A-2. Tensile Specimens

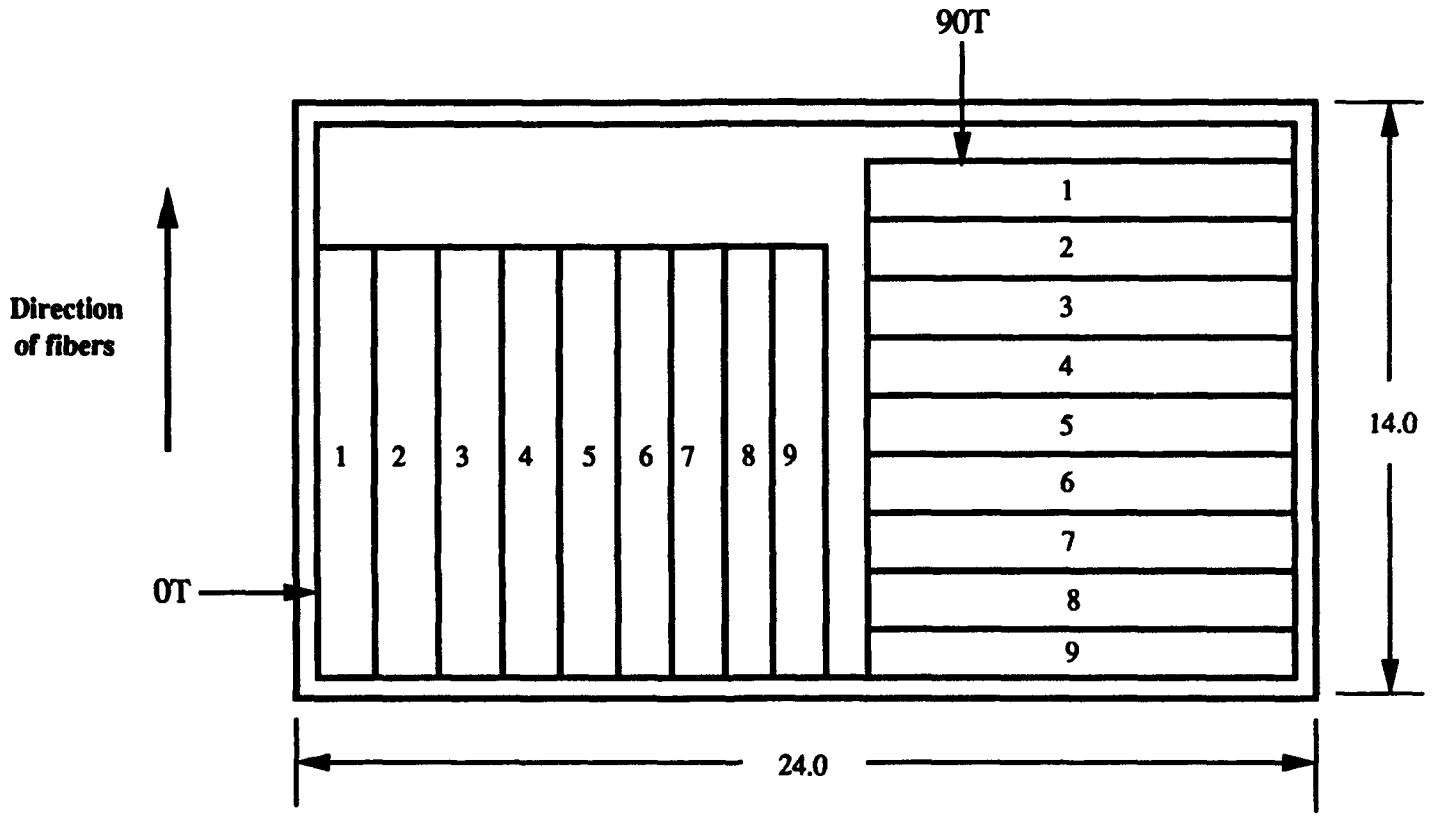

Figure A-3. Panel A: (0) and (90) Specimens

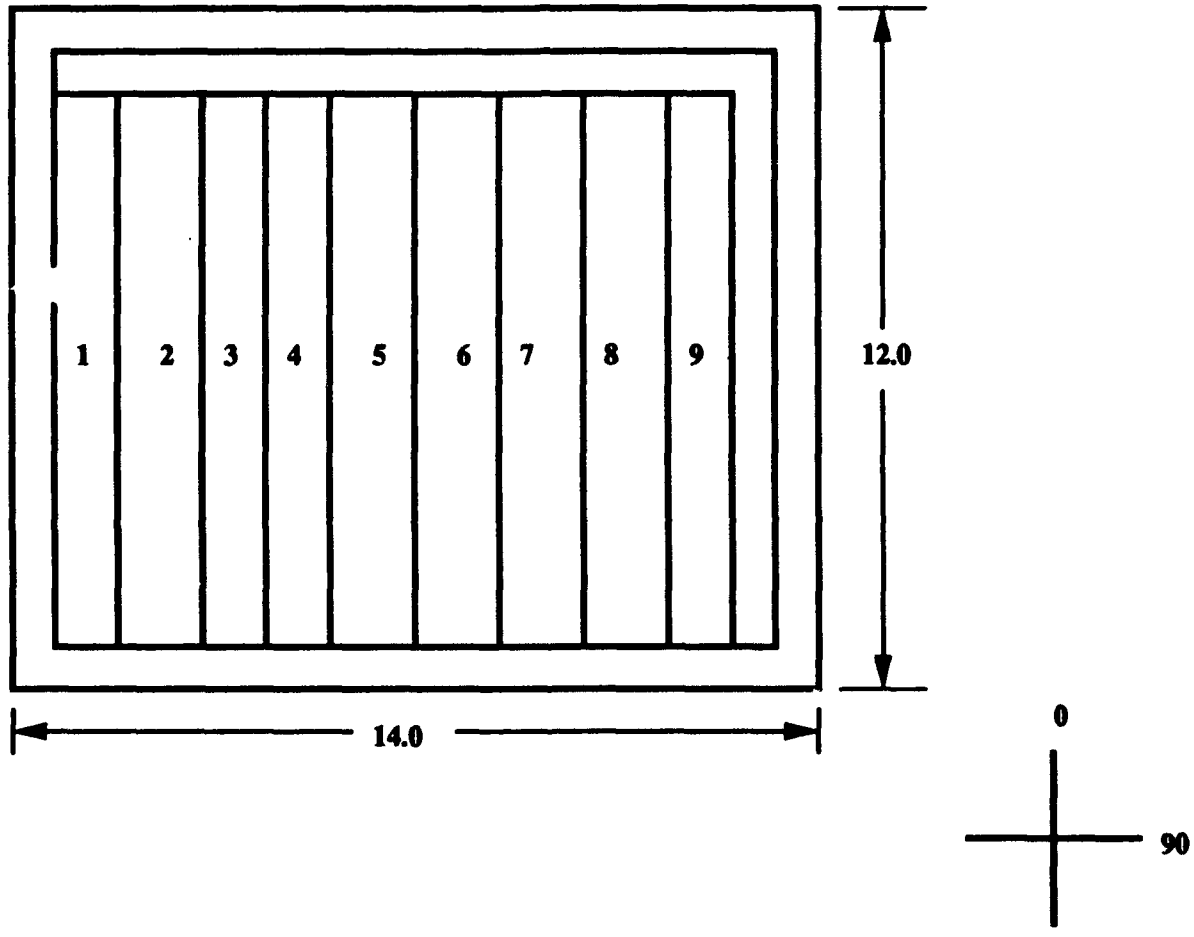

Figure A-4. Panel B: (0/90) Specimens

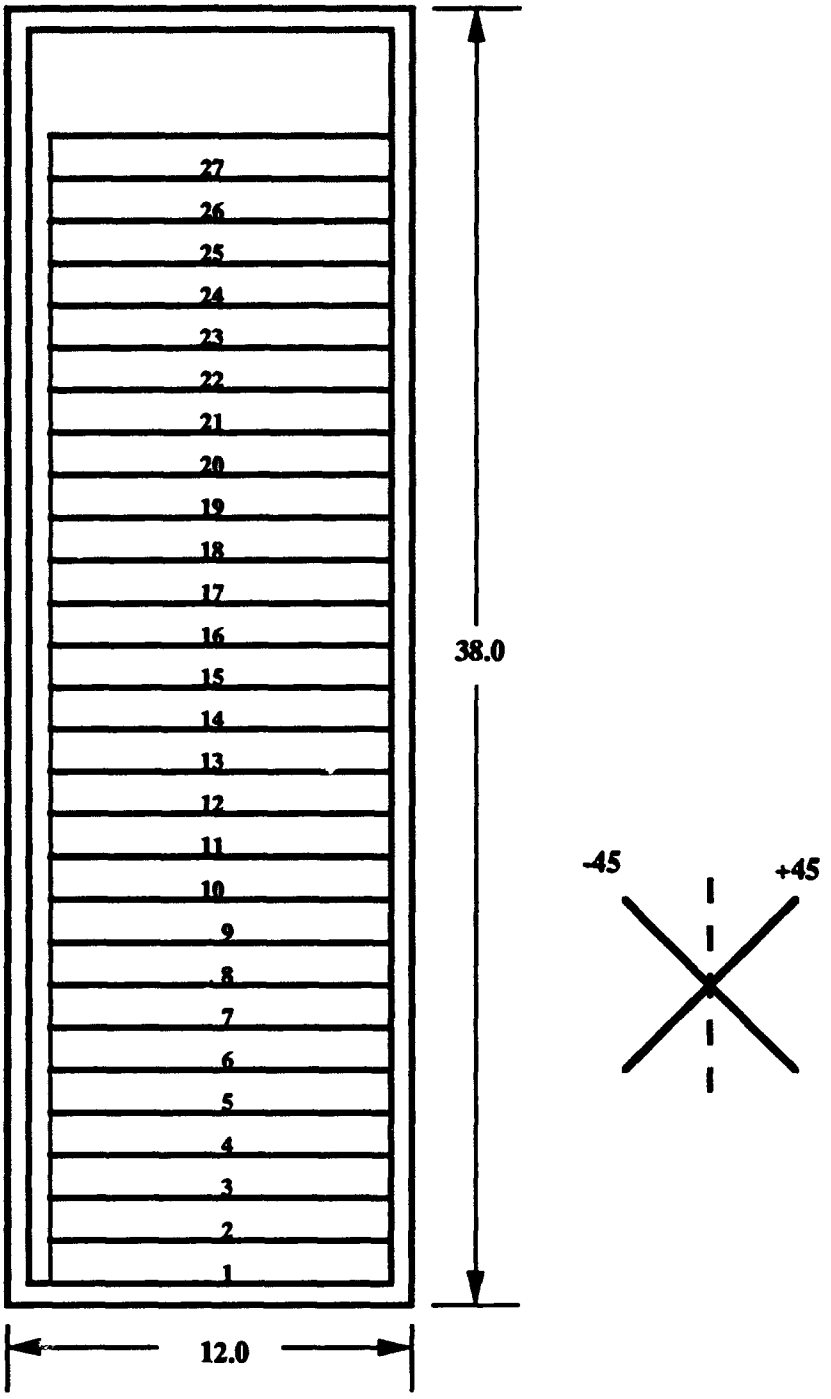

Figure A-5. Panel C: (± 45) Tension Specimen

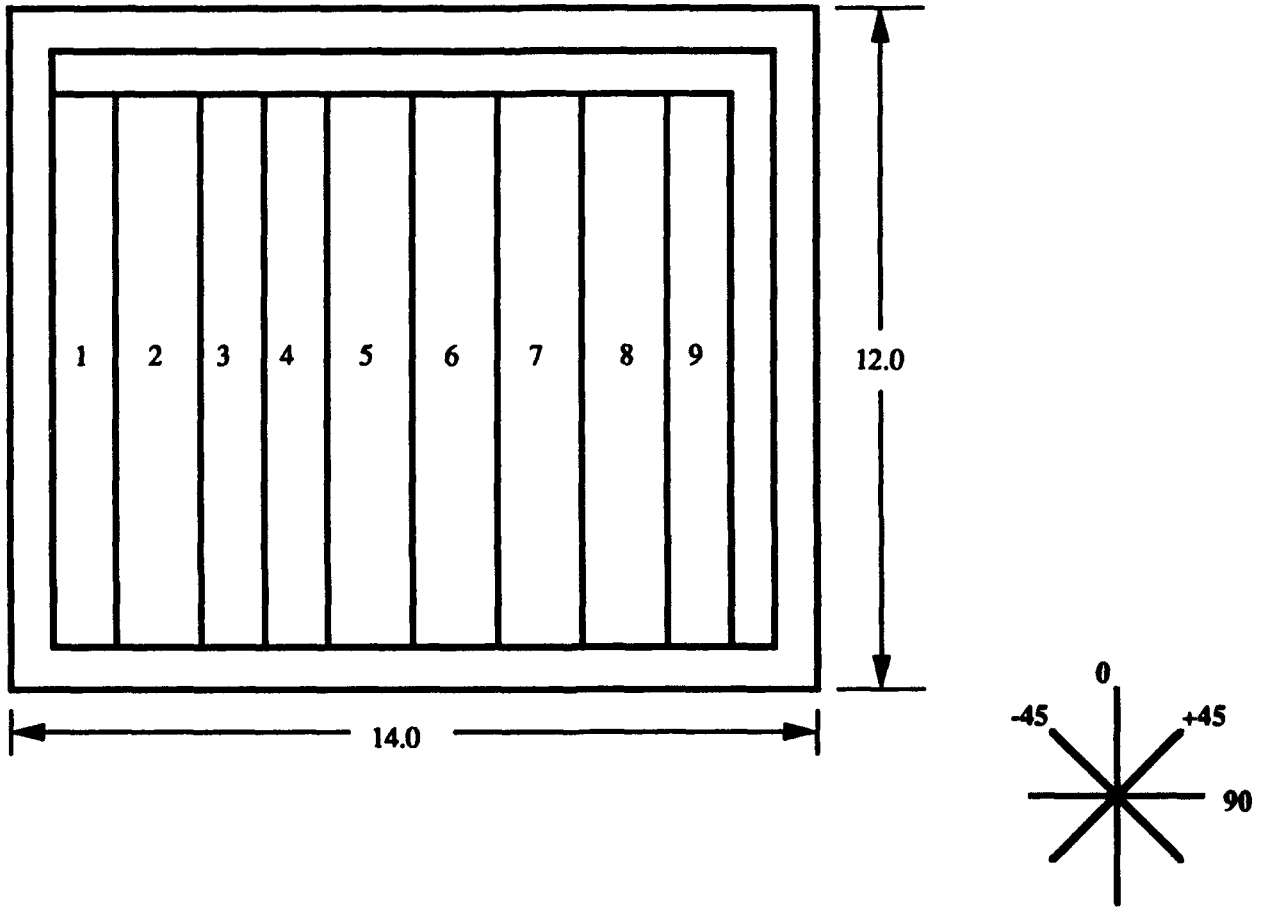

Figure A-6. Panel D: QI Specimens

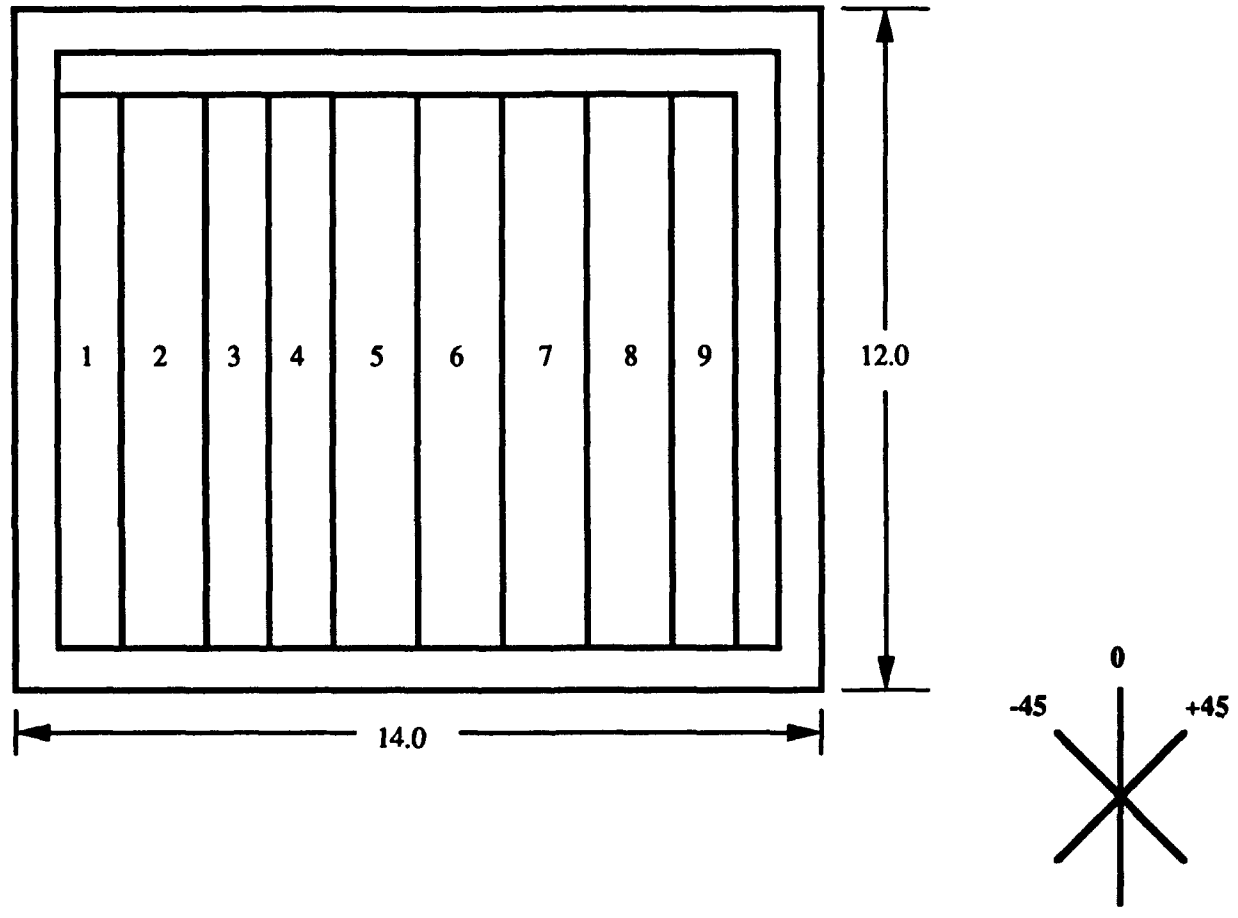

Figure A-7. Panel E: (0(2)/± 45) Specimens

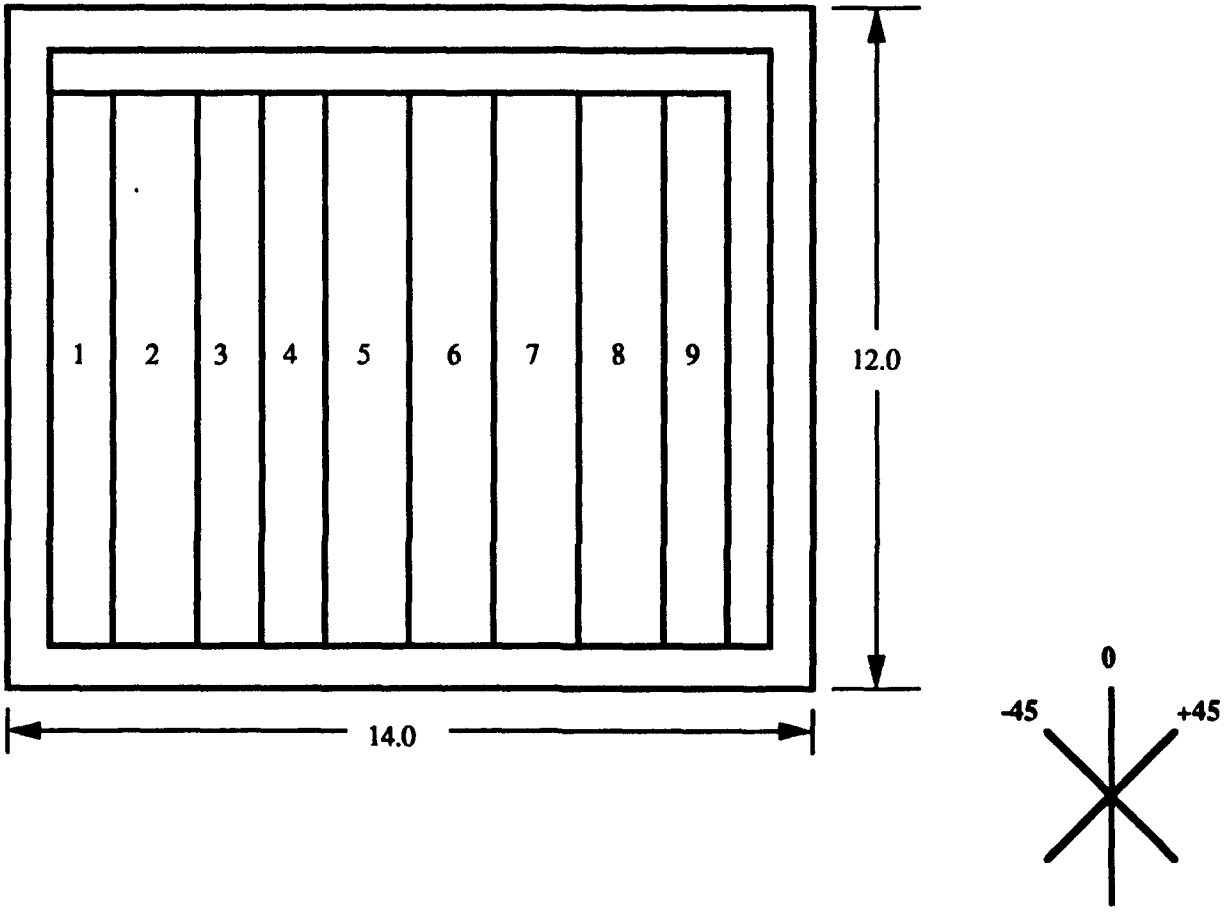

Figure A-8. Panel F: (0/$\pm$ 45)Specimens

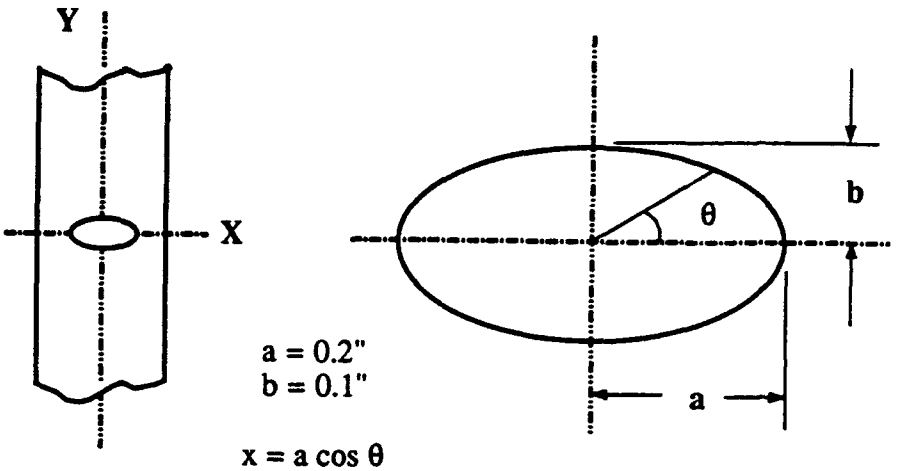

a = 0.2"
b = 0.1"

$x = a \cos \theta$

$y = b \sin \theta$

(i)

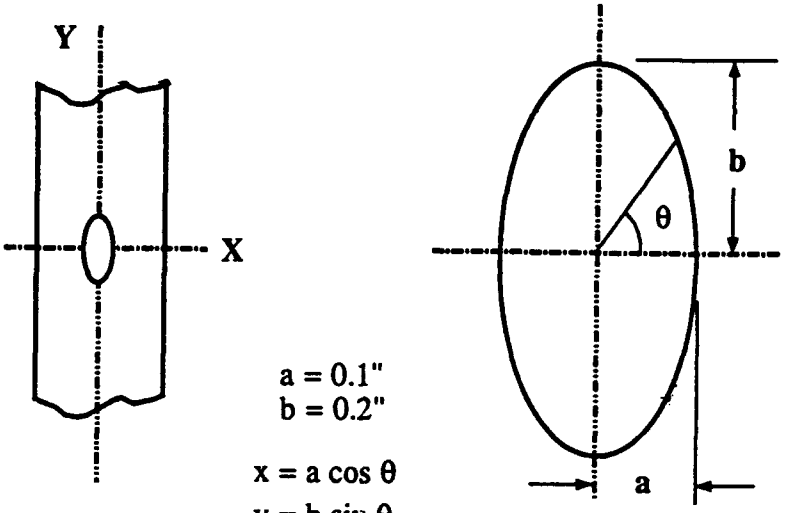

a = 0.1"
b = 0.2"

$x = a \cos \theta$

$y = b \sin \theta$

(ii)

See Table I for (x,y) coordinate data

Figure A-9. Hole Type II & III (Elliptical)

Hole Type II - Figure 9 (i)		Hole Type III - Figure 9 (ii)	
X-coordinate (in)	Y-coordinate (in)	X-coordinate (in)	Y-coordinate (in)
0.200	0.000	0.100	0.000
0.193	0.026	0.097	0.052
0.173	0.050	0.087	0.100
0.141	0.071	0.071	0.141
0.100	0.087	0.050	0.173
0.052	0.097	0.026	0.197
0.000	0.100	0.000	0.200
-0.052	0.097	-0.026	0.197
-0.100	0.087	-0.050	0.173
-0.141	0.071	-0.071	0.141
-0.173	0.050	-0.087	0.100
-0.193	0.026	-0.097	0.052
-0.200	0.000	-0.100	0.000
-0.193	-0.026	-0.097	-0.052
-0.173	-0.050	-0.087	-0.100
-0.141	-0.071	-0.071	-0.141
-0.100	-0.087	-0.050	-0.173
-0.052	-0.097	-0.026	-0.197
0.000	-0.100	0.000	-0.200
-0.052	-0.097	0.026	-0.197
-0.100	-0.087	0.050	-0.173
-0.141	-0.071	0.071	-0.141
-0.173	-0.050	0.087	-0.100
-0.193	-0.026	0.097	-0.052
-0.200	0.000	0.100	0.000

Table A-I -Elliptical Hole Coordinates

Appendix B - Input File Format

This appendix presents the basic format and content of the input files used by the analysis program PLNRS. PLNRS is a fortran code, and the source code should be referenced for futher information. The following information is valid for the version of the program used in this study. The reader is advised to review the program for any minor changes in input term labels or format which may occur. The basic input file format is presented first, followed by an explanation of the various terms. The fortran format for each entry is listed in parentheses (i.e., integer or real number, and size).

Input file format

HED

NUMNP NUMEL NUMMAT NUMPC ACELX ACELY Q NISO MISO LVECT NAXI NCONTR NONLIN NOPSHN MAXINR MAXEL MINEL MAXDPT MDIS NTIME ISOL NVECT ITUR

N KODE(N) X(N) Y(N) UU(N,1) UU(N,2) T(N)

(This is repeated for the number of node points)

THETAK

DEPTHK

MATK

EL I J K L MAT THETA DEPTH

(This is repeated for the number of elements)

MAT

NUMDAT: 1T 1C 2T 2C SH12 NU12T NU12C

(Stress-strain data goes here in 6 columns)

E1T E1C E2T E2C G12

Explanation of input terms

HED	Header or title, up to 80 characters
NUMNP	Total number of node points in mesh (I5)
NUMEL	Total number of elements in mesh (I5)
NUMMAT	Number of different materials used (I5)
NUMPC	Number of pressure cards used (N/A for tensile panel - enter 0) (I5)

ACELX	Acceleration in x-direction (F10.0)
ACELY	Acceleration in y-direction (F10.0)
Q	Reference temperature (F10.0)
NISO	Identifies type of material (I5) - 1 = isotropic 2 = anisotropic 3 = both
MISO	Number of isotropic materials (I5)
LVECT	Load vector; 0 or 1 (I5)
NAXI	1 if axisymmetric, 0 otherwise (I5)
NCONTR	1 writes data for contours, 0 does not (I5)
NONLIN	1 if nonlinear analysis, 0 if linear (I5)
NOPSHN	Element unloading option - 1, 2, 3, or 4 - see source code for details (I5)
MAXINR	Maximum number of increments to compute in analysis run (I5)
MAXEL	Maximum element number to include in output (I5)
MINEL	Minimum element number to include in output (I5)
MAXDPT	Number of elements depth-wise (I5)
MDIS	0 if force loading, 1 if displacement loading (I5)
NTIME	CPU time limit (I5)
ISOL	Type of solution scheme - 1 if incore, 2 if banded
NVECT	*Lowest node # where force applied* - will run through highest node # (I5)
ITUR	Same as NVECT, but for displacement (I5)
N	Node number (I5)
KODE(N)	Nodal constraint (I5) - 0 = free 1 = constrained in x-direction 10 = constrained in y-direction 11 = load or displacement applied at node
X(N), Y(N)	x and y coordinates of point (2F10.6)
UU(N,1 or 2)	Initial x and y displacements of node (if non-zero, KODE=11) (2F10.6)
T(N)	Initial temperature of node (F10.5)
THETAK	Orientation angle of each direction present in layup (KF10.0)
DEPTHK	Total thickness of each group of ply directions (KF10.0)
MATK	Material number for each group of ply directions (KF10.0) In these 3 terms, K represents the number of directions in the layup.
EL	Element number (I5)
I, J, K, L	Nodal connections forming element - see Figure B1 (4I5)
MAT	Material number for the element (I5)
THETA	Orientation angle of fibers (F10.6)

DEPTH	Thickness of element - one element used for each direction (F10.6)
MAT	Material number for data to follow (I5)
NUMDAT	Number of data points for the following material data entries (7I5):
1T, 1C	Stress-strain data along fiber direction in tension, compression
2T, 2C	Stress-strain data transverse to fiber in tension, compression
SH12	Shear data
NU12T,C	Poisson's ratio data in tension, compression The data itself is entered in pairs as strain and either stress or Poisson's ratio, in a total of 6 columns across (3 pairs across). Each entry is (F10.6) in size.
E1T, E1C	Initial modulus, fiber direction, tension and compression (F10.6)
E2T, E2C	Initial modulus, transverse to fibers, tension and compression (F10.6)
G12	Initial shear modulus (F10.6)

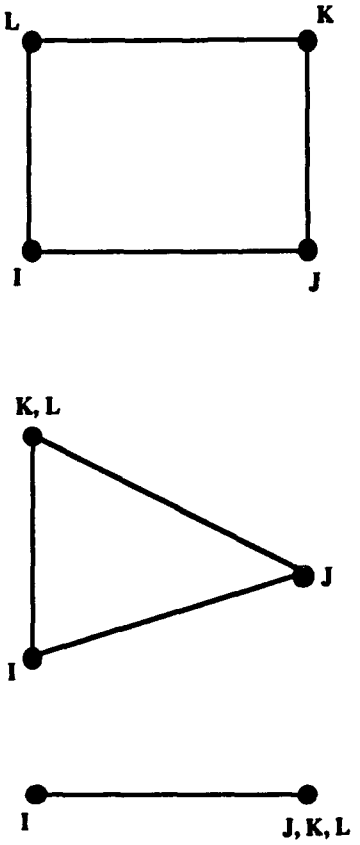

Figure B1. Nodal Connections for Various Element Types

Appendix C - GENELP Source Code

The source code for the GENELP program is included here; this is a Fortran program designed to generate a finite element mesh around an elliptical hole. It produces a mesh of concentric ellipses, given an existing mesh of concentric circles. It is designed for use with the PLNRS nonlinear analysis program. The existing mesh is expected to model one-quarter of a panel or test specimen. The user specifies the ratio of the semi-axes of the elliptical hole and the number of divisions desired around the quarter-hole.

```
      PROGRAM GENELP
C
C*****************************************************************
C
C     ELLIPSE GENERATING PROGRAM
C
C*****************************************************************
C
C       This program takes the existing nodal data for a finite
C       element mesh around a circular hole and modifies it for
C       an elliptical hole.  Required inputs include the name of
C       the existing file, ratio of the semi-axes of the ellipse,
C       number of divisions around the quarter-hole, and the
C       radius number at which grading begins.  The existing
C       data is expected to be for a circle whose diameter equals
C       the major axis of the ellipse.
C
C       Written by:     Capt Bill J. Lau
C
C                       Air Force Institute of Technology
C                       School of Engineering
C                       AFIT/ENY
C                       Class GAE-93D
C                       WPAFB, OH  45425
C
C       Date:           19 July 93
C
C       Last Modified:  22 July 93
C
C*****************************************************************
C
C       List of Variables:
C
C       AXRAT  : ratio of the semi-axes of the ellipse, taken
C                as y:x, or transverse:longitudinal (real)
C
C       NDI    : number of divisions around the quarter-hole
C                which the mesh is divided into (integer)
C
C       NRL    : number of radial lines in the mesh (integer)
C
C       ANDI   : same as NDI, but converted to real # (real)
C
C       DTH    : delta theta, or angle between mesh radial
C                lines, in radians (real)
C
C       NGRAD  : radius number of first graded circle (integer)
C
C       NCE    : number of concentric ellipses (integer)
C
C       NNOD   : number of nodes used (integer)
C
C       NN     : node number (integer)
C
C       NC     : node counter (integer)
C
C       ND     : node counter (integer)
C
C       ANG    : angle from x-axis to given radial line,
C                in radians (real)
```

```
C
C*****************************************************************
C
C       Resident FORTRAN Functions Used:
C
C       DFLOAT : convert integer to double precision real #
C
C       COS    : cosine of angle (in radians)
C
C       SIN    : sine of angle (in radians)
C
C*****************************************************************
C
      IMPLICIT DOUBLE PRECISION (A-H, O-Z)
      DIMENSION X(1000), Y(1000), UU(1000,2), KODE(1000)
     1         ,X1(1000), Y1(1000)
      DATA PI/3.1415927/
      CHARACTER *40 FILENAME
C
      PRINT *,'Enter the name of the file to be modified.'
      READ 6, FILENAME
    6 FORMAT(A)
      OPEN(5,NAME=FILENAME,STATUS='OLD')
C
      PRINT *,'Enter a name for the new data file.'
      READ 6, FILENAME
      OPEN(6,NAME=FILENAME,STATUS='NEW')
C
      PRINT *,'Enter the ratio of the ellipse semi-axes, b:a;'
      PRINT *,'i.e., transverse to longitudinal ratio, or y:x.'
      READ *, AXRAT
C
      PRINT *,'Enter the number of divisions along the quarter-hole.'
      READ *, NDI
C
C       Compute the number of radial lines in the mesh, as well
C       as the angle, in radians, between mesh lines.  (Must
C       convert NDI from integer to real number.)
C
      NRL=NDI+1
      ANDI=DFLOAT(NDI)
      DTH=(PI/2.0)/ANDI
C
      PRINT *,'Enter the radius number where grading begins.'
      READ *, NGRAD
C
C       Compute the number of concentric ellipses for which
C       coordinates will be generated.
C
      NCE=NGRAD-1
C
C       Compute number of nodes involved.
C
      NNOD=NRL*NCE
C
C       Read in the existing nodal data for these nodes.
C
      READ(5,1000) (ND,KODE(ND),X(ND),Y(ND),UU(ND,1)
     1             ,UU(ND,2),ND=1,NNOD)
C
```

```
C       Loops to compute x- and y-coordinates of nodal points
C       for concentric ellipses, based on data read in above.
C       For case of axis ratio less than one, value of "a" is
C       x-coordinate where y=0; the input ratio of the semi-axes
C       gives "b", and the sine and cosine relationships are
C       used to compute coordinates, using the angle between the
C       radial lines.  For case of axis ratio greater than one,
C       value of "b" is y-coordinate where x=0; procedure is
C       the same, with ratio determining "a".
C
      NN=0
      IF(AXRAT.GT.1.0)THEN
          A1=(1.0/AXRAT)*X(1)
      ELSE
          B1=AXRAT*X(1)
      ENDIF
C
      DO 20 I=1,NCE
          NC=NRL*(I-1)+1
          IF(AXRAT.GT.1.0)THEN
              B=X(NC)
              A=A1+(X(NC)-X(1))
          ELSE
              A=X(NC)
              B=B1+(X(NC)-X(1))
          ENDIF
C
          DO 10 J=1,NRL
             NN=NN+1
             ANG=DTH*(J-1)
             X1(NN)=A*COS(ANG)
             Y1(NN)=B*SIN(ANG)
C
   10     CONTINUE
   20 CONTINUE
C
C       Save the new coordinate data in the new file.
C
      WRITE(6,1000) (ND,KODE(ND),X1(ND),Y1(ND),UU(ND,1)
     1              ,UU(ND,2),ND=1,NNOD)
 1000 FORMAT(2I5,4F10.7)
C
      STOP
      END
```

Appendix D - STACK Source Code

The source code for the fortran program STACK is included here. STACK takes an existing finite element mesh for one ply orientation and generates data for the same mesh with multiple ply orientations. The nodes are taken to extend through the laminate thickness. Thus, the same nodes are used to create multiple elements; one for each ply orientation through the thickness. The format generated is that required in the PLNRS nonlinear analysis program. Appendix B presents this input file format.

In STACK, the user must input the number of ply orientations in the laminate, the orientation (angle) of each, and the total thickness of the plies in each direction.

```
      PROGRAM STACK
C
C*****************************************************************
C
C        Program takes existing mesh for one ply orientation
C        and generates data for same mesh with mutiple ply
C        orientations.  User inputs the number of different
C        ply orientations, orientation angle, and thickness
C        of each ply orientation.
C
C        Written by:      Capt Bill J. Lau
C
C                         Air Force Institute of Technology
C                         School of Engineering
C                         AFIT/ENY
C                         Class GAE-93D
C                         WPAFB, OH  45433
C
C        Date:            4 August 93
C
C        Last Modified:   25 August 93
C
C        Thanks to Dr. R.S. Sandhu of Wright Labs for the concept
C        and preliminary code, and helpful suggestions for
C        improvements!
C
C*****************************************************************
C
      IMPLICIT DOUBLE PRECISION (A-H,O-Z)
      DIMENSION KODE(1000),R(1000),Z(1000),T(1000)
     1          ,UU(1000,2),IX(1000,5),AN(1000)
     2          ,ZA(1000),HED(18),JX(5000,5)
     3          ,TH(10),TK(10),ANJ(5000),ZAJ(5000)
      CHARACTER *40 FILENAME
C
C        Read in the data from the existing data file.
C
      PRINT*,'Enter input file name:'
      READ 6, FILENAME
    6 FORMAT(A)
      OPEN(5,NAME=FILENAME,STATUS='OLD')
C
      PRINT*,'Enter output file name:'
      READ 6, FILENAME
      OPEN(6,NAME=FILENAME,STATUS='NEW')
C
      READ(5,40)HED,NUMNP,NUMEL,NUMMAT,NUMPC
     1          ,AX,AZ,Q,NISO,MISO,LVECT,NAXI
     2          ,NCONTR,NONLIN
   40 FORMAT(18A4/4I5,3F10.0,6I5)
C
      READ(5,80)NOPSHN,MAXINR,MAXEL,MINEL,MAXDPT
     1          ,MDIS,NTIME,ISOL,NVECT,ITUR
   80 FORMAT(10I5)
C
      READ(5,100)(N,KODE(N),R(N),Z(N),UU(N,1)
     1          ,UU(N,2),T(N),N=1,NUMNP)
  100 FORMAT(2I5,4F10.6,F10.5)
C
      READ(5,110)(M,(IX(M,I),I=1,5),AN(M)
     1          ,ZA(M),M=1,NUMEL)
  110 FORMAT(6I5,2F10.0)
C
C        Specify the number of ply orientations,
C        the angles, and thicknesses of each.
C
```

```
      PRINT*,'Enter the number of ply orientations;
     1 MAXPLY='
      READ*,MAXPLY
C
      DO 200 I=1,MAXPLY
         PRINT*,'Enter orientation of ply; TH(I)='
         READ*,TH(I)
         PRINT*,'Enter thickness of ply; TK(I)='
         READ*,TK(I)
  200 CONTINUE
C
C        Generate the additional element data for each
C        ply; nodes remain the same.
C
      JK=0
      DO 300 I=1,NUMEL
         DO 250 K=1,MAXPLY
            JK=JK+1
            DO 230 J=1,5
               JX(JK,J)=IX(I,J)
  230       CONTINUE
            ANJ(JK)=TH(K)
            ZAJ(JK)=TK(K)
  250    CONTINUE
  300 CONTINUE
C
      NUMTOT=NUMEL*MAXPLY
C
C        Output the new data in the desired form.
C
      WRITE(6,1000)HED,NUMNP,NUMTOT,NUMMAT,NUMPC
     1             ,AX,AZ,Q,NISO,MISO,LVECT,NAXI
     2             ,NCONTR,NONLIN
 1000 FORMAT(18A4/4I5,3F10.7,7I5)
      WRITE(6,1100)NOPSHN,MAXINR,MAXEL,MINEL
     1             ,MAXPLY,MDIS,NTIME,ISOL,NVECT,ITUR
 1100 FORMAT(10I5)
      WRITE(6,1200)(N,KODE(N),R(N),Z(N),UU(N,1)
     1             ,UU(N,2),T(N),N=1,NUMNP)
 1200 FORMAT(2I5,4F10.6,F10.5)
      WRITE(6,1300)(M,(JX(M,I),I=1,5),ANJ(M)
     1             ,ZAJ(M),M=1,NUMTOT)
 1300 FORMAT(6I5,2F10.5)
C
      STOP
      END
```

Bibliography

1. Mall, S., Class handouts and notes in MECH 541, Mechanics of Composite Materials, School of Engineering, Air Force Institute of Technology (ETC), Wright-Patterson AFB, OH, 1992

2. Missile Airframe Guidelines - A Handbook for Composite Applications, report of Low Cost Composite Weapons (LCCW) contract by McDonnell Douglas Missile Systems Co., 15 Sep 88 - 30 Jun 91

3. Hua, C.T., Chu, J.-N., Ko, F.K., "Damage Tolerance of Three-Dimensional Commingled PEEK/Carbon Composites", Composite Materials: Testing and Design, Tenth Volume, ASTM STP 1120, Philadelphia, PA, 1992, pp. 400-413

4. Silverman, E.M., Wiacek, C.R., and Griese, R.A., "Characterization of IM7 Graphite/Thermoplastic Polyetheretherketone (PEEK) for Spacecraft Structural Applications", Composite Materials: Testing and Design, Tenth Volume, ASTM STP 1120, Philadelphia, PA, 1992, pp. 118-130

5. Tan, S.C., "Tensile and Compressive Notched Strength of PEEK Matrix Composite Laminates", Journal of Reinforced Plastics and Composites, Vol. 6, No. 3, July 1987, pp. 253-267

6. Morrocco, John D., "Lockheed Concentrates on F-22 Risk Reduction," Aviation Week and Space Technology, Vol. 139, No. 10, September 6, 1993, pp. 50-53

7. Calcote, L.R., The Analysis of Laminated Composite Structures, New York: Van Nostrand Reinhold Co., 1969

8. Sandhu, R.S. "Nonlinear Behavior of Unidirectional and Angle Ply Laminates", Journal of Aircraft, Vol. 13, No. 2, (February 1976), pp. 104-111

9. Martin, R.J. A Study of Failure Characteristics in Thermoplastic Composite Material, MS Thesis, AFIT/GA/AA/88M-2. School of Engineering, Air Force Institute of Technology (AU), Wright-Patterson AFB, OH. March 1988

10. Daniels, J.A. A Study of Failure Characteristics in Thermoplastic Composite Laminates Due to an Eccentric Circular Discontinuity, MS Thesis, AFIT/GAE/ENY/89D-06. School of Engineering, Air Force Institute of Technology (AU), Wright-Patterson AFB, OH. December 1989

11. Fisher, J.M. A Study of Failure Characteristics in a Thermoplastic Composite Material at High Temperature, MS Thesis, AFIT/GAE/AA/88D-15. School of Engineering, Air Force Institute of Technology (au), Wright-Patterson AFB, OH. December 1988

12. Wham, B. An Investigation of Graphite PEEK Composite Under Compression with a Centrally Located Circular Discontinuity, MS Thesis, AFIT/GA/93M-01. School of Engineering, Air Force Institute of Technology (AU), Wright-Patterson AFB, OH. March 1993

13. Halpin, J.C., Primer on Composite Materials: Analysis (Revised Ed.), Lancaster, PA: Technomic Publishing Co., 1984

14. Vinson, J.R. and Sierakowski, R.L., The Behavior of Structures Composed of Composite Materials, Boston: Kluwer Academic Publishers, 1986

15. Tsai, S.W., Composites Design (Third Edition), Dayton, OH: Think Composites, 1987

16. Agarwal, B.D., and Broutman, L.J., Analysis and Performance of Fiber Composites, Second Edition, New York: John Wiley & Sons, 1990

17. Palazotto, A.N., Class handouts and notes in MECH 600, Elasticity, MECH 605, Fracture Mechanics, MECH 644, Finite Element Methods for Structural Analysis II, and MECH 741, Advanced Topics in Composites, School of Engineering, Air Force Institute of Technology (ETC), Wright-Patterson AFB, OH, 1992-1993

18. Jones, R.M., Mechanics of Composite Materials, New York: Hemisphere Publishing Corp., 1975

19. Cook, R.D., Malkus, D.S., and Plesha, M.E., Concepts and Applications of Finite Element Analysis, Third Ed., New York: John Wiley & Sons, 1989

20. Broek, D., Elementary Engineering Fracture Mechanics, Fourth Edition, Boston: Kluwer Academic Publishers, 1991

21. Saada, A.S. Elasticity: Theory and Applications, Malabar, Florida: Robert E. Krieger Publishing Company, 1989.

22. Savin, G.N. "Stress Distribution Around Holes" NASA Technical Translation NASA TT F-607, November 1970.

23. Peterson, R.E. Stress Concentration Factors, New York: John Wiley and Sons, 1974, pp. 110-112, 126/7, 150, 196.

24. Zienkiewicz, O.C., The Finite Element Method, Third Ed., London: McGraw-Hill, 1977

25. Cron, S.M., Palazotto, A.N., and Sandhu, R.S., "A Failure Criterion Evaluation for Composite Materials", Composite Materials: Testing and Design, Ninth Volume, ASTM STP 1059, American Society for Testing and Materials, Philadelphia, PA, 1990, pp. 494-507

26. Daniels, J.A., Palazotto, A.N., amd Sandhu, R.S., "Failure Characteristics in Thermoplastic Composite Laminates Due to an Eccentric Circular Discontinuity", AIAA Journal, Vol. 29, No. 5, May 1991, pp. 830-837.

27. Martin, R.J., Sandhu, R.S., and Palazotto, A.N., "Experimental and Analytical Comparisons of Failure in Thermoplastic Composite Laminates", accepted for publication in Experimental Mechanics, March or June 1994 issue

28. Sandhu, R.S., Gallo, R.L., and Sendeckyj, G.P., "Initiation and Accumulation of Damage in Composite Laminates", Composite Materials: Testing and Design (Sixth Conference), ASTM STP 787, I.M. Daniel, Ed., 1982, pp.163-182

29. Hart-Smith, L.J., "A Scientific Approach to Composite Laminate Strength Prediction", Composite Materials: Testing and Design, Tenth Volume, ASTM STP 1120, Philadelphia, PA, 1992, pp.142-169

30. Canfield, R., Capt, Class handouts and notes in MECH 642, Finite Element Method for Structural Analysis I, School of Engineering, Air Force Institute of Technology (ETC), Wright-Patterson AFB, OH, 1992

31. Sandhu, R.S., Personal conversations, Aug/Sep 1993

32. Pagano, N.J., and Soni, S.R., "Free Edge Delamination Prevention in Composite Laminates", Debonding/Delamination of Composites, AGARD-CP-530, 1992, pp. 1-1 - 1-11

33. Sandhu, R.S., Sendeckyj, G.P., Schoeppner, G.A., and Pappas, J.E., "Initiation and Prevention of Edge Delamination With and Without Residual Stresses", Debonding/Delamination of Composites, AGARD-CP-530, 1992, pp. 3-1 - 3-20

34. Poon, C., Bellinger, N.C., Xiong, Y., and Gould, R.W., "Edge Delamination of Composite Laminates", Debonding/Delamination of Composites, AGARD-CP-530, 1992, pp. 12-1 - 12-13

35. Sandhu, R.S. and Sendeckyj, G.P., "Edge Delamination of $(\pm\theta_m/90_{n/2})_s$ Laminates Subjected to Tensile Loading", Journal of Composite Technology and Research, Vol. 13, No. 2, Summer 1991, pp. 78-90.

Vita

Capt. Bill Lau was born 10 December 1962 in Milwaukee, Wisconsin. He graduated in 1981 from Nathan Hale Senior High School in West Allis, Wisconsin. In 1981 he attended Parks College of St. Louis University in Cahokia, Illinois. He graduated Cum Laude in 1985 with a bachelor's degree in aerospace engineering. His Air Force career started in 1987 when he went through the commissioning program at Officer Training School (OTS), at the Medina Annex to Lackland Air Force Base, San Antonio, Texas. In 1988 Capt. Lau was assigned to the Eastern Test Range at Patrick AFB, Florida, where he worked as a Program Support Manager and later Range Operations Officer coordinating launch support for the Space Shuttle program. He is currently assigned to Wright Laboratory in the Structural Analysis and Optimization Branch. He is married to the former Lorraine Suzanne Slusser; they have a daughter, Sarah.

Permanent Address: 5232 Cobb Dr.
Dayton, OH 45431

REPORT DOCUMENTATION PAGE

Form Approved
OMB No. 0704-0188

1. AGENCY USE ONLY *(Leave blank)*	2. REPORT DATE	3. REPORT TYPE AND DATES COVERED
	December 1993	Master's Thesis

4. TITLE AND SUBTITLE
A STUDY OF GRAPHITE PEEK COMPOSITE WITH CENTRAL ELLIPTICAL HOLES UNDER TENSION

5. FUNDING NUMBERS

6. AUTHOR(S)
Bill J. Lau, Captain, USAF

7. PERFORMING ORGANIZATION NAME(S) AND ADDRESS(ES)
Air Force Institute of Technology, WPAFB, OH 45433-6583

8. PERFORMING ORGANIZATION REPORT NUMBER
AFIT/GAE/ENY/93D-20

9. SPONSORING / MONITORING AGENCY NAME(S) AND ADDRESS(ES)
Dr. R.S. Sandhu
WL/FIBCA
Bldg 45, Wright-Patterson AFB, OH 45433-6553

10. SPONSORING / MONITORING AGENCY REPORT NUMBER

11. SUPPLEMENTARY NOTES

12a. DISTRIBUTION / AVAILABILITY STATEMENT
Approved for public release; distribution unlimited

12b. DISTRIBUTION CODE

13. ABSTRACT *(Maximum 200 words)*

This study investigated the stress-strain response and failure modes of Graphite/Polyetheretherketone (Gr/PEEK) tension specimens containing a central elliptical hole. Both experiments and finite element numerical analyses were conducted. Test specimens included seven layups and three hole geometries; three of each combination were tested. The holes consisted of an ellipse with major axis aligned with the load axis, an ellipse with major axis transverse to the load axis, and a circle. Strain gages were located adjacent to the hole and midway between the hole and tab on all specimens. Strain data was used to plot stress-strain response. The analysis utilized a nonlinear finite element program, assuming plane stress. Linear stress-strain relationships are applied incrementally; piecewise cubic spline interpolation functions represent the material data provided to the program, accounting for the material nonlinearity. A strain energy failure criterion determines element failures. Analytical stress-strain results correlated well with experiment, with some divergence noted. Damage progression of the finite element models agreed with observed failure surfaces, except for unidirectional and crossply layups. These failed more suddenly, and the program is unable to capture this phenomenon. Interlaminar stresses developing in the actual tests and coarse regions of the finite element meshes were identified as probable sources of error.

14. SUBJECT TERMS
Composites, Thermoplastic Matrix, Elliptical Holes, Finite Elements, Nonlinear Analysis, Graphite/PEEK, Stress Concentration

15. NUMBER OF PAGES
123

16. PRICE CODE

17. SECURITY CLASSIFICATION OF REPORT	18. SECURITY CLASSIFICATION OF THIS PAGE	19. SECURITY CLASSIFICATION OF ABSTRACT	20. LIMITATION OF ABSTRACT
Unclassified	Unclassified	Unclassified	UL